論文 / 著書情報
Article / Book Information

題目(和文)	糖類を有用化学品へ変換するゼオライト触媒の開発に関する研究
Title(English)	Study on development of zeolite catalysts for conversion of sugars into useful chemicals
著者(和文)	大友亮一
Author(English)	Ryoichi Otomo
出典(和文)	学位:博士(工学), 学位授与機関:東京工業大学, 報告番号:甲第9498号, 授与年月日:2014年3月26日, 学位の種別:課程博士, 審査員:野村　淳子,富田　育義,原　亨和,馬場　俊秀,松下　伸広
Citation(English)	Degree:Doctor (Engineering), Conferring organization: Tokyo Institute of Technology, Report number:甲第9498号, Conferred date:2014/3/26, Degree Type:Course doctor, Examiner:,,,,
学位種別(和文)	博士論文
Type(English)	Doctoral Thesis

Doctor thesis

Study on development of zeolite catalysts for conversion of sugars into useful chemicals

(和訳: 糖類を有用化学品へ変換するゼオライト触媒の開発に関する研究)

This thesis was submitted to Tokyo Institute of Technology for the degree of Doctor of Engineering.

Ryoichi Otomo

Department of Electronic Chemistry

Interdisciplinary Graduate School of Science and Engineering

Tokyo Institute of Technology

Contents

Chapter 1

General Introduction

1-1 Background

In recent years, an increasing effort has been devoted to find a new way to utilize biomass as feedstock for the production of useful chemicals and fuels because of its abundance, renewability and worldwide distribution [1-5]. Nature produces annually renewable biomass in 170 billion metric tons, which consists of complex components e.g. carbohydrates, lignin, fatty acids, lipids, proteins, and others. Carbohydrate such as cellulose, hemicellulose and starch accounts for ~75 % of biomass resources. Therefore, the conversion of sugars to value-added chemicals is very important for the potential biorefinery. US DOE proposed the potential bio-based chemicals as "Top 10" in 2004 [6] and later it was revised by Bozell and Petersen as "Top 10 + 4" in 2010 [7]. The revised list includes 11 chemicals that are derived from carbohydrates.

This study focuses on particular routes, namely, dehydration of sugars to furfurals and dehydration of sorbitol to isosorbide. These "plat-form" materials have a wide possible downstream route to form various types of useful chemicals [8-10]. Hence, these types of reactions have attracted a great research attention in the field of catalytic biomass conversion.

Table 1 "Top10 + 4" chemical opportunities listed by Bozell and Petersen

Furans	Ethanol	Lactic acid	Sorbitol
Furfural	Isoprene	Succinic acid	Xylitol
5-hydroxymethylfurfural	Biohydrocarbons	Levulinic acid	
2,5-furandicarboxylic acid	Glycerol derivatives	Hydroxypropionic acid	

1-2 Synthesis of zeolites

1-2-1 Synthesis mechanism

Zeolites are microporous materials formed by TO_4 tetrahedra (T = Si, Al…) interconnected by the oxygen atoms, creating pores and cavities with uniform size and shape in the molecular dimension range (3-15 Å). Opportunity to create zeolitic structures with different framework topology and also different chemical composition have allowed their diverse application such as separation, gas adsorption, ion exchange catalysis and recent new applications including biomedicine and electronics [11]. Principally, zeolites are synthesized in aqueous media under hydrothermal conditions in the presence of organic and/or inorganic cations and a mobilizing agent. A large number of variables influence the hydrothermal crystallization and determines the kinetics and the final crystalline phases formed. There have been very nice reviews on the principal and the theory for zeolite synthesis [12-14]. This and the next sections briefly summarize the development of zeolite synthesis with reference to these reports.

Since the first example of synthetic zeolite reported by Barrer, several mechanisms have been proposed for the zeolite growth. Those mechanisms are generally based on a phase transformation of the initial reactants in amorphous form towards a crystalline product. This type of transformation is roughly divided into two pathways; one is solution-mediated transportation mechanism and the other is solid transformation.

The first possible mechanism for zeolite synthesis was proposed by Barrer *et al*. [15]. They discussed that aluminosilicates are created by secondary building units, which are rings of polyhedral, and not form additions of individual Al or Si tetrahedra (Table 2, Entry 1).

Years later, Flanigen *et al*. depicted a complementary mechanism, in which the crystal growth primarily takes place in the solid phase (Table 2, Entry 2). Extensive heterogeneous nucleation occurs and the nuclei subsequently develop to a critical size composed of polyhedra (e.g. hexagonal prism). Growth of the crystal proceeds through a type of polymerization and depolymerization mediated by excess hydroxyl ions [16].

In 1966, Kerr introduced the hypothesis of the solution-mediated growth mechanism [17]. He claimed that a zeolite could be formed via dissolution of gel by sodium hydroxide followed by deposition of zeolite crystals from gel-derived species in solution (Table 2, Entry 3). Ciric presented the most detailed study of zeolite synthesis at that date in 1968 [18]. The work pointed out in the solution-mediated growth mechanism, transport of growth species to crystals embedded in gel is restricted by diffusion through the gel.

A more chemically detailed picture of zeolite crystallization was reported by Zhdanov in 1970 [19]. In this mechanism the solid and liquid phases are connected by the solubility equilibrium. Condensation reactions give rise to ‘‘primary aluminosilicate blocks (4- and 6-membered rings)’’ and crystal nuclei. Crystal growth occurs from solution until dissolution of the amorphous phase is complete. The composition of the formed crystals depended on that of the liquid phase from which they crystallized (Table 2, Entry 4).

In 1961, two groups of workers disclosed the effect of introducing quaternary ammonium cations into zeolite synthesis [20,21]. The introduction of these organic reactants provided new possibilities for probing the chemistry of the zeolite synthesis. Derouane *et al.* proposed two different pathways for ZSM-5 formation depending on the silica source shown in Table 2, Entry 5 [22,23]. The use of polymeric silica led to the generation of a small number of nuclei which grew by a liquid phase transportation process to yield large ZSM-5singl e crystals (synthesis A). This is a type of the solution-mediated crystallization pathways and is similar to the scheme proposed by Zhdanov. When monomeric silicates were used, a large number of nuclei was generated and then very small crystallites were rapidly and directly yielded within the hydrogel through a solid hydrogel phase transformation, which is a type of solid-phase transformation pathways (synthesis B). Chang and Bell studied the formation of ZSM-5 from Al-free precursor gels using multiple analytical methods and found the ion sieve effects, where embryonic structures are formed with tetrapropylammonium (TPA) cation rapidly upon heating [24]. These first-formed units had the composition of Si/TPA = 20-24, and may resemble ZSM-5 channel intersections (4 per unit cell of

96 tetrahedralatoms). Each intersection of the crystal formed through this way essentially contains y one TPA cation. Based on these results, they proposed a possible mechanism for ZSM-5nucleation (Table 2, Entry 6). First clathrate-like water structure is formed around the template, followed by the conversion of the clathrate-like hydrate to a clathrate-like silicate by isomorphous substitution of silicate for water in the embryonic units. Such units are initially randomly connected but in time become ordered (‘‘annealed’’) through repeated cleavage and recombination of siloxane bonds, mediated by hydroxide ion. Thus, nucleation occurs through progressive ordering of these entities into the final crystal structure.

Burkett and Davis examined the role of TPA as structure-directing agent in the synthesis of silicalite-1 and proposed that the inorganic-organic composite is formed at early stages and subsequently nucleation proceeds through aggregation of these composite species (Table 2, Entry 7).

Table2 Summary of the proposed synthesis mechanism.

Entry	Authors	Ref.	Studied system	Schematic illustration
1	Barrer	15	Various low-silica phase	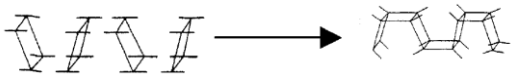
2	Flanigen Breck	16	Na-A Na-X	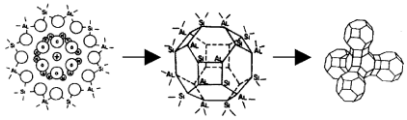
3	Kerr	17	Na-A	$\text{Amorphous solid} \xrightarrow{\text{fast}} \text{soluble species(S)}$ $\text{(S)} + \text{nuclei(or zeolite crystals)} \xrightarrow{\text{slow}} \text{zeolite A}$
4	Zhdanov	19	Na-A Na-X	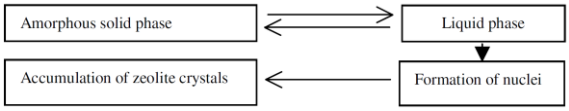
5	Derouane Detremmerie Gabelica Blom	22,23	Na,TPA-silicalite-1	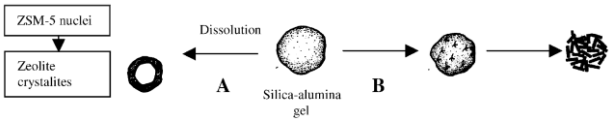
6	Chang Bell	24	Na,TPA-silicalite-1	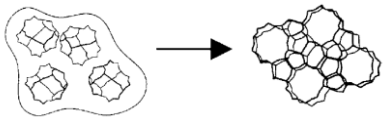
7	Burkett Davis	25-27	Silicalite-1	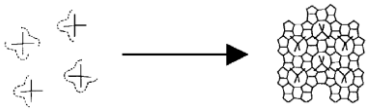

1-2-2 Organic structure-directing agent (OSDA)

The first zeolites were synthesized in alkaline media. Aluminum-rich zeolites were crystallized due to the presence of extraframework sodium ions. In 1961, the OSDA was introduced for the first time in zeolite synthesis by Barrer *et al* [15]. The use of tetraalkylammonium cations allowed increasing the framework Si/Al ratio, determined by the OSDA incorporated into the zeolite. Less positive charges are introduced by the organic molecule than by the small inorganic cations in the sodalite cage, as shown in Figure 1, requiring less anionic charges in the zeolite framework [28]. Therefore, the organic molecule can determine the amount of trivalent elements in the zeolite framework, but also the structural characteristics, such as pore dimensions and cavities, depending on shape, size, hydrophobicity, and number of charges of the OSDA molecule.

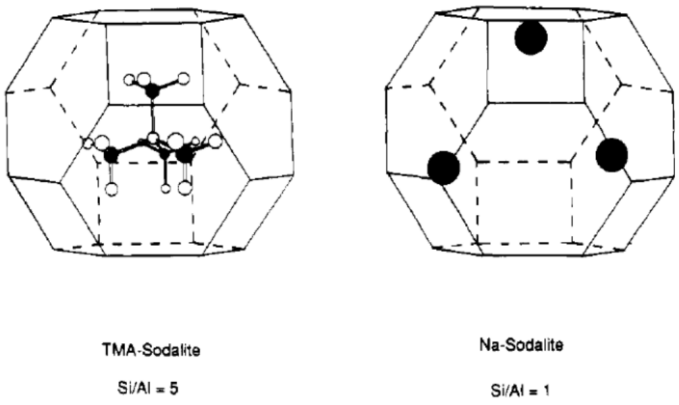

Figure 1 Tetramethylammonium (left) and sodium (right) cations in sodalite cage.

The use of organic molecules in zeolite synthesis was quickly expanded after the initial work of Barrer. Many new high-silica zeolites were crystallized using organic molecules including amines and quaternary ammonium cations in aluminosilicate gels. For example, zeolites Beta (*__BEA__), ZSM-5 (**MFI**), and ZSM-11 (**MEL**) were synthesized using tetraethyl-, tetrapropyl- and tetrabutylammonium cations, respectively [29-31]. These types of zeolites are of high importance for their catalytic applications.

A series of significant studies on the interaction of OSDA molecules and silicate species,

which is strongly related to the role of OSDA, were reported by Burkett and Davis [25-27]. In this series of papers, they examined the role of tetrapropylammonium (TPA) cation as structure-directing agent in silicalite synthesis by solid-state NMR spectroscopy. The schematic illustration is shown in Figure 2. ^{1}H-^{29}Si CP MAS NMR results provide direct evidence to the initial formation of an inorganic-organic composite. TPA molecules in this composite adopt a conformation similar to that in the zeolite product. The initial formation of the inorganic-organic composite is initiated by overlap of the "hydrophobic hydration" spheres of the inorganic and organic components. Aggregation of these composite species occurs accompanied with subsequent release of ordered water to establish favorable van der Waals interactions. Finally, crystal growth occurs through diffusion of the same species to the surface of the growing crystallites to give a layer-by-layer growth mechanism.

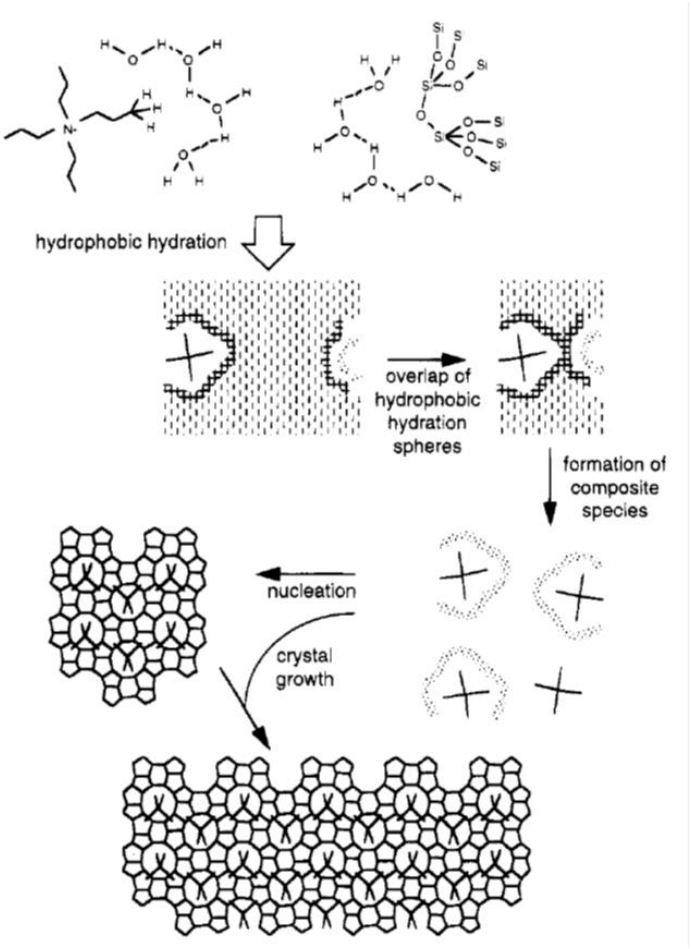

Figure 2 Mechanism for structure-direction of TPA cation in the synthesis of silicalite-1.

The relationship between OSDA properties and the characteristics of cages and pores of formed zeolites have been studied [32]. Continuing in this direction, Gies et al. established a series of properties that has to be fulfilled to be a successful OSDA [33], as summarized below.

1) A molecule must be stable under the hydrothermal synthesis conditions.
2) A molecule should fit into the desired cage.
3) A molecule should form as many Van der Waals contacts as possible with the inner surface of the cage but with the least deformation.
4) A molecule should have only a weak tendency to form complexes with the solvent.
5) A molecule should be rigid because rigid molecules will tend to form clathrasils more easily than flexible molecules.
6) A tendency to form a clathrasil will increase with the increase in the basicity or polarizability of the guest molecule.

Since the middle in 1990s, extensive research effort has been devoted to rationalize the synthesis of a new type of zeolite by using a wide variety of OSDAs. For example, extra-large pore zeolites with 14-memebered ring structures have been synthesized by using relatively large and rigid OSDAs. The first example of the synthesis of extra-large pore zeolite is UTD-1, which was synthesized in the presence of bis(pentamethylcyclopentadienyl)cobalt complex [34]. The second is CIT-5 with **CFI**-type structure reported by Davis et al. [35]. Original CIT-5 was a pure-silica zeolite, but it was also reported later that **CFI**-type aluminosilicate analogue with high hydrothermal stability can be also synthesized [36]. Corma and co-workers in Instituto de Tecnología Química (ITQ) have reported a large number of new types of zeolites including extra-large pore zeolites. They have employed fluoride anion as mineralizing agent instead of traditional alkaline metals. One advantage of the fluoride anion route is that syntheses can be performed at near neutral pH, resulting in the improved stability of OSDA molecules. Another is related to the number of defects

that the formed zeolites have. This is because fluoride anion can balance the positive charge of OSDA cations, whereas the framework of high-silica zeolites prepared in high pH must balance the positive charge. Not only following the fluoride method but also introducing germanium in the synthesis mixture, Corma's group have been successfully synthesized many kinds of extra-large pore zeolites; e.g. ITQ-15 (14- and 12-rings), ITQ-33 (18-, 10-, and 10-rings), ITQ-40 (16-, 15-, and 15-rings) and ITQ-44 (18-, 12-, and 12-rings) [37-40] and many other successful examples are shown below.

OSDA molecules involved in the synthesis enable innovative, unique zeolite frameworks and tunable chemical compositions, which may have significant implications in relevant chemical processes, surely including catalysis.

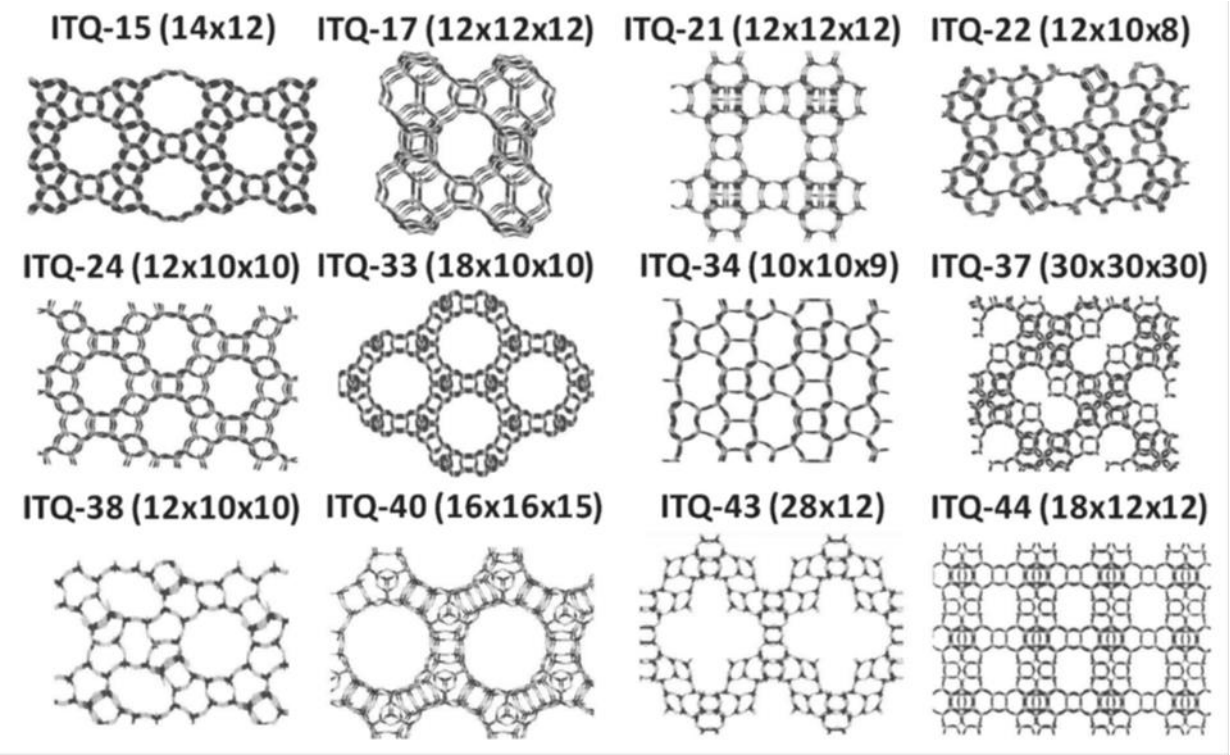

Figure 3 New types of germanosilicates synthesized at ITQ.

1-2-3 OSDA-free synthesis of zeolites

In early days of zeolite synthesis, limited types of zeolites such as A, X, Y, L, mordenite, were hydrothermally synthesized from aluminosilicate gels. Later a number of zeolites with new types of topologies have been successfully synthesized by employing OSDAs. Those successful syntheses include some industrially important zeolites with high-silica compositions; for example, ZSM-5, ZSM-12, ZSM-22, MCM-22, SSZ-13, and Beta. Now, reduction of manufacturing cost and environmental risk in the design and synthesis of zeolites is strongly desired for industrial application.

The elimination of OSDA in the final solid usually requires high temperature combustion that destroys this high-cost component. Davis et al. developed a new methodology that can completely recycle the OSDAs (Figure 4) in the synthesis of ZSM-5 [41]. These organic molecules can be disassembled in the zeolite pore after crystallization and the fragments can be removed from the zeolite pores, followed by the reassembly and reuse. With this methodology, several types of zeolites like ZSM-5, ZSM-11, and ZSM-12 were successfully synthesized [42,43].

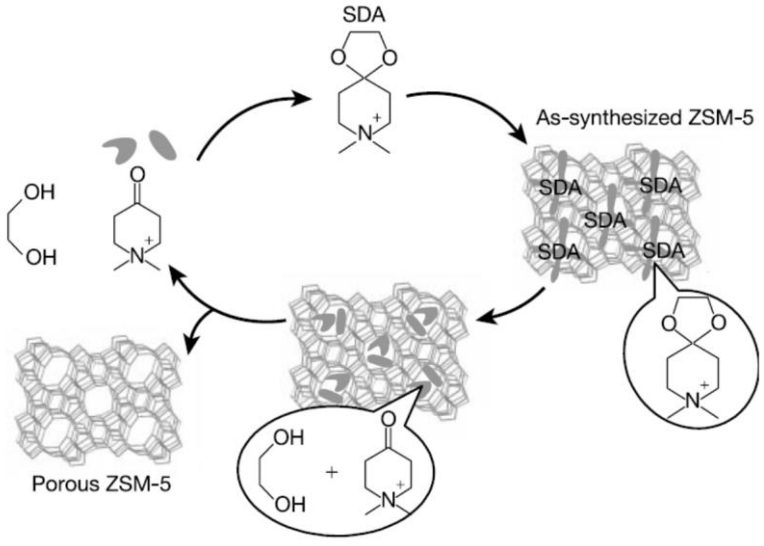

Figure 4 Synthesis of ZSM-5 with the combustion-free OSDAs.

Another improved methodology for synthesis of zeolites that have conventionally been synthesized by using OSDAs emerges. It is very simple, that is OSDA-free synthesis of zeolites. For example ZSM-5 is typically synthesized by employing TPA cation as OSDA, but it can be actually synthesized without using any OSDAs. In fact, the first series of publications to demonstrate the OSDA-free synthesis of well crystallized ZSM-5 was presented by Grose and Flanigen in 1970s [44,45]. Later, Shiralkar and Clearfield investigated the compositional constraints and optimized the synthesis conditions for the OSDA-free synthesis of ZSM-5 [46].

Recently there emerges a new method for the OSDA-free synthesis of zeolites. In this method, zeolites were hydrothermally synthesized from (metallo)aluminosilicate gel containing alkali metal cations with the assistance of seed crystal, which is therefore, called “seed-directed” or “seed-assisted” OSDA-free synthesis. By employing this method, an increasing number of zeolites has been successfully synthesized; for example, ECR-1 [47], ZSM-34 [48], Beta [49-54], ZSM-5 small crystal [55,56], RUB-13 [57,58], ZSM-12 [59,60], high-silica ferrierite [61], Levyne [62], and Fe-Beta [63].

1-3 Dehydration of saccharides to furfurals

1-3-1 5-Hydroxymethylfurfural (HMF)

There have been already a considerable range of chemical building blocks derived from renewable resources. One of them, 5-hydroxymethylfurfural, abbreviated as HMF, plays an important role, because it can be obtained not only from fructose but also (more recently) from glucose as well as directly from cellulose as shown in Figure 5 [64].

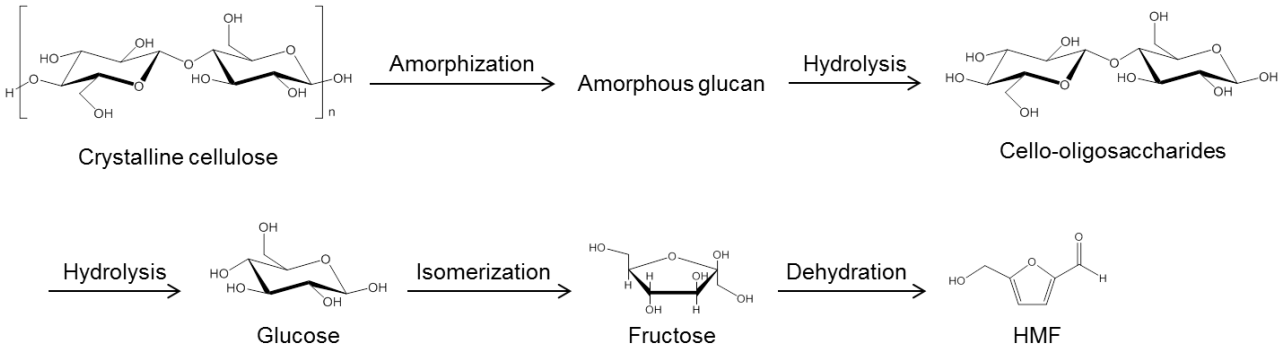

Figure 5 Conversion of cellulose to HMF via a multi-step reaction.

HMF is a very important building block for a wide range of chemical products. Particularly, HMF can be a potential precursor for the production many types of furan derivatives (Figure 6). Its structural motifs present in HMF, namely furan, primary hydroxyl and formyl functionalities, allow synthetic transformation to other target molecules [8,9]. Some examples of applications of HMF are shown in the following sentences.

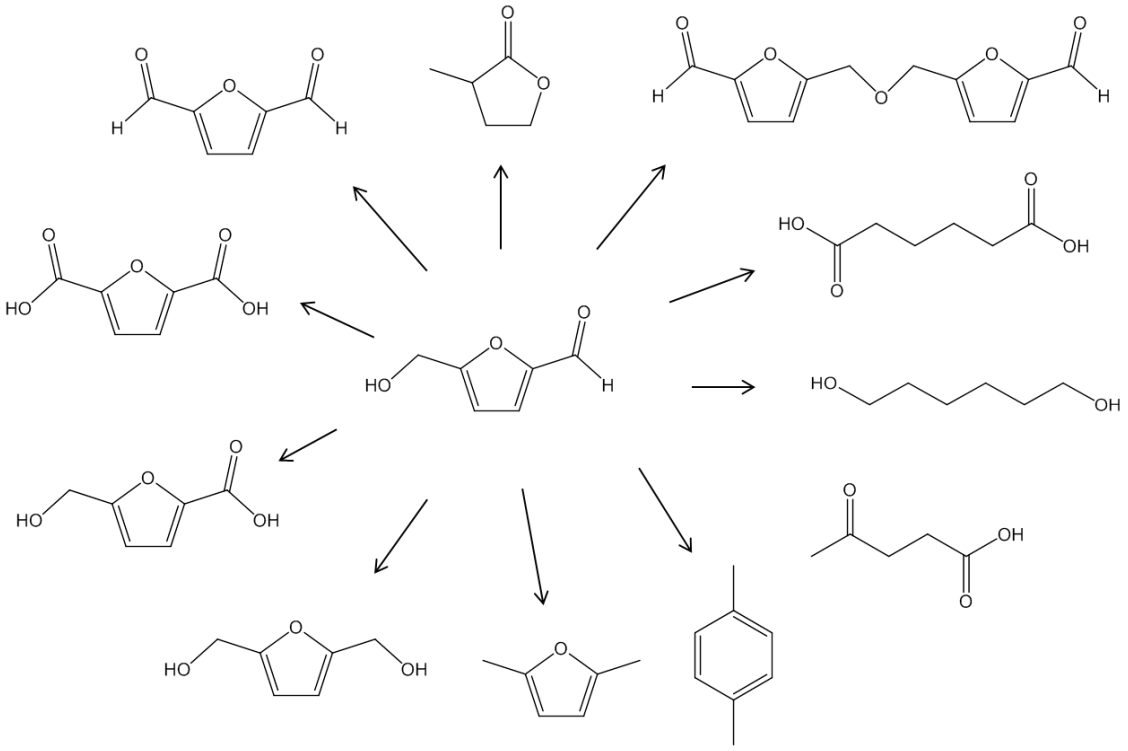

Figure 6 HMF as plat-form material transformed to various derivatives.

The most important molecule that can be derived from HMF is 2,5-furandicarboxylic acid (FDCA). It can be obtained *via* the oxidation of HMF. FDCA was identified by the US DOE to be a key bio-based platform chemical [6,7]. It can be utilized in a wide range of applications, but the application as an alternative to terephthalic acid is the most important. It can serve as a potential bio-renewable monomer for a widely used component in various polyesters such as polyethyleneterephthalate and polybutyleneterephthalate. Several oxidation methods have been described in the literature. The oxidation reaction was achieved with several different stoichiometric oxidants like N_2O_4, HNO_3 and $KMnO_4$ [65]. The catalyst which is currently used for terephthalic acid production (Co/Mn/Br) was used for the oxidation under high pressure of air (~70 bar) [66,67]. Heterogeneous catalysts have been also effective in the oxidation HMF to FDCA with molecular oxygen. Supported platinum catalysts were first used in the presence of base, resulting in near quantitative FDCA yield [68]. Gorbanev *et al.* demonstrated that Au/TiO_2 was able to oxidize HMF into FDCA in 71% yield at near room temperature [69]. Casanova et al. showed that Au/CeO_2 was

more active and selective [70]. Davis *et al.* compared a number of different catalysts and found that Pt/C and Pd/C oxidized HMF to FDCA an order of magnitude faster than Au/C or Au/TiO_2 [71]. Recently, Gupta *et al.* reported the base free oxidation over gold catalysts supported on hydrotalcite and achieved ~100 % yield [72].

There are several examples in the literature for the selective oxidation of the formyl group of HMF to 5-hydroxylmethyl-2-furancarboxylic acid (HMFCA) by using silver oxide [73] or mixture of silver and copper(II) oxides [74] under basic conditions. Supported gold catalysts were reported to be promising oxidation catalysts for the selective production of HMFCA. Gorbanev *et al.* reported the formation of HMFCA as an intermediate product during the aerobic oxidation of HMF to 2,5-furandicarboxylic acid (FDCA) with Au/TiO_2 catalyst in basic aqueous solution at room temperature [69]. Casanova *et al.* also observed the formation of HMFCA as an intermediate product during gold-nanoparticle-catalyzed aerobic oxidation of HMF. They described that selective oxidation to HMFCA took place at 25 ◦C after 4 h and reported 100% yield [75]. Very recently, Davis *et al.* described 92–93% selectivity towards HMFCA with 100% conversion of HMF promoted by Au/C and Au/TiO_2 in basic conditions [71].

Another interesting material derived from HMF is 2,5-dimethylfuran (DMF). DMF is a very promising liquid fuel in the future, with a high energy density, 31.5 MJ/L, which is similar to that of gasoline (35.0 MJ/L), and is 40% higher than that of ethanol (23.0 MJ/L) [76,77]. Moreover, DMF (bp: 92-94 ºC) is less volatile than ethanol (bp: 78 ºC) and is immiscible with water, so that it is especially suitable to be used as a transportation fuel. DMF was obtained with 71% yield by vapor phase hydrogenolysis of 10 wt% 5-HMF in 1-butanol solution in a flow reactor loaded with a Cu-Ru/C catalyst [77]. 95% yield of DMF was obtained by heating a solution of 5-HMF in refluxing tetrahydrofuran in the presence of formic acid, H_2SO_4, and Pd/C catalyst [78]. Recently, it has been reported that *para*-xylene, which is the precursor for terephthalic acid, can be produced with 75 % selectivity from DMF through Diels-Alder type cycloaddition reaction with ethylene over Y zeolite [79].

1-3-2 Dehydration of fructose to HMF

The dehydration of D-fructose can be catalyzed generally by protonic acids [80,81]. Nearly one hundred inorganic and organic acidic compounds have been positively identified as catalysts for the synthesis of HMF. The most commonly used inexpensive acids have been H_2SO_4, H_3PO_4 and HCl [82-84]. Antal *et al.* reported the dehydration of d-fructose with H_2SO_4 as catalyst in sub-critical water at 250 ºC and attained 53 % yield of HMF [85]. A biphasic reaction system was reported by Dumesic *et al.* [86]; in this process, fructose is dehydrated to HMF in HCl aqueous solution containing poly(1-vinyl-2-pyrrolidinone) or dimethyl sulfoxide. This biphasic system suppresses the undesired side reactions. Furthermore, the produced HMF is continuously extracted into the organic solvent (Figure 7). These advantages enables as high as 82 % selectivity at 87 % conversion.

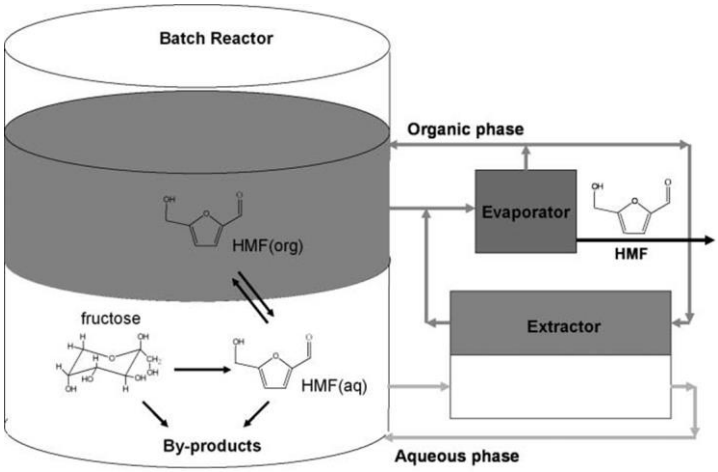

Figure 7 Bi-phasic reaction system proposed by Dumesic *et al.*

The dehydration of fructose to HMF can also be catalyzed by many types of heterogeneous catalysts including ion exchange resins [87-89], metal phosphates [90,91], metal oxides [92,93] and zeolites [94,95]. Extensive research effort has been devoted to application of ion-exchange resins for the dehydration reaction. Nakamura *et al.* investigated a strongly acidic ion-exchange resin in D-fructose dehydration and Diaion PK-216 resin was reported to be an efficient catalyst for the

dehydration and 90% yield of 5-HMF was obtained [87]. Further investigations by Chheda and Dumesic reported very good yields of HMF from fructose by using the Diaion PK216 resin as catalyst in the water-MIBK biphasic system [88]. Recently, Qi et al. used an acetone–water reaction medium and got a yield of 5-HMF as high as 73 % with 94 % fructose conversion by microwave heating at 150 ºC with the presence of a cationic exchange resin (Dowex50wx8-100) catalyst [89]. Vanadium phosphate and niobium phosphate were reported be good catalysts for the dehydration of fructose in water [90,91]. Watanabe *et al.* examined the production of 5-HMF from fructose catalyzed by TiO_2 [92] and ZrO_2 [93] under microwave irradiation. In the case of TiO_2, the yield of HMF reached 38 % with fructose conversion of 84 % at 200 ºC after 5min. Moreau et al. studied the dehydration of fructose in the presence of H-mordenite and achieved 70 % yield of HMF at 93 % conversion of fructose [94,95].

1-3-3 Production of HMF from glucose

Glucose is the most abundant building block in renewable biomass resources, which constitutes cellulose, hemicellulose and starch in nature. Because glucose is cheap and available in a large scale, it has been regarded as promising “plat-form” raw material for manufacturing bio-based chemical products. Therefore, increasing research interest has been paid to utilization of glucose including conversion to HMF.

H_2SO_4 and H_3PO_4 were used as representative homogeneous acid catalysts in the transformation of glucose to HMF in water [96,97]. However, HMF yields obtained in these systems were less than 5 %. Because glucose is more stable and less reactive than fructose, severe conditions are necessary for conversion of glucose. HMF is, unfortunately, unstable under such conditions and subsequently consumed, leading to the low yields. This problem can be avoided by the biphasic reaction system and HMF yield was remarkably improved; 53 % yield of HMF was achieved in HCl *aq* containing DMSO in the combination with MIBK/2-butanol as extracting solvent [98]. Heteropoly acid, $Ag_3PW_{12}O_{40}$ in water combined with MIBK showed 85 % selectivity

to HMF at 90 % conversion of glucose at 130 ºC for 4 h [99].

Although the dehydration of fructose has been extensively investigated by many researchers and many excellent results have been achieved as seen in the preceding section, it is much more difficult to transform glucose to HMF, though it would be preferable to develop a process using glucose as feedstock. Recently, Huang *et al.* reported a breakthrough to improve the HMF yield [100]. They used a combination of isomerase enzyme and HCl *aq* as catalysts. In this system, glucose is isomerized to fructose catalyzed by the enzyme. Thus produced fructose was dehydrated to HMF in HCl *aq*/1-butanol biphasic solvent to achieve 63 % yield of HMF based on glucose. Since it has been found that fructose is readily dehydrated to HMF, such a tandem reaction system combining the isomerization of glucose with the subsequent dehydration of fructose to HMF has been a promising reaction strategy. Following this report, a wide variety of combinations were reported. For example, the combination of metal salts such as $AlCl_3$ and HCl aq showed 70 % selectivity to HMF at 88 % conversion of glucose with 2-*sec*-butylphenol as extracting solvent [101]. Herein, $AlCl_3$ as water-compatible Lewis acid promoted the isomerization of glucose to fructose.

Ionic liquids, particularly imidazolium salts were found to be effective solvents (in some cases, also as catalysts). Zhao *et al.* first reported conversion of glucose to HMF with $CrCl_2$ in 1-ethyl-3-methylimidazolium chloride (denoted as [EMIm]Cl) solvent and achieved 72 % selectivity to HMF at 94 % conversion of glucose[102]. Chromium chlorides in ionic liquids in combination with N-heterocyclic carbene ligands showed better performance, 81 % yield of HMF [103]. Lima *et al.* used $CrCl_3$ in [BMIm]Cl and toluene mixture to obtain 91% HMF yield with 100 % selectivity after 4 h at 100 ºC [104]. Chidambaram and Bell reported that the catalytic performance of 12-molybdophosphoric acid in [EMIm]Cl or [BMIm]Cl was improved by the combination with acetonitrile and this reaction system showed 98 % yield of HMF [105].

Many types of heterogeneous catalysts have been investigated for the transformation of glucose to HMF. Among them, metal oxide catalysts showed outstanding catalytic performances in

the reaction. TiO_2 catalyst showed 39 % conversion of glucose and 27 % yield of HMF in water at 250 ºC [106]. Under the same conditions, TiO_2-ZrO_2 catalyst showed better performance; 44 % conversion and 29 % yield [107]. McNeff et al. described the transformation of a number of carbohydrate feedstocks including glucose in a two-phase flow process. In the reaction system, an aqueous solution containing sugar substrate and organic extraction solvent were pumped into the reactor kept at 160-200 ºC in the presence of a TiO_2 catalyst. Methylisobutylketone (MIBK) was better as extracting solvent than *n*-butanol because *n*-butanol is miscible with water under the reaction conditions. 30 % yield of HMF was achieved from 50 wt% glucose solution at 180 ºC [108]. Recently, it has been reported that the performance of a metal oxide catalyst is remarkably improved by the modification with phosphoric acid. Du et al. reported that niobium oxide modified with phosphoric acid showed 72 % conversion and 49 % yield of HMF in water with *n*-butanol [109]. They also reported TiO_2 modified in the same way showed 70 % conversion and 58 % yield of HMF [110]. Hara et al. reported showed that $Nb_2O5{\cdot}nH_2O$ modified with phosphoric acid as water-tolerant Lewis acid catalyst showed 92 % conversion of glucose and 52 % yield of HMF [111]. Yan et al. studied HMF formation from glucose in DMSO. The highest HMF yield of 48% at 97 % conversion was obtained whenSO_4^{2-}/ZrO_2-Al_2O_3 catalysts with an Al/Zr molar ratio of 1 was used at 20 wt % relative to glucose [112]. Later, they also reported 56 % yield of HMF [113].

Ebitani et al. first introduced the combination of two or higher kinds of catalysts, each of which promotes the different steps in the transformation of glucose to HMF [114,115]. In this paper, they also introduced the concept of the separation of acid and base in a one pot. They used the combination of hydrotalcite as solid base and Amberlyst-15 as solid acid. Solid base and solid acid cannot contact each other, even when contained in the same reactor and therefore, they are not deactivated by neutralization. Hydrotalcite promoted the isomerization of glucose to fructose and Amberlyst resin promoted the subsequent dehydration of fructose to HMF. In DMF solvent, the combination catalyst showed 42 % yield of HMF at 73 % conversion of glucose.

Davis et al. showed a promising breakthrough by using Sn-Beta zeolite for the isomerization

of glucose to fructose [116]; Sn-Beta zeolite as Lewis acid catalyst promoted the reaction in water to give the equilibrium mixture of glucose, fructose and mannose at 110 ºC. The NMR experiment using deuterated glucose revealed that Sn-Beta zeolite catalyzes the glucose isomerization through an intramolecular hydride shift to form fructose [117]. Following these reports, reaction systems pairing Sn-Beta and some types of Brønsted acid catalysts were proposed. For example, the combination of Sn-Beta and HCl acidic solution gave 57 % yield of HMF in water-THF biphasic system [118]. Dumesic et al. employed the combination of Sn-Beta and Amberlyst resins in a monophasic solvent composed of water and THF and achieved excellent results, 63 % yield of HMF [119]. Tsapatsis et al. have combined Sn-Beta with Amberlyst 131 to perform the one-pot formation of glucose to 5-(ethoxymethyl)-furfural in ethanol [120].

As shown above, extensive research effort has been devoted to the transformation of glucose to HMF and some promising results have been reported. However, the performances of heterogeneous catalysts are generally lower than those of homogeneous catalysts. The development of easily available catalyst with higher catalytic performance and environmentally benign reaction system is strongly desired.

1-4 Dehydration of sorbitol to isosorbide

1-4-1 Isosorbide

Sorbitol is a promising material derived from biomass and it is ranked as one of the top 12 important targets from biomass [6,7,10]. Sorbitol is produced industrially (ca. 700,000 tons per year) by catalytic hydrogenation of glucose [121]. Most of the industrial processes rely on batch-wise hydrogenation of glucose derived from starch by using Raney nickel catalysts promoted with electropositive metal atoms such as Mo and Cr and other supported metal catalysts [122,123].

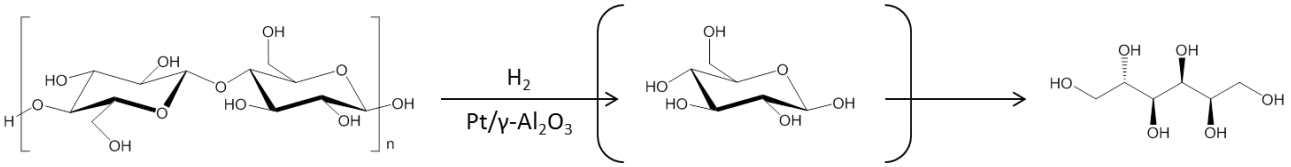

Figure 8 One-pot sorbitol production from cellulose.

In the past decade, however, increasing research effort has been devoted to the production of sorbitol from cellulose as non-food biomass because it is renewable, abundant in the worldwide, available in a large scale, and cheap. In 2006 Fukuoka et al. first reported the hydrogenolysis of cellulose to sorbitol and mannitol over Pt/γ-Al_2O_3 [124]. Later other research groups reported the production of sorbitol from cellulose by using the supported metal catalysts [125-132]. Recently, Schüth et al. reported the two-step process combining mechanocatalytic depolymerization of cellulose and subsequent hydrogenolysis to achieve 91% yield of sorbitol [133].

Isosorbide (1,4:3,6-dianhydro-D-sorbitol) is one of the most important derivatives derived from sorbitol, which is produced through double intramolecular dehydration of sorbitol (Figure 9).

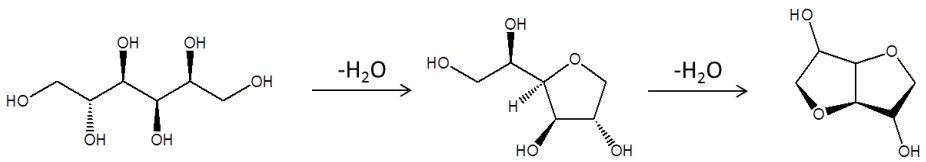

Figure 9 Dehydration of sorbitol to isosorbide

Isosorbide is a V-shaped molecule of two *cis*-fused connected tetrahydrofuran rings with an opening angle of 120 º and secondary hydroxyl groups at C-2 and C-5 positions as shown in Figure 10. Isosorbide has two isomers, isomannide and isoidide. The difference between these three isomers is the configuration of the two hydroxyl groups. Isosorbide has *exo* configuration at C-2 and *endo* at C-5, whereas isomannide has *endo* configuration for both positions, and isoidide has *exo* configuration for both (Figure 11). This difference results in different physical and chemical properties of the isomers such as melting temperature and reactivity [134]. The reactivity of the two hydroxyl groups of isosorbide differs significantly. Nucleophilic character of the hydroxyl oxygen at C-5 is increased by the intramolecular hydrogen bond, which results in higher reactivity than the other hydroxyl oxygen at C-2. However, the substitution reaction with sterically hindered substituents might occur preferentially at C-2 despite its less reactivity because *endo* configuration hinders the approach of the bulky substituents. The two hydroxyl groups of isomannide show significantly lower reactivity than those of isosorbide probably due to strong intramolecular hydrogen bonds. Besides, isomannide is produced from fructose or mannitol, but these compounds are more expensive than glucose and sorbitol. Therefore, isomannide is less attractive for large-scale application. The other isomer, isoidide, shows much higher reactivity than the other two isomers, but its precursor L-idose is a rare sugar, leading to a high cost of L-iditol. Thus isosorbide has higher importance in comparison to the isomers. Therefore, this study deals with the production of isosorbide from sorbitol.

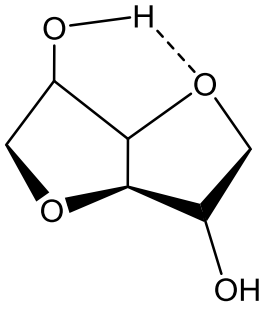

Figure 10 Molecular structure of isosorbide

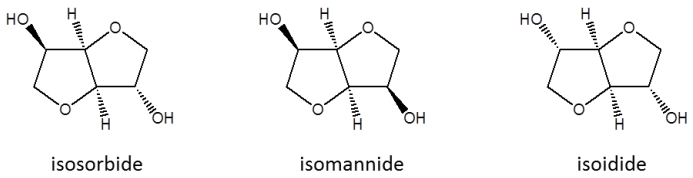

Figure 11 Dianhydrohexitol isomers.

1-4-2 Application of isosorbide

Because of tis high stability and two functional groups, isosorbide has many applications in wide industrial fields. One of the most important applications of isosorbide is in the pharmaceutical field. It can reduce blood pressure for brain tumors, head injuries and glaucoma. It is also the medicine for Ménière's disease and a diuretic agent [5]. Isosorbide mononitrate and dinitrate are medicines for angina pectoris and they are more effective than glycerol trinitrate in several points [135]. Isosorbide dimethyl ether is used commercially available, non-toxic, versatile, pharmaceutical solvent.

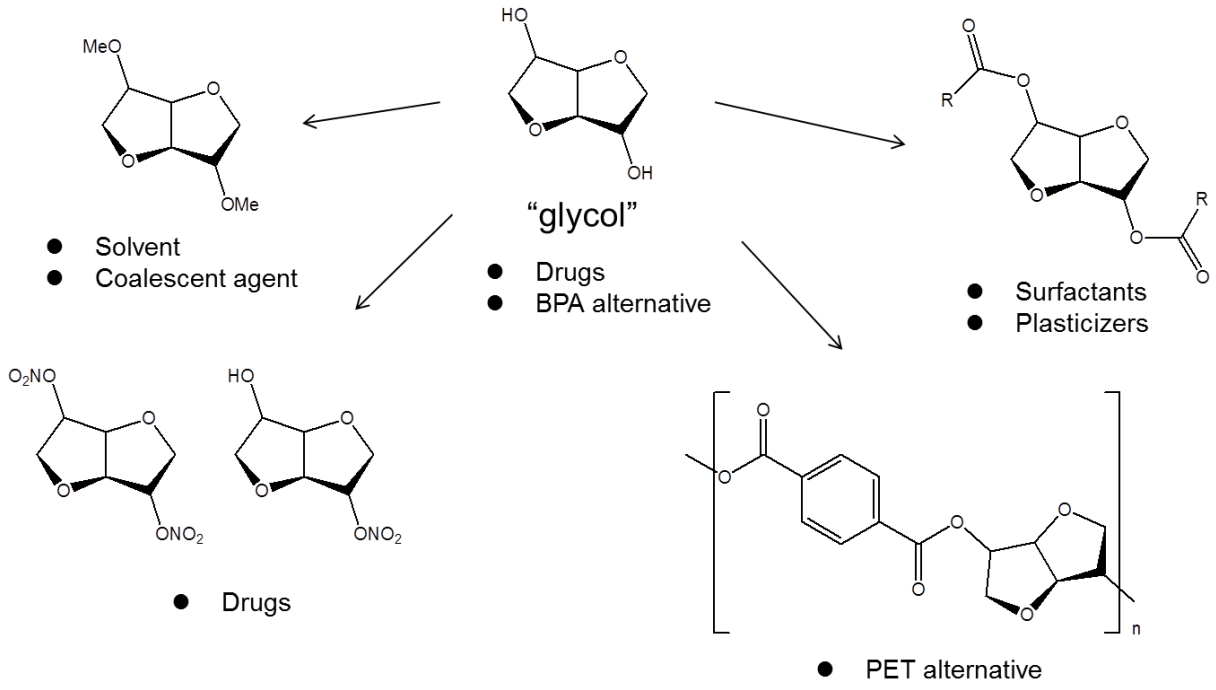

Figure 12 Isosorbide derivatives and their applications

Low-melting or room-temperature liquid isosorbide derivatives can be obtained by breaking the intra- and/or intermolecular hydrogen bonds. Etherification or esterification of the hydroxyl group(s) is an easy method for attaining that purpose. Sorbitan, which is an intermediate for the production of isosorbide, is commercially used as raw material in the production of surfactants. Unfortunately, isosorbide ester and ether are not commercially applied as surfactant, but they are

used as replacement of plasticizers. Roquette has commercialized the isosorbide diester POLYSORB ID37 to replace phthalates in the production of soft PVC polymers [136,137]. Recently, short-chain aliphatic isosorbide ethers as hydrotropes or coalescents have been investigated [138,139]. In these publications etherification of isosorbide was performed by Williamson ether synthesis using organohalides as reactants. New possible methods for the etherification have been proposed. Sauthier et al. described the use of homogenous palladium catalyst for the production of isosorbide octyl ethers. They observed ~60 % selectivity to diether at 100 % conversion [140]. Recently, Palkovits et al. proposed the etherification of isosorbide with *tert*-butanol over Amberlyst-15. They found a significant solvent effect and dimethyl carbonate is the best. After 6 h of the reaction, the mixtures of the mothers and diether at >90 % yield [141].

Recently, application of isosorbide as plastic monomer has attracted increasing interest and there are excellent reviews summarizing recent advances in the area [142,143]. Thus this section focuses on selected important polymers. Poly-(ethylene-co-isosorbide)terephthalate (PEIT) shows a high glass transition temperature (T_g) up to ~200 ºC by increasing the proportion of isosorbide monomer, while PET has T_g at ~80 ºC. This is advantageous for using the PEIT bottle with hot water filled [144,145]. Similarly, poly(isosorbide oxalate) has a remarkably high T_g (~170 ºC) and good biodegradable properties [146]. Isosorbide as diol monomer is also considered as valuable replacement of bisphenol A (BPA) in the production of epoxy resins and polycarbonates with high functionality [147,148]. Isosorbide diglycidyl ether have been employed as monomer for epoxy resins [147]. Comparative studies showed that thus prepared resins had significantly high tensile and impact strength compared to BPA resins. Poly(isosorbide carbonate), abbreviated as PIC, is a bio-based and harmless plastic that is highly transparent, heat-resistant (T_g, ~175 ºC) and water-tolerant. PIC is a promising alternative to BPA polycarbonate [149]. Teijin Chemicals established a mass production technology of PIC in 2011 and Mitsubishi Chemical started a 5000 t/year-scale plant for PIC in 2012. Roquette constructed a plant for themanufacture of polymer-grade isosorbide in 2007 and the current capacity is about 5000 t/year. Its feedstock is

starch mainly from corn and wheat at this moment, and the substrate is converted to isosorbide *via* the hydrolysis to glucose by enzymes, hydrogenation to sorbitol by a Ni catalyst and dehydration to the product [5].

1-4-3 Production of isosorbide from sorbitol and other precursors

Dehydration of sorbitol to isosorbide has been investigated by many researchers and many types of acid catalysts including homogeneous [150-159] and heterogeneous catalysts [160-169] have been used. Huchette and Flèche reported that sorbitol was dehydrated to isosorbide in 77 % yield by using sulfuric acid as catalyst *in vacuo* at 135 ºC for 15 h [152]. This process achieved the high yield, but requires neutralization and decoloration of the dark-colored mixture. Later, Yamaguchi et al. reported the dehydration of sorbitol in water at high temperature without any acid catalysts added [155]. Recently, Makkee et al. reported the production of isosorbide from cellulose in molten salt hydrate medium and they achieved 95 % yield from cellulose and glucose [156,157]. Heteropoly acids were also employed for the dehydration reaction by some groups [158] Sels et al. reported the direct conversion of cellulose to isosorbide using heteropoly acids [159]. For industrial application, a heterogeneous system has advantages in many points. Therefore, many types of heterogeneous catalysts have been explored; for example, modified metal oxides [160-164], metal phosphates [165], supported heteropoly acids [166], supported metals [167,168], and ion-exchange resin [152,169]. Among those solid acid catalysts, sulfated titania catalyst exhibited the best performance, ~75 % yield of isosorbide under reduced pressure (0.3 bar) [162].

Considerable effort has been devoted to the development of catalyst and reaction systems for isosorbide production from cellulosic biomass. Nevertheless, to establish a new large-scale process, several challenges such as energy efficiency, a kind of feedstock, inexpensive solvent, catalytic activity and selectivity, and product separation must be solved. This study approaches such problems from the development of a heterogeneous catalyst with high performance.

References

1. Y. Román-Leshkov, J. N. Chheda, J. A. Dumesic, Science, 312 (2006) 1933-1937.
2. A. Corma, S. Iborra, A. Velty, Chem. Rev. 107 (2007) 2411-2502.
3. J. N. Chheda, G. W. Huber, J. A. Dumesic, Angew. Chem. Int. Ed. 46 (2007) 7164-7183.
4. P. Gallezot, Chem. Soc. Rev. 41 (2012) 1538-1558.
5. H. Kobayashi, A. Fukuoka, Green Chem. 15 (2013) 1740-1763.
6. T. Werpy, G. Petersen, A. Aden, J. Bozell, J. Holladay, A. Manheim, D. Eliot, L. Lasure, S. Jones, *Top Value Added Chemicals from Biomass;* U.S. Department of Energy: Oak Ridge, TN, 2004; vol. 1.
7. J. J. Bozell, G. R. Petersen, Green Chem. 12 (2010) 539-554.
8. A. A. Rosatella, S. P. Simeonov, R. F. M. Frade, C. A. M. Afonso, Green Chem. 13 (2011) 754-793.
9. R.-J. van Putten, J. C. van der Waal, E. de Jong, C. B. Rasrendra, H. J. Heeres, J. G. de Vries, Chem. Rev. 113 (2013) 1499-1597.
10. J. Zhang, J. Li, S.-B. Wu, Y. Liu, Ind. Eng. Chem. Res. 52 (2013) 11799-11815.
11. M. E. Davis, Nature, 417 (2002) 814-821.
12. M. E. Davis, R. F. Lobo, Chem. Mater. 4 (1992) 756-768.
13. C. S. Cundy, P. A. Cox, Chem. Rev. 103 (2003) 663-701.
14. C. S. Cundy, P. A. Cox, Micropor. Mesopor. Mater. 82 (2005) 1-78.
15. R.M. Barrer, J.W. Baynham, F.W. Bultitude, W.M. Meier, J. Chem. Soc. (1959) 195-208.
16. E.M. Flanigen, D.W. Breck, 137th Meeting of the ACS, Division of Inorganic Chemistry, Cleveland, OH, April 1960, Abstracts, p. 33
17. G.T. Kerr, J. Phys. Chem. 70 (1966) 1047-1050.
18. J. Ciric, J. Colloid Interface Sci. 28 (1968) 315-324.
19. S.P. Zhdanov, in: E.M. Flanigen, L.B. Sand (Eds.), Molecular Sieve Zeolites-I, ACS Adv. Chem. Ser., vol. 101, 1971, p. 20-43.

20. R.M. Barrer, P.J. Denny, J. Chem. Soc. (1961) 971-982.

21. G.T. Kerr, G.T. Kokotailo, J. Am. Chem. Soc. 83 (1961) 4675.

22. E.G. Derouane, S. Detremmerie, Z. Gabelica, N. Blom, Appl. Catal. 1 (1981) 201-224.

23. Z. Gabelica, N. Blom, E.G. Derouane, Appl. Catal. 5(1983) 227-248.

24. C.D. Chang, A.T. Bell, Catal. Lett. 8 (1991) 305-316.

25. S.L. Burkett, M.E. Davis, J. Phys. Chem. 98 (1994) 4647-4653.

26. S.L. Burkett, M.E. Davis, Chem. Mater. 7 (1995) 920-928.

27. S.L. Burkett, M.E. Davis, Chem. Mater. 7 (1995) 1453-1463.

28. Ch. Baerlocher, W. M. Meier, Helv. Chim. Acta. 52 (1969) 1853-1860.

29. R. L. Wadlinger, G. T. Kerr, E. J. Rosinski, U.S. Patent 3308069, 1967.

30. R. J. Argauer, G. R. Landolt, US Patent 3702886, 1972.

31. P. Chu, US Patent 3709979, 1973.

32. R. Lobo, S. I. Zones, M. E. Davis, J. Incl. Phenom. Mol. Rec. 21 (1995) 47-48.

33. H. Gies, B. Marker, Zeolits, 12 (1992) 42-49.

34. C. C. Freyhardt, M. Tsapatis, R. F. Lobo, K. J. Balkus, M. E. Davis, Nature, 381 (1996) 295-298.

35. P. Wagner, M. Yoshikawa, K. Tsuji, M. E. Davis, M. Lovallo, M. Tsapatis, Chem. Commun. (1997) 2179-2180.

36. M. Yoshikawa, P. Wagner, M. Lovallo, K. Tsuji, T. Takewaki, C.-Y. Chen, L. W. Beck, C. Jones, M. Tsapatsis, S. I. Zones, M. E. Davis, J. Phys. Chem. B, 102 (1997) 7139-7147.

37. A. Corma, M. J. Díaz-Cabañas, F. Rey, S. Nicolopoulusa, K. Boulahya, Chem. Commun. (2004) 1356-1357.

38. A. Corma, M. J. Díaz-Cabañas, J. L. Jordá, C. Martínez, M. Moliner, Nature, 443 (2006) 842-845.

39. A. Corma, M. J. Díaz-Cabañas, J. Jiang, M. Afeworki, D. L. Dorset, S. L. Soled, K. G. Strohmaier, Proc. Natl. Acad. Sci. U.S.A. 107 (2010) 13997-14002

40. J. Jiang, J. L. Jordá, M. J. Diaz- Cabañas, J. Yu, A. Corma, Angew. Chem. Int. Ed. 49 (2010) 4986-4988.

41. H. Lee, S. I. Zones, M. E. Davis, Nature, 425 (2003) 385-388.

42. H. Lee, S. I. Zones, M. E. Davis, J. Phys. Chem. B, 109 (2005) 2187-2191.

43. H. Lee, S. I. Zones, M. E. Davis, Micropor. Mesopor. Mater. 88 (2006) 266-274.

44. R. W. Grose, E. M. Flanigen, Belgian Patent (BE) 851066, 1977.

45. R. W. Grose, E. M. Flanigen, U.S. Patent 4257885, 1981.

46. V.P. Shiralkar, A. Clearfield, Zeolites, 9 (1989) 363-370.

47. J. W. Song, L. Dai, Y. Y. Ji, F.-S. Xiao, Chem. Mater. 18 (2006) 2775-2777.

48. Z. F. Wu, J. W. Song, Y. Y. Ji, L. M. Ren, F.-S. Xiao, Chem.Mater. 20 (2008) 357-359.

49. B. Xie, J. W. Song, L. Ren, Y. Ji, J. Li, F.-S. Xiao, Chem. Mater. 20 (2008) 4533-4535.

50. G. Majano, L. Delmotte, V. Valtchev, S. Mintova, Chem. Mater. 21 (2009) 4184-4191.

51. Y. Kamimura, W. Chaikittisilp, K. Itabashi, A. Shimojima, T. Okubo, Chem. Asian J. 5 (2010) 2182-2191.

52. B. Xie, H. Zhang, C. Yang, S. Liu, L. Ren, L. Zhang, X. Meng, B. Yilmaz, U. Müller, F.-S. Xiao, Chem. Commun. 47 (2011) 3945-3947.

53. Y. Kamimura, S. Tanahashi, K. Itabashi, A. Shimojima, T. Okubo, J. Phys. Chem. C, 115 (2011) 744-750.

54. H. Zhang, B. Xie, X. Meng, U. Müller, B. Yilmaz, M. Feyen, S. Maurer, H. Gies, T. Tatsumi, X. Bao, W. Zhang, D. De Vos, F.-S. Xiao, Micropor. Mesopor. Mater.180 (2013) 123-129.

55. G. Majano, A. Darwiche, S. Mintova, V. Valtchev, Ind. Eng. Chem. Res. 48 (2009) 7084-7091.

56. N. Ren, Z.-J. Yang, X.-C. Lv, J. Shi, Y.-H. Zhang, Y. Tang, Micropor. Mesopor. Mater. 131 (2010) 103-114.

57. T. Yokoi, M. Yoshioka, H. Imai, T. Tatsumi, Angew. Chem. Int. Ed. 48 (2009) 9884-9887.

58. M. Yoshioka, T. Yokoi, M. Liu, H. Imai, S. Inagaki, T. Tatsumi, Micropor. Mesopor. Mater.

153 (2012) 70-78.

59. K. Iyoki, Y. Kamimura, K. Itabashi, A. Shimojima, T. Okubo, Chem. Lett. 39 (2010) 730-731.

60. Y. Kamimura, K. Itabashi, T. Okubo, Micropor. Mesopor. Mater. 147 (2012) 149-156.

61. H. Zhang, Q. Guo, L. Ren, C. Yang, L. Zhu, X. Meng, C. Li, F.-S. Xiao, J. Mater. Chem. 21 (2011) 9494-9497.

62. H. Zhang, C. Yang, L. Zhu, X. Meng, B. Yilmaz, U. Müller, M. Feyen, F.-S. Xiao, Micropor. Mesopor. Mater. 155 (2012) 1-7.

63. H. Zhang, L. Chu, Q. Xiao, L. Zhu, C. Yang, X. Meng, F.-S. Xiao, J. Mater. Chem. A, 1 (2013) 3254-3257.

64. X. Tong, Y. Ma, Y. Li, Appl. Catal. A: Gen. 385 (2010) 1-13.

65. T. Miura, H. Kakinuma, T. Kawano, H. Matsuhisa, U.S. Patent 7411078, 2008.

66. W. Partenheimer, V. V. Grushin, Adv. Synth. Catal. 343 (2001) 102-111.

67. K. Yutaka, T. Miura, S. Eritate, T. Komuro, U.S. Patent 0092720, 2011.

68. P. Vinke, W. V. Poel, H. van Bekkum, Stud. Surf. Sci. Catal. 59 (1991) 385-394.

69. Y. Y. Gorbanev, S. K. Klitgaard, J. M. Woodley, C. H. Christensen, A. Riisager, ChemSusChem, 2 (2009) 672-675.

70. O. Casanova, S. Iborra, A. Corma, J. Catal. 265 (2009) 109-116.

71. S. E. Davis, L. R. Houkb, E. C. Tamargoa, A. K. Datyeb and R. J. Davis, Catal. Today, 160 (2011) 55-60.

72. N. K. Gupta, S. Nishimura, A. Takagaki, K. Ebitani, Green Chem. 13 (2011) 824-827.

73. T. Elhajj, A. Masroua, J. C. Martin and G. Descotes, Bull. Soc. Chim. Fr. 1987, 855-860.

74. B. W. Lew, Chem. Abstr. 68 (1968) P49434n.

75. O. Casanova, S. Iborra, A. Corma, ChemSusChem, 2 (2009) 1138-1144.

76. H.B. Nisbet, J. Inst. Petrol. 32 (1946) 162–166.

77. Y. Roman-Leshkov, C.J. Barrett, Z.Y. Liu, J.A. Dumesic, Nature, 447 (2007) 982-985.

78. T. Thananatthanachon, T. B. Rauchfuss, Angew. Chem. Int. Ed. 49 (2010) 6616-6618.

79. C. L. Williams, C.-C. Chang, P. Do, N. Nikbin, S. Caratzoulas, D. G. Vlachos, R. F. Lobo, W. Fan, P. J. Dauenhauer, ACS Catal. 2 (2012) 935-939.

80. C.J. Moye, Rev. Pure Appl. Chem. 14 (1964) 161-170.

81. M.S. Feather, J.F. Harris, Adv. Carbohydr. Chem. 28 (1973) 161-224.

82. D.W. Harris, M.S. Feather, J. Org. Chem. 39 (1974) 724-725.

83. B.F.M. Kuster, H.S. van der Baan, Carbohydr. Res. 54 (1977) 165-176.

84. C.F. Moye, R.J. Goldsack, J. Appl. Chem. 16 (1966) 206-208.

85. M. J. Antal, W. S. L. Mok, G. N. Richards, Carbohydr. Res. 199 (1990) 91-109.

86. Y. Román-Leshkov, J. N. Chheda, J. A. Dumesic, Science, 312 (2006) 1933-1937.

87. Y. Nakamura, S. Morikawa, Bull. Chem. Soc. Jpn. 53 (1980) 3705-3706.

88. J.N. Chheda, J.A. Dumesic, Catal. Today 123 (2007) 59-70.

89. X. Qi, M. Watanabe, T.M. Aida, R.L. Smith Jr., Green Chem. 10 (2008) 799-805.

90. C. Carlini, P. Patrono, A.M.R. Galletti, G. Sbrana, Appl. Catal. A: Gen. 275 (2004) 111-118.

91. F. Benvenuti, C. Carlini, P. Patrono, A.M. Raspolli Galletti, G. Sbrana, M.A. Massucci, P. Galli, Appl. Catal. A: Gen. 193 (2000) 147-153.

92. M. Watanabe, Y. Aizawa, T. Iida, R. Nishimura, H. Inomata, Appl. Catal. A: Gen. 295 (2005) 150-156.

93. X. Qi, M. Watanabe, T.M. Aida, R.L. Smith Jr., Catal. Commun. 9 (2008) 2244-2249.

94. C. Moreau, R. Durand, C. Pourcheron, S. Razigade, Ind. Crops Prod. 3 (1994) 85-90.

95. C. Moreau, R. Durand, S. Razigade, J. Duhamet, P. Faugeras, P. Rivalier, P. Ros, G. Avignon, Appl. Catal. A: Gen. 145 (1996) 211-224.

96. M. Watanabe, Y. Aizawa, T. Iida, T. M. Aida, C. Levy, K. Sue, H. Inomata, Carbohydr. Res. 340 (2005) 1925-1930.

97. N. H. Smith, U.S. Patent 3118912, 1960.

98. J. N. Chheda, Y. Román-Leshkov, J. A. Dumesic, Green Chem. 9 (2007) 342-350.

99. C. Fan, H. Guan, H. Zhang, J. Wang, S. Wang, X. Wang, Biomass Bioenergy 35 (2011) 2659-2665.

100. R. Huang, W. Qi, R. Su, Z. He, Chem. Commun. 46 (2010) 1115-1117.

101. Y. J. Pagán-Torres, T. Wang, J. M. R. Gallo, B. H. Shanks, J. A. Dumesic, ACS Catal. 2 (2012) 230-234.

102. H. Zhao, J. E. Holladay, H. Brown, Z. C. Zhang, Science, 316 (2007) 1597-1600.

103. G. Yong, Y. Zhang, J. Y. Ying, Angew. Chem. Int. Ed. 47 (2008) 9345-9348.

104. S. Lima, P. Neves, M. M. Antunes, M. Pillinger, N. Ignatyev, A. A. Valente, Appl. Catal. A: Gen. 363 (2009) 93-99.

105. M. Chidambaram, A. T. Bell, Green Chem. 12 (2010) 1253-1262.

106. A. Chareonlimkun, V. Champreda, A. Shotipruk, N. Laosiripojana, Fuels, 89 (2010) 2873-2880.

107. A. Chareonlimkun, V. Champreda, A. Shotipruk, N. Laosiripojana, Bioresour. Technol. 101 (2010) 4179-4186.

108. C. V. McNeff, D. T. Nowlana, L. C. McNeff, B. Yana, R. L. Fedie, Appl. Catal. A: Gen. 384 (2010) 65-69.

109. F. Yang, Q. Liu, X. Bai, Y. Du, Bioresour. Technol. 102 (2011) 3424-3429.

110. F. Yang, Q. Liu, M. Yue, X. Bai, Y. Du, Chem. Commun. 47 (2011) 4469-4471.

111. K. Nakajima, Y. Baba, R. Noma, M. Kitano, J. N. Kondo, S. Hayashi, M. Hara, J. Am. Chem. Soc. 133 (2011) 4224-4227.

112. H. Yan, Y. Yang, D. Tong, X. Xiang, C. Hu, Catal. Commun. 10 (2009) 1558-1563.

113. Y. Yang, X. Xiang, D. Tong, C. Hu M. M. Abu-Omar, Bioresour. Technol.116 (2012) 302-306.

114. A. Takagaki, M. Ohara, S. Nishimura, K. Ebitani, Chem. Commun. (2009) 6276-6278.

115. M. Ohara, A. Takagaki, S. Nishimura, K. Ebitani, Appl. Catal. A: Gen. 383 (2010) 149-155.

116. M. Moliner, Y. Román-Leshkov, M. E. Davis, Proc. Natl. Acad. Sci. USA, 107 (2010)

6164-6168.

117. Y. Román-Leshkov, M. Moliner, J. A. Labinger, M. E. Davis, Angew. Chem. Int. Ed. 49 (2010) 8954-8957.

118. E. Nikolla, Y. Román-Leshkov, M. Moliner, M. E. Davis, ACS Catal. 1 (2011) 408-410.

119. J. M. R. Gallo, D. M. Alonso, M. A. Mellmer, J. A. Dumesic, Green Chem. 15 (2013) 85-90.

120. C. M. Lew, N. Rajabbeigi and M. Tsapatsis, Ind. Eng. Chem. Res., 51 (2012) 5364-5366.

121. P. J. Cerino, G. Fleche, P. Gallezot, Stud. Surf. Sci. Catal. 59 (1991) 231-236.

122. A P. Gallezot, P. Cérino, B. Blanc, G. Flèche and P. Fuertes, J. Catal. 146 (1994) 93-102.

123. B. W. Hoffer, E. Crezee, P. R. M. Mooijman, A. D. van Langeveld, F. Kapteijn, J. A. Moulijn, Catal. Today, 79/80 (2003) 35-41.

124. A. Fukuoka, P. L. Dhepe, Angew. Chem., Int. Ed. 45 (2006) 5161-5163.

125. W. Deng, X. Tan, W. Fang, Q. Zhang, Y. Wang, Catal. Lett. 133 (2009) 167-174.

126. J. Geboers, S. Van de Vyver, K. Carpentier, K. de Blochouse, P. A. Jacobs, B. F. Sels, Chem. Commun. 46 (2010) 3577-3579.

127. R. Palkovits, K. Tajvidi, A. M. Ruppertc, J. Procelewska, Chem. Commun. 47 (2011) 576-578.

128. H. Kobayashi, Y. Ito, T. Komanoya, Y. Hosaka, P. L. Dhepe, K. Kasai, K. Hara, A. Fukuoka, Green Chem. 13 (2011) 326-333.

129. J. Geboers, S. Van de Vyver, K. Carpentier, P. A. Jacobs, B. F. Sels, Chem. Commun. 47 (2011) 5590-5592.

130. J. W. Han, H. Lee, Catal. Commun. 19 (2012) 115-118.

131. P. Yang, H. Kobayashi, K. Hara, A. Fukuoka, ChemSusChem, 5 (2012) 920-926.

132. S. Van de Vyver, J. Geboers, W. Schutyser, M. Dusselier, P. Eloy, E. Dornez, J. W. Seo, C. M. Courtin, E. M. Gaigneaux, P. A. Jacobs, B. F. Sels, ChemSusChem, 5 (2012) 1549-1558.

133. J. Hilgert, N. Meine, R. Rinaldi and F. Schüth, Energy Environ. Sci. 6 (2013) 92-96.

134. M. Rose, R. Palkovits, ChemSusChem, 5 (2012) 167-176.

135. J. D. Parker, J. O. Parker, N. Engl. J. Med. 338 (1998) 520-531.

136. H. Luitjes, J. Jansen, WO 9945060, 1999.

137. D. S. Van Es, A. E. Frissen, H. Luitjes, WO 0183488A1, 2001.

138. M. Durand, A. Mouret, V. Molinier, T. Féron, J.-M. Aubry, Fuel, 89 (2010) 2729-2734.

139. M. Durand, V. Molinier, T. Féron, J.-M. Aubry, Prog. Org. Coat. 69 (2010) 344-351.

140. J. Lai, S. Bigot, M. Sauthier, V. Molinier, I. Suisse, Y. Castanet, J.-M. Aubry, A. Morteux, ChemSusChem, 4 (2011) 1104-1111.

141. M. Rose, K. Thenert, R. Pfützenreuter, R, Palkovits, Catal. Sci. Technol. 3 (2013) 938-941.

142. H. R. Kricheldorf, J. Macromol. Sci., Rev. Macromol. Chem. Phys. C37 (1997) 599-631.

143. F. Fenouillot, A. Rousseau, G. Colomines, R. Saint-Loup, J.-P. Pascault, Prog. Polym. Sci. 35 (2010) 578-622.

144. R. M. Gohil, Polym. Eng. Sci. 49 (2009) 544-553.

145. F. Fenouillot, A. Rousseau, G. Colomines, R. Saint-Loup, J.-P. Pascault, Prog. Polym. Sci., 35 (2010) 578–622.

146. K. Kurachi, M. Shimokawa, JP Pat, 4692057, 2011.

147. X. Feng, A. J. East, W. B. Hammond, Y. Zhang, M. Jaffe, Polym. Adv. Technol. 22 (2011) 139-150.

148. M. Chrysanthos, J. Galy, J.-P. Pascault, Polymer, 52 (2011) 3611-3620.

149. A. Ono, K. Toyohara, H. Minematsu, Y. Kageyama, US Pat, 7365148, 2008.

150. J. C. Goodwin, J. E. Hogde, D. Weisleder, Carbohydr. Res. 79 (1980) 133-141.

151. K. Bock, C. Pedersen, H. Thøgersen, Acta. Chem. Scand. B, 35 (1981) 441-449.

152. G. Flèche, M. Huchette, Starch, 38 (1986) 26-30.

153. J. Defaye, A. Gadelle, C. Pedersen, Carbohydr. Res. 205 (1990) 191-202.

154. L. Dosen-Micovic and Z. Cekovic, J. Phys. Org. Chem. 11 (1998) 887-894.

155. A. Yamaguchi, N. Hiyoshi, O. Sato, M. Shirai, Green Chem. 13 (2011) 873-881.

156. R. Menegassi de Almeida, J. Li, C. Nedelof, P. O'Connor, M. Makkee, J. A. Moujin, ChemSusChem, 3 (2010) 325-328.

157. J. Li, A. Spina, J. A. Moujin, M. Makkee, Catal. Sci. Technol. 3 (2013) 1540-1546.

158. J. U. Oltmanns, S. Palkovits, R. Palkovits, Appl. Catal. A: Gen. 456 (2013) 168-173.

159. B. O. de Beek, J. Geboers, S. Van der Vyver, J. Van Lishout, J. Snelders, W. J. J. Huijgen, C. M. Courtin, P. A. Jacobs, B. F. Sels, ChemSusChem, 6 (2013) 199-208.

160. Z.-C. Tang, D. H. Yu, P. Sun, H. Li, H. Huang, Bull. Korean Chem. Soc. 31 (2010) 3679-3683.

161. J. Xia, D. Yu, Y. Hu, B. Zou, P. Sun, H. Li, H. Huang, Catal. Comm. 12 (2011) 544-547.

162. N. A. Khan, D. K. Mishra, I. Ahmed, J. W. Yoon, J.-S. Hwang, S. H. Jhung, Appl. Catal. A: Gen. 452 (2013) 34-38.

163. I. Ahmed, N. A. Khan, D. K. Mishra, J. S. Lee, J.-S. Hwang, S. H. Jhung, Chem. Eng. Sci. 93 (2013) 91-95.

164. A. A. Dabbawala, D. K. Mishra, J.-S. Hwang, Catal. Commun. 42 (2013) 1-5.

165. M. Gu, D. Yu, H. Zhang, P. Sun, H. Huang, Catal. Lett. 133 (2009) 214-220.

166. P. Sun, D. H. Yu, Y. Hu, Z. C. Tang, J. J. Xia, H. Li, H. Huang, Korean J. Chem. Eng. 28 (2011) 99-105.

167. C. Montassier, J. C. Menezo, J. Moukolo, J. Naja, L. C. Hoang, J. Barbier and J. P. Boitiaux, J. Mol. Catal. 70 (1991) 65-84.

168. N. Li, G. W. Huber, J. Catal., 270 (2010) 48-59.

169. N. A. Khan, D. K. Mishra, J.-S. Hwang, Y.-W. Kwak, S. H. Jhung, Res. Chem. Intermed. 37 (2011) 1231-1238.

Chapter 2

Dealuminated Beta zeolite as Effective Bifunctional Catalyst for Direct Transformation of Glucose to 5-Hydroxymethylfurfural

Abstract:

To improve the catalytic performance of Beta zeolite in the direct transformation of glucose into 5-hydroxymethylfurfural (HMF), effects of calcination and steam treatment on the structure of Al atoms in the framework and acid properties of Beta zeolite were examined in detail. ^{27}Al MAS NMR measurement and IR observation revealed that a part of Si-O-Al bonds in the framework were cleaved to form Al species out of the ***BEA** framework during the treatments and these species showed Lewis acidity. Especially, when the ammonium-type Beta was calcined over 700 ºC or treated with steam (50 kPa in N_2 balance) over 500 ºC, the amount of Lewis acid sites was increased at the expense of Brønsted acid sites. Thus prepared Beta zeolite catalysts having a sufficient amount of Lewis acid sites were found to be effective bifunctional catalysts in synthesis of HMF from glucose; for example, Beta zeolite prepared by the calcination at 750 ºC showed 55 % selectivity to HMF at 78 % conversion of glucose. I clarified the roles of Lewis and Brønsted acid sites on the Beta zeolite in the direct transformation of glucose to HMF. Furthermore, the reaction mechanism for the isomerization of glucose was investigated by means of isotope experiment using deuterated glucose. Finally, reusability of the Beta zeolite was also investigated.

2-1 Introduction

Effective utilization of biomass resources into useful materials such as chemicals and fuels has attracted considerable attention as a potential alternative to crude oil [1-4]. Carbohydrates accounts for 75 % of annually renewable biomass [5]. Biomass carbohydrates are divided into two types of polysaccharides. One is cellulose, which is a glucose polymer, and the other is hemicellulose, which has some types of polysaccharides containing pentoses *e.g.*, xylose and arabinose. These carbohydrates can be converted into useful materials through furfural or 5-(hydroxymethyl)-furfural abbreviated as HMF. These compounds have been regarded as a platform material for the production of polymers [6], fine chemicals [7-8] and transportation fuels [9-10]. Increasing attention has been paid to the dehydration of fructose to HMF. Nearly one hundred homogeneous and heterogeneous catalysts have been positively identified as catalysts for the synthesis of HMF from fructose and the promising results have been achieved [11]. Antal *et al.* conducted the dehydration reaction in sub-critical water containing H_2SO_4 to achieve 53 % yield of HMF [12]. A biphasic reactor system was reported by Román-Leshkov *et al.* [13]; in this process, fructose is dehydrated to HMF in HCl aqueous solution containing poly(1-vinyl-2-pyrrolidinone) or dimethyl sulfoxide. This biphasic system suppresses the undesired side reactions. Furthermore, the produced HMF is continuously extracted into the organic solvent. Moreau *et al.* studied the dehydration of fructose in the presence of H-mordenite and achieved 73 % yield of HMF at 93 % conversion of fructose [14].

In contrast, it is much more difficult to transform glucose to HMF, though it would be preferable to develop a process using glucose as feedstock because glucose is the most abundant component of biomass and less expensive than fructose. Since it has been found that fructose is readily dehydrated to HMF, recently, a tandem reaction system combining isomerization of glucose with subsequent dehydration of fructose to HMF has been extensively investigated. In those reports, the combinations of two types of catalysts assisting each step were employed and various types of combinations have been reported so far. Huang *et al.* achieved 63 % yield of HMF by employing

glucose isomerase enzyme and HCl aqueous solution containing borate ion as catalysts for the isomerization of glucose and the dehydration of fructose, respectively [15]. Takagaki *et al.* reported a combination of hydrotalcite and Amberlyst-15 as base and acid catalysts, respectively. In *N,N*-dimethylformamide media, this combination led to 76 % selectivity to HMF at 60 % of glucose conversion [16].

Water-tolerant Lewis acids that catalyze the isomerization of glucose to fructose even in aqueous media have been reported. It is desirable that the transformation of glucose to HMF is performed in water or in mixed solvents containing water because glucose is produced through hydrolysis of glucose polymers such as cellulose and starch. Ishida *et al.* reported lanthanide chlorides catalyzed the production of HMF from glucose [17]. Heterogeneous Lewis acid catalysts were also reported to be active in the isomerization reaction in water. Recently, Moliner *et al.* reported that Sn-Beta catalyzed the isomerization of glucose in water at 110 - 140 ºC and the catalyst can be used multiple times [18]. Following this report, the reaction systems pairing Sn-Beta and some types of Brønsted acid catalysts were developed. Nikolla and co-workers reported the combination of Sn-Beta and HCl acidic solution that gave 57 % yield of HMF in a water-THF biphasic system [19]. The combination of Sn-Beta and Amberlyst resins in a monophasic solvent composed of water and THF was found to give excellent results (63 % yield of HMF based on glucose) [20]. Although these catalysts showed good performance, the preparation of Sn-Beta generally require cost and time and some special additives are required to achieve a high catalytic performance. The developments of easily available catalysts with higher catalytic performance and a simple reaction system have been desired. Some research groups reported examples of a reaction system using transition metal oxides modified with H_3PO_4 as “single catalyst” that shows an activity in both isomerization and dehydration in water [21-23].

In the present study, I performed calcination at high temperature or steam treatment on Beta zeolite (***BEA**-type aluminosilicate zeolite) to induce a type of dealumination, which is a partial cleavage of Si-O-Al bonds in the framework to form Al species out of the framework. I found that

Beta zeolites, which have two types of acid sites, are effective bifunctional catalysts in the tandem reaction combining the isomerization of glucose to fructose and the dehydration of fructose to HMF. Lewis acid sites on the zeolites are active in promoting the isomerization through a hydride transfer mechanism as clarified by an isotope experiment using deuterated glucose. On the other hand, their Brønsted acid sites accelerate the subsequent dehydration of fructose to HMF.

2-2 Experimental

2-2-1 Catalyst preparation

The aluminosilicate zeolite with ***BEA** topology was synthesized in the media containing fluoride anion according to the previous report [24]. Tetraethylammonium cation was used as structure-directing agent (SDA) in the synthesis. Aluminum isopropoxide (Kanto chemical) was added to tetraethylammonium hydroxide solution (Alfa aesar) with stirring. Then, tetraethyl orthosilicate (TEOS) purchased from Tokyo Chemical Industries was added and the mixture was stirred until the complete evaporation of ethanol. Finally, HF *aq* (Wako) was added. The molar composition of the gel was 1.0 TEOS : 0.5 TEAOH : 0.067 $Al(O^iPr)_3$: 8 H_2O : 0.5 HF. Thus obtained thick gel was transferred to a Teflon-lined stainless steel autoclave and crystallized at 140 ºC for 5 days with tumbling. The solid product was recovered by filtration, washed with distilled water and dried overnight at 100 ºC followed by calcination at 580 ºC to remove SDA. This sample is denoted as Beta-SDAcal. The calcined sample was stirred in 1.0 M NH_4NO_3 solution at 80 ºC for ion-exchange. This treatment was repeated two times to obtain an ammonium form, denoted as Beta-NH_4.

Beta-NH_4 was calcined in air at different temperatures (500 – 750 ºC) to obtain the proton-form samples. Thus prepared samples are designated as Beta-Cal*x*, where *x* is the calcination temperature. Steam-treatment of ammonium-form samples was also performed at 500 - 600 ºC. The 1 g of the sample packed in a quartz tube was heated to the desired temperature at the rate of 3 ºC /min in air flow and then the gas flow was switched to a steam flow (50 kPa in N_2 balance) at the

flow rate of 50 ml/min. After 1 h of the treatment, the steam flow was stopped and the sample was cooled down under nitrogen flow. The steam-treated samples are designated as Beta-ST*y*, where *y* is the treatment temperature.

2-2-2 Characterization of the prepared catalysts

Powder X-ray diffraction (XRD) patterns of the prepared samples were collected on a Rigaku Ultima III diffractmeter using a Cu Kα radiation (40 kV, 20 mA). Chemical compositions of the zeolites were analyzed by a Shimadzu ICPE-9000 analyzer. Solid-state ^{27}Al MAS NMR spectra of hydrated samples were obtained on a JEOL ECA-600 spectrometer at a resonance frequency of 156.4 MHz using a 4 mm sample rotor with a spinning rate of 15 kHz. ^{29}Si MAS NMR spectra were measured on a JEOL ECA-400 spectrometer at a resonance frequency of 399.0 MHz using a 6 mm sample rotor with a spinning rate of 5.5 kHz.

The catalyst samples were characterized by FT-IR spectroscopy. FT-IR spectra were obtained by a Jasco FT-IR 4100 spectrometer equipped with an MCT detector. For FT-IR observation, a self-supporting disk of each sample was placed in a quartz cell connected to a closed gas-circulation system. After the sample was pretreated at 450 ºC *in vacuo*, a spectrum was recorded at 150 ºC. Acid properties of the samples were evaluated by using pyridine as probe molecule. After the record of the spectra at 150 ºC, an excess amount of pyridine (~ 1 kPa) was introduced into the cell and the sample was held at that temperature for 15 min. Then the sample was heated to 250 ºC and then the cell was evacuated for 10 min to pump off pyridine desorbed from silanol groups and weak acid sites. The sample was cooled to 150 ºC and IR spectra were recorded. This process was repeated with the temperature varied ranging from 250 to 450 ºC. For quantitative calculation of adsorbed pyridine, the reported molar extinction coefficient was used [25].

2-2-3 Catalytic tests

Catalytic tests were performed in a Teflon-lined stainless-steel autoclave (50 ml). The

reaction mixture was heated by a heating jacket outside the autoclave. At a set time, the reaction was quenched by cooling the autoclave in an ice bath. The reaction mixture was filtered prior to quantitative analysis to remove the solid catalyst. For the reaction in a mixed solvent, the homogeneous solution after the filtration was separated into aqueous and organic phases by adding NaCl as salting-out agent. Sugar substrates and water-soluble products in the aqueous phase were analyzed by an HPLC (Shimadzu, LC-20A) with refractive index and UV (280 nm) detectors in the ion-exclusion mode. HMF and furfural in the organic phase were analyzed by another HPLC (Shimadzu LC-10A) with UV detector (260nm).

^{13}C NMR spectra of the collected fractions (shown in Section *3.3.2*) were recorded on a JEOL GX500 spectrometer with ^{1}H broadband decoupling. To a 5 mm sample tube containing the collected aqueous solution was added a capillary tube packed with D_2O for locking.

2-3 Results and discussion

The as-synthesized sample showed a typical XRD pattern assigned to the ***BEA**-type structure. After the calcination at 580 ºC (Beta-SDAcal) followed by the ion-exchange to the ammonium form (Beta-NH_4), the framework structure was retained (Figure 1). Figure 2 shows ^{27}Al MAS NMR spectra of these three samples. The as-synthesized sample with the Si/Al atomic ratio of 15 gave peaks at around 55 ppm, which are assigned to tetrahedral Al atoms in the framework (Figure 2(a)). For Beta-SDAcal, a sharp peak was newly observed at 0 ppm, indicating the formation of octahedral Al species during the calcination of SDA (Figure2(b)). Note that the peak at 0 ppm completely disappeared after the ion-exchange to the ammonium form. These results suggest that octahedral Al species were re-incorporated into the framework by the ion-exchange. This phenomenon has been already reported by some research groups [26-27].

Thus obtained ammonium-form Beta zeolite having only tetrahedral Al species in the framework (Beta-NH_4) was used as a parent sample in further studies to clarify the effect of calcination and steam treatment; calcination or steam treatment of the parent ammonium-form

sample at different temperatures was conducted. The Si/Al ratio of the ammonium-form sample was 15, which is equal to that of the gel, and the Si/Al ratio of the whole solid samples was changed neither by the calcination nor the steam treatment.

2-3-1 Structural properties of the catalysts

XRD patterns of the catalyst samples are shown in Figure 3. All the samples showed typical XRD patterns assigned to the *__BEA__-type structure. Although calcination or steam treatment at high temperatures slightly decreased the diffraction intensities, the framework structure was definitely retained after the treatments.

Figure 4 shows the ^{27}Al MAS NMR spectra of the catalyst samples and Beta-NH_4. In the spectrum of Beta-NH_4, the overlapped two peaks appeared at 54 and 57 ppm. These peaks are assigned to tetrahedral Al species at T1, T2 sites and T3 – T9 sites in the framework, respectively [28]. Beta-Cal500 showed the two peaks assigned to tetrahedral Al atoms of which the peak at 57 ppm was remarkably decreased. In addition, a sharp peak was seen at 0 ppm, indicating that the dealumination from the framework occurred during the calcination; a part of the framework Al species located at T3-T9 sites apparently got out of the framework. The intensity of the peak at 57 ppm was further decreased by the calcination at above 600 ºC, suggesting that dealumination was enhanced by raising the calcination temperature.

Similar behavior was observed in the steam-treated samples. The peak at 57 ppm was remarkably decreased along with the increase in the steam-treatment temperature, and finally the peak was hardly seen in the spectrum of Beta-ST600. Compared with calcination, the steam-treatment caused severer dealumination because hydrolysis of Si-O-Al bonds, which is the cause of dealumination, was highly promoted by high-pressure of H_2O vapor at high temperature.

In the spectra of the samples calcined at > 700 ºC or steam-treated, the sharp peak at 0 ppm was not increased but gradually decreased and broadened into the lower field, when the calcination or treatment temperature was increased. Simultaneously, another broad peak at ~ 4 ppm appeared,

indicating the generation of another type of octahedrally-coordinated Al species. The total intensities of all the peaks of octahedral Al species decreased along with an increase in the calcination temperature. This would be because the Al species generated by the severe treatments are in distorted coordination environment, having low NMR sensitivity.

Figure 5 shows IR spectra of the samples measured at 150 ºC after the pretreatment. Beta-Cal500 exhibited absorption peaks attributed to bridging OH groups (~ 3600 cm^{-1}) and silanol groups (~ 3750 cm^{-1}) overlapping with a broad band (3000 – 3700 cm^{-1}) derived from the hydrogen-bond of OH groups. Note that in addition to these peaks, a small but clear peak can be seen at 3782 cm^{-1}. The spectrum of Beta-Cal600 was similar to those of Beta-Cal500 and the sample calcined at 580 ºC, while there was a marked difference in the spectra between these three samples and Beta-Cal700; the peak attributed to bridging OH groups was decreased by raising the temperature from 600 to 700 ºC along with the increase in the peak at 3782 cm^{-1}. The peak at 3782 cm^{-1} has been called "VHF band" attributed to partially hydrolyzed Al species showing Lewis acidity bearing an OH group(s) [29-30], indicating a cleavage of Si-O-Al bonds in the framework. Similar trends were observed in the spectra of the steam-treated samples. The IR study also indicates the enhanced dealumination by the calcination or steam treatment at high temperature, as observed in the Al NMR spectra.

^{29}Si MAS NMR spectra of the catalyst samples are given in Figure 6. The spectrum of Beta-Cal500 consists of four peaks centered at -102, -106, -112 and -116 ppm. The peaks at -102 and -106 ppm are assigned to Q^3 and Q^4 species connected with an Al atom (Q^n: $Si(OM)_n(OH)_{4-n}$, M = Si or Al), respectively. The peaks at -112 and -116 ppm are assigned to Q^4 (T3 – T9 sites) and Q^4 (T1and T2 sites) species [28,31]. As the calcination temperature was increased, the peaks at -102 and -106 ppm were decreased progressively with a sharpening of the peaks at -112 and -116 ppm. The decrease in the peak at -102 ppm indicates a condensation of two Si-OH groups in close vicinity, forming a Si-O-Si linkage. Similar phenomena were also observed in the steam-treated samples. Note that in the spectrum of Beta-ST600, the broad peak at -112 ppm was split into the

two distinct peaks at -113 and -112 ppm and the peak at -106 ppm almost completely disappeared, although the peak derived from tetrahedral Al atoms in the framework was still observed at around 54 ppm in the ^{27}Al NMR spectrum (Figure 2(g)).

2-3-2 Acid properties of the catalysts

Acid properties of the catalyst samples were assessed by IR observation employing pyridine as probe molecule. The amount of adsorbed pyridine after evacuation at 250 ºC is summarized in Table 1. The amount of adsorbed pyridine on Brønsted and Lewis acid sites of Beta-Cal500 were 0.25 and 0.13 mmol/g, respectively. As the calcination temperature was increased, Brønsted acid sites were decreased but Lewis acid sites were increased; for Beta-Cal750, the amounts of Brønsted and Lewis acid sites were 0.17 and 0.18 mmol/g, respectively. Namely, the ratio of Brønsted acid sites to Lewis acid sites (B/L ratio) was decreased from 1.9 to 0.94; the dealumination by the calcination led to the decrease in tetrahedral Al species, which are Brønsted acid sites, and thus dealuminated Al species act as Lewis acid sites.

The acid properties of the samples were also evaluated by using CO as probe molecule (Figure S2). For Beta-Cal750, the total intensity of the stretching band of CO adsorbed on Lewis acid sites appearing at > 2200 cm^{-1} was higher than that for Beta-Cal500. These findings indicate that Lewis acid sites were undoubtedly increased by the calcination at a high temperature, being in accordance with the IR observation employing pyridine as probe molecule.

The total amount of acid sites was slightly decreased for the samples calcined at high temperature. This is probably because the calcination resulted in the generation of weak Lewis acid sites that release adsorbed pyridine molecule below 250 ºC or the generation of non-acidic Al species. Note that the acid properties of the steam-treated samples were more remarkably changed depending on the treatment temperature, compared to the calcined samples. This is because the steam-treated samples had undergone severer dealumination at a temperature than the calcined samples.

2-3-3 Catalytic isomerization of glucose to fructose

2-3-3-1 Kinetic isotope effect in the isomerization reaction

The consecutive reaction mechanism has been reported for the transformation of glucose to HMF (Scheme 1). Zhao *et al.* reported metal chlorides in ionic liquid effectively catalyzed the transformation of glucose to HMF in which case metal chloride catalysts promoted both the isomerization of glucose to fructose and the subsequent dehydration of fructose to HMF [32]. Nikolla *et al.* reported that the combination of Sn-Beta and HCl aq was effective for the direct transformation of glucose and other sugars to HMF [19]. If Lewis acid site generated by the dealumination catalyze the isomerization of glucose, the dealuminated Beta zeolites can act as bifunctional catalyst in the direct transformation of glucose to HMF in combination with original Brønsted acid sites.

First, the catalytic activity of Beta-ST600 in the isomerization of glucose was representatively investigated. Figure 7 gives the product distributions in the isomerization of glucose in water at 170 ºC with the reaction time changed. Fructose was obtained as main product with 71 % selectivity for the reaction time of 0.25 h. HMF, furfural, anhydroglucose (abbreviated as AHG), and C_3 products were also formed in small amounts in addition to fructose. Furthermore, there were missing products that were not detected by HPLC (less than 10 % selectivity based on carbon atoms). At the prolonged reaction time, the conversion of glucose was increased. Concurrently the selectivity to fructose was decreased and those to HMF and missing products were increased due to consecutive reactions of fructose.

To clarify the reaction mechanism of the isomerization, I have also performed the isomerization of deuterated glucose. The sum of the yields of fructose, HMF and furfural, which are the products resulting from the isomerization, is plotted in Figure 8. There was a remarkable difference in the reaction rates between these substrates, implying that the C-H cleavage at the C-2 position of glucose is involved in the rate-determining step of the isomerization reaction promoted by the dealuminated Beta zeolite.

2-3-3-2 Reaction mechanism of the isomerization over dealuminated Beta zeolite

The products in the isomerization of glucose-D2 over Beta-ST600 were separated by ligand-exchange chromatography using HPLC with a Ca^{2+}-form column, which can completely separate monosaccharides such as glucose and fructose. Each fraction passing through the column was collected and concentrated by evaporation of eluent water. Figure 9 shows the NMR spectra of glucose, fructose and their deuterated isotopes. The signals in the spectra are assigned according to the previous reports [33-34]. The peaks at 72.2 and 74.9 ppm in the spectrum of unlabeled glucose were assigned to C-2 atoms of α-glucopyranose and β-glucopyranose, respectively (Figure 9(a)). In the spectrum of glucose-D2 (Figure 9(b)), these peaks were not observed, indicating virtually complete deuteration. Furthermore, a new triplet peak centering at 74.7 ppm with low intensity was observed. This peak is derived from C-2 atom bonded with deuterium. The ^{13}C NMR spectra were recorded with proton decoupling pulse, which caused the nuclear Overhauser effect. Therefore, the carbon atoms coupled with hydrogen atoms were observed with high intensity, but the C-2 atom coupled with deuterium was not affected and observed with relatively low intensity. Note that the chemical shifts of the other peaks were totally the same as those of unlabeled glucose (Figure 10).

Figures 9(d) and (e) show the spectra of unlabeled fructose and fructose fraction collected after the catalytic run of glucose-D2 for 1 h, respectively. Although the peaks at 62.6 and 63.8 ppm were clearly found in the spectrum of unlabeled fructose, these peaks were not found in the spectrum of the products. They are assigned to C-1 atoms of β-fructofuranose and β-fructopyranose, respectively. At the expense of their disappearance, a triplet peak centering at 63.3 ppm was newly observed for the fructose produced from glucose-D2, which can be assigned to the C-1 atom coupled with deuterium. Obviously, fructose deuterated at the C-1 position was dominantly produced in the isomerization of glucose-D2 over Beta-ST600. The glucose fraction collected after the catalytic run contained only glucose-D2 (Figure 9(c)), indicating that glucose substrate was not scrambled with hydrogen atom derived from H_2O solvent during the reaction. In the isomerization of glucose catalyzed by base, the reaction proceeds *via* enediol intermediate and consequently the

hydrogen atom derived from H_2O solvent is scrambled in the fructose product and residual glucose. Based on the findings that hydrogen scrambling was absolutely not observed and that the deuterated fructose was dominantly produced, it is concluded that fructose was not produced *via* enediol intermediate as is the case with the base- catalyzed reaction but *via* intramolecular hydride transfer from C-2 to C-1 atom in the glucose molecule. Román-Leshkov *et al.* also suggested an intramolecular hydride transfer mechanism for the isomerization of glucose to fructose over Lewis acid sites of Sn-Beta [35].

The mechanism was further confirmed by a control experiment using the opposite combination of isotope labeling; the isomerization of unlabeled glucose in D_2O solvent. Figure 11 shows the NMR spectra of glucose and fructose fractions obtained in the experiment, indicating that neither fraction contain the deuterated molecules. Furthermore, D NMR analysis gave a single peak derived from D_2O solvent (not shown). These results clearly showed that dealuminated Beta zeolites have an activity to promote the isomerization of glucose to fructose *via* the intramolecular hydride transfer mechanism over Lewis acid sites on dealuminated Beta zeolites.

2-3-4 Influence of acid properties and reaction conditions

2-3-4-1 Effect of the solvent

HMF was obtained from glucose in the solvent of water at 170 ºC but the yield was below 5 % (Figure 7). In order to increase the yield, the reaction conditions were altered. It has been claimed in copious literature that the dehydration of glucose is strongly affected by solvent systems. Therefore, I first investigated the effect of the solvent by using Beta-Cal750. Table 2 summarizes the reaction results in different solvent systems. For the reaction in water of 5 ml, the conversion of glucose was 74 % at 1 h and the selectivities to fructose and HMF were 17 and 14%, respectively. The carbon balance was not good; the selectivity to missing products was 59%. This is probably due to the formation of polymerized products, which were not detected by HPLC. The color of the reaction mixture was changed from transparent to black.

The replacement of 10 % water with dimethylsulfoxide (DMSO) (i.e., water, 4.5 ml; DMSO 0.5 ml) suppressed the formation of the undetected products. The selectivities to fructose and HMF at 50 % conversion were improved to 26 and 33 %, respectively. Vlachos *et al.* reported the solvent effects of DMSO in the DMSO-water mixture [36]; they stated that DMSO protects (i) fructose from side reactions other than its dehydration to HMF and (ii) HMF from rehydration and humins formation reaction.

Unfortunately, the selectivity to HMF was not remarkably improved at high conversion; at 89 % conversion of glucose, the selectivity to HMF was only 36 %. This is probably because successive reactions of HMF including humins formation might not be completely suppressed in this solvent system. Then tetrahydrofuran (THF) was added into the reaction mixture to protect HMF (water, 4.5 ml; DMSO 0.5 ml; THF 15 ml) [37-38]. The selectivity to HMF turned out to be improved at high conversion; 55 % selectivity to HMF was achieved at 78 % conversion of glucose. Note that glucose molecule is solvated by water and DMSO molecules but not solvated by THF molecules because glucose is almost immiscible with THF. Thus, the solvent system was optimized and the further catalytic reactions were operated in the optimized solvent system (water, 4.5 ml; DMSO 0.5 ml; THF 15 ml).

2-3-4-2 Effect of the calcination or steam treatment

The reaction results on the transformation of glucose to HMF using Beta catalysts calcined or steam-treated at different temperatures are shown in Table 3. For the calcined samples, the conversion of glucose was increased with an increase in the calcination temperature; the sample calcined at 500, 600, 700, 750 ºC gave 57, 61, 69, and 78 % conversions of glucose, respectively. Then the selectivities to HMF were 36, 37, 50, and 55%, respectively. A sample calcined at higher temperature has a larger amount of Lewis acid sites, as described in Section 3.1; *i.e.*, there is a good relationship between the amount of Lewis acid sites and catalytic activity. The relationship is also applicable to Beta-SDAcal, which showed 57 % of glucose conversion and 38 % HMF selectivity.

It implies that the isomerization of glucose, which is the rate-determining step in the total reaction as shown in Section *3.5*, was promoted by Lewis acid sites on aluminosilicate Beta zeolites.

The Beta-Cal500 catalyst required 5 h to reach *ca.* 81 % of glucose conversion with 50 % selectivity to HMF, while Beta-Cal750 gave almost the same conversion (78 %) in 3 h with a higher selectivity to HMF (ca. 55 %). In addition to fructose and HMF, several by-products, such as levulinic acid (LVA) and decomposed products, were found in the reaction mixture. These results clearly showed that a catalyst with lower amount of Lewis acid required longer reaction time to reach the same level of glucose conversion and that long reaction time did not contribute to the improvement of the selectivity to HMF but escalated consecutive reactions. Levulinic acid was formed in 5 – 7 % selectivity *via* hydration of HMF. Besides, furfural was also formed in 4 % selectivity, which would be formed not *via* consecutive reaction of HMF but *via* a side reaction of fructose with loss of a carbon atom [39]. The formation of AHG was also observed, which might be produced over Brønsted acid sites [40]; actually, the sample having a larger amount of Brønsted acid sites (*e.g.*, Bta-Cal500) gave the higher selectivity to AHG. It was revealed that Brønsted acid sites do not contribute to the isomerization of glucose but promote the formation of an ether bond between C-1 and C-6.

Steam-treated Beta zeolites gave similar reaction results. The conversion of glucose was 77 and 78 % for Beta-ST500 and Beta-ST600, respectively. The product distributions were also similar to those for the calcined catalysts; the catalytic performance of Beta-ST500 and Beta-ST600 was similar to that of Beta-Cal700 and Beta-Cal750, respectively. Although Beta-ST600 has a little lower amount of Lewis acid sites than Beta-Cal700, Beta-Cal750 and Beta-ST500 catalysts, it showed the highest conversion of glucose. I assume that Beta-ST600 had relatively weak Lewis acid sites that desorb pyridine molecule below 250 ºC and that even such weak acid sites can also promote the isomerization of glucose to fructose.

The ^{27}Al MAS NMR spectra (Figure 4) imply that severe treatments promote the generation of another type of octahedrally-coordinated Al species that shows the peak at 4 ppm. Furthermore,

the samples prepared by the severe treatments showed a “VHF band” in the IR spectra (Figure 5). Although the details of Lewis-acidic Al species active for hydride transfer reactions on aluminosilicate zeolite have not been fully understood [41-43], thus generated new Al species might work as the active species for the isomerization of glucose. The details of dealumination mechanism and nature of the active Lewis-acidic species are under investigation.

The HMF yields at the reaction time of 3 h are plotted against the amount of Lewis acid sites in Figure 12. The HMF yield was increased along with an increase in the amount of Lewis acid sites except for Beta-ST600. The reason for the deviating behavior for Beta-ST600 would be due to the presence of relatively weak Lewis acid sites. The catalysts prepared by the harsh treatments have large amounts of Lewis acid sites and showed the high reaction rates in the isomerization of glucose, which should be the rate-determining step in the total reaction, contributing to the high yield of HMF.

2-3-5 Dehydration of fructose to HMF

Transformation of glucose to HMF is a two-step reaction consisting of the isomerization of glucose to fructose followed by the dehydration of fructose to HMF (Scheme 1). The yield of HMF could be strongly affected by the selectivity in the dehydration step. I performed the dehydration of fructose using the catalysts (Table 4). The catalytic run for 1 h gave the conversions over 90 % for all the catalysts. The reaction rates of the fructose dehydration were much faster than those of glucose isomerization. Therefore, the isomerization step should be the rate-determining step in the transformation of glucose to HMF. The selectivity to HMF was slightly decreased by the high-temperature calcination. In the steam-treated samples, the selectivity rather depended on the treatment temperature; the increase in the treatment temperature led to the decrease in the selectivity to HMF. The steam-treatments caused severe dealumination, resulting in a decrease in the Brønsted acid sites accompanied with an increase in the Lewis acid sites. Thus steam-treatment led to the low selectivities to HMF but undesired reactions of fructose over Lewis acid sites.

Aluminosilicate Beta zeolite showed a lower activity in the isomerization of glucose than Sn-Beta and Ti-Beta [18,44]. Hence, aluminosilicate Beta catalysts required higher temperature to promote the isomerization than Sn-Beta and Ti-Beta. Nevertheless, the low activity of Lewis acid sites of aluminosilicate Beta would be a benefit in a one-pot formation of HMF from glucose. High Lewis acidity should result not only in the rapid isomerization but also in rapid undesired side-reactions of fructose [18, 19]. To effectively produce HMF from glucose in one pot, it is important that fructose should be dehydrated to HMF faster than undesired reactions over Lewis acid sites. Therefore, highly active Brønsted acids such as mineral acids are required in the presence of highly active Lewis acids. The Dealuminated Beta zeolites prepared by the harsh treatments (calcination at > 700 ºC and steam treatment at >500 ºC) have Lewis acid sites much enough to promote the isomerization of glucose and they have originally Brønsted acid sites that accelerate the dehydration of fructose more rapidly than undesired side reactions of fructose over Lewis acid sites. In this way, thus prepared Beta zeolites have both Lewis and Brønsted acidity suitable for the direct transformation, leading to the high catalytic performance.

I performed the catalytic transformation of glucose to HMF by using the commercial Beta, mordenite, USY and ZSM-5 and silica-alumina (Table 5). The commercial Beta zeolite showed a poorer catalytic performance than Beta-Cal750 in spite of its higher acid amounts. Besides, Beta-Cal750 showed higher conversion of glucose than other types of 12-membered ring zeolites such as mordenite and USY. ZSM-5 showed a much poorer catalytic performance; 19 % selectivity to HMF at 33 % conversion of glucose probably because glucose molecule is too large to enter the 10-membered pores of the **MFI**-type structure. The catalytic performance of silica-alumina was also evaluated. Its large amount of Lewis acid sites contributed to the high conversion, but its small amount of Brønsted acid sites resulted in the low selectivity to HMF. Our best catalyst, Beta-Cal750, gave 43 % yield of HMF at reaction time of 3 h. However, Sn-W mixed oxide, which has been reported as bifunctional catalyst for conversion of sugars to HMF, required the reaction time of 18 h to achieve 48 % yield of HMF [45]. Hence, I concluded that Beta zeolites dealuminated at high

temperature were effective bifunctional catalyst for the transformation of glucose to HMF

2-3-6 Regeneration of catalyst

Regeneration of the Beta zeolite catalysts was investigated. The catalyst after each run was recovered by filtration, thoroughly washed with water and dried in an oven at 100 ºC. At this point, the color of the catalyst was light brown. Prior to the next run, the recovered catalyst was calcined at 550 ºC to remove residual organic moieties deposited on the catalyst. Figure 13 shows the conversion of glucose and product distributions in five consecutive runs. In the course of the repeated runs, the conversion of glucose was slightly decreased from 78 to 70 %, but the selectivity to HMF remained constant. Consequently the HMF yield was only slightly decreased from 43 to 40 %. Although the selectivity to fructose was gradually increased in the course, the selectivity to unknown products was decreased. After five times of usage, the recovered catalyst was calcined at 550 ºC and characterized. The Si/Al ratio of the recovered catalyst was 15, unchanged from the fresh one. The change in the product distribution might be due to the change of the acid properties of the catalyst. The acid properties of the recovered catalyst were evaluated by using pyridine as probe molecule. The amounts of pyridine molecule adsorbed on Lewis and Brønsted acid sites after the evacuation at 250 ºC were decreased from 0.17 to 0.14 mmol/g and from 0.18 to 0.13 mmol/g, respectively. The repeated calcination at 550 ºC resulted in the decrease in Lewis acid sites and also in the decrease of the glucose conversion.

2-4 Conclusions

I successfully found that the proportion of Lewis acid sites on the zeolite was remarkably increased when *__BEA__-type aluminosilicate was simply calcined over 700 ºC or treated with steam over 500 ºC, and that thus treated Beta zeolite catalysts were found to be an effective bifunctional catalyst for the synthesis of HMF from glucose. During these treatments, a part of Si-O-Al bonds surrounding an Al atom were cleaved to form Al species showing Lewis acidity. Beta zeolites

prepared by harsh treatments had sufficient amount of Lewis acid sites to promote the isomerization of glucose in addition to the original Brønsted acid sites. Those zeolites with acid properties controlled were effective bifunctional catalysts for the direct transformation of glucose to HMF (55 % selectivity at 78 % glucose conversion). A ^{13}C NMR technique revealed that glucose molecule was isomerized to fructose through an intramolecular hydride transfer. The generated fructose was dehydrated to HMF over Brønsted acid sites. The Beta zeolite catalyst can be recovered by filtration and regenerated by simple calcination and the HMF yield remained fairly constant during five consecutive runs.

References:

1. A. Corma, S. Iborra, A. Velty, Chem. Rev. 107 (2007) 241-2502.
2. J. N. Chheda, G. W. Huber, J. A. Dumesic, Angew. Chem. Int. Ed. 46 (2007) 7184-7201.
3. J. J. Bozell, G. R. Petersen, Green Chem. 12 (2010) 539-554.
4. P. Gallezot, Chem. Soc. Rev. 41 (2012) 1538-1558.
5. F. W. Lichtenthaler, The Key Sugars of Biomass: Availability, Present Non-Food Uses and Potential Future Development Lines, in: B. Kamm, P. R. Gruber, M. Kamm (Eds), Biorefineries - Industrial Processes and Products, Volume 2, Wiley-VCH, Germany, 2006, pp. 3-51.
6. A. Gandini, M. N. Belgacem, Prog. Polym. Sci. 22 (1997) 1203-1379.
7. M. J. Climent, A. Corma, S. Iborra, Green Chem. 13 (2011) 520-540.
8. A. A. Rosatella, S. P. Simeonov, R. F. M. Frade, C. A. M. Afonso, Green Chem. 13 (2011) 754-793.
9. G. W. Huber, S. Iborra, A. Corma, Chem. Rev. 106 (2006) 4044-4098.
10. D. M. Alonso, J. Q. Bond, J. A. Dumesic, Green Chem. 12 (2010) 1493-1513.
11. X. Tong, Y. Ma, Y. Li, Appl. Catal. A: Gen. 385 (2010) 1-13.
12. M. J. Antal, W. S. L. Mok, G. N. Richards, Carbohydr. Res. 199 (1990) 91-109.
13. Y. Román-Leshkov, J. N. Chheda, J. A. Dumesic, Science, 312 (2006) 1933-1937.
14. C. Moreau, R. Durand, S. Razigade, J. Duhamet, P. Faugeras, P. Rivalier, P. Ros, G. Avignon, Appl. Catal. A: Gen. 45 (1996) 211-224.
15. R. Huang, W. Qi, R. Su, Z. He, Chem. Commun. 46 (2010) 1115-1117.
16. A. Takagaki, M. Ohara, S. Nishimura, K. Ebitani, Chem. Commun. 2009, 6276-6278.
17. H. Ishida, K. Seri, J. Mol. Catal. A: Chem. 112 (1996) L163-L165.
18. M. Moliner, Y. Román-Leshkov, M. E. Davis, Proc. Natl. Acad. Sci. USA, 107 (2010) 6164-6168.
19. E. Nikolla, Y. Román-Leshkov, M. Moliner, M. E. Davis, ACS Catal. 1 (2011) 408-410.

20. J. M. R. Gallo, D. M. Alonso, M. A. Mellmer, J. A. Dumesic, Green Chem. 15 (2013) 85-90.

21. K. Nakajima, Y. Baba, R. Noma, M. Kitano, J. N. Kondo, S. Hayashi, M. Hara, J. Am. Chem. Soc. 133 (2011) 4224-4227.

22. F. Yang, Q. Liu, M. Yue, X. Bai, Y. Du, Chem. Commun. 47 (2011) 4469-4471.

23. V. V. Ordomsky, V. L. Sushkevich, J. C. Schouten, J. van der Schaaf, T. A. Nijhuis, J. Catal. 300 (2013) 37-46.

24. M. A. Camblor, A. Corma, S. Valencia, J. Mater. Chem. 8 (1998) 2137-2145.

25. C. A. Emeis, J. Catal. 141 (1993) 347-354.

26. B. H. Wouters, T.-H. Chen, P. J. Grobet, J. Am. Chem. Soc. 120 (1998) 11419-11425.

27. G. H. Kuehl, H. K. C. Timken, Micropor. Mesopor. Mater. 35 – 36 (2000) 521-532.

28. G. Valerio, A. Goursot, R. Vetrivel, O. Malkina, V. Malkin, D. R. Salahub, J. Am. Chem. Soc. 120 (1998) 11426-11431.

29. I. Kiricsi, C. Flego, G. Pazzuconi, W. O. Parker, R. Millini, C. Perego, G. Bellussi, J. Phys. Chem. 98 (1994) 4627-4634.

30. A. Vimont, F. Thibault-Starzyk, J. C. Lavalley, J. Phys. Chem. B, 104 (2000) 286-291.

31. J. Pérez-Pariente, J. Sanz, V. Fornés, A. Corma, J. Catal. 124 (1990) 217-223.

32. H. Zhao, J. E. Holladay, H. Brown, Z. C. Zhang, Science, 316 (2007) 1597-1600.

33. M. U. Roslund, P. Tähtinen, M. Niemitzc, R. Sjöholm, Cabohydr. Res. 343 (2008) 101-112.

34. W. Funcke, C. von Sontang, C. Triantaphylides, Carbohydr. Res. 75 (1979) 305-309.

35. Y. Román-Leshkov, M. Moliner, J. A. Labinger, M. E. Davis, Angew. Chem. Int. Ed. 49 (2010) 8954-8957.

36. S. H. Mushrif, S. Caratzoulas, D. G. Vlachos, Phys. Chem. Chem. Phys. 14 (2012) 2637-2644.

37. Y. Román-Leshkov, J. A. Dumesic, Top. Catal. 52 (2009) 297-303.

38. J. Wang, J. Ren, X. Liu, G. Lu, Y. Wang, AIChE J. 59 (2013) 2558-2566.

39. J. Zhang, E. Weitz, ACS Catal. 2 (2012) 1211-1218.

40. M. Ohara, A. Takagaki, S. Nishimura, K. Ebitani, Appl. Catal. A: Gen. 383 (2010) 149-155.

41. P. J. Kunkeler, B. J. Zuurdeeg, J. C. van der Waal, J. A. van Bokhoven, D. C. Koningsberger, H. van Bekkum, J. Catal. 180 (1998) 234-244.

42. O. Bortnovsky, Z. Sobalík, B. Wichterlová, Z. Bastl, J. Catal. 210 (2002) 171-182.

43. B. Akata, J. Warzywoda, A. Sacco Jr., J. Catal. 222 (2004) 397-403.

44. A. Corma, M. E. Domine, S. Valencia, J. Catal. 215 (2003) 294–304.

45. K. Yamaguchi, T. Sakurada, Y. Ogasawara, N. Mizuno, Chem. Lett. 40 (2011) 542-543.

Table 1 Amount of adsorbed pyridine after desorption at 250 ºC[a, b].

Sample	Amount of adsorbed pyridine		
	Brønsted (mmol/g)	Lewis (mmol/g)	B/L
Beta-SDAcal	0.23	0.14	1.6
Beta-Cal500	0.25	0.13	1.9
Beta-Cal600	0.24	0.14	1.7
Beta-Cal700	0.20	0.17	1.2
Beta-Cal750	0.17	0.18	0.94
Beta-ST500	0.11	0.17	0.65
Beta-ST600	0.09	0.15	0.60

a: each acid amount (mmol/g) was calculated by using the reported molar extinction coefficient in Ref. 26.

b: the Si/Al ratios of all the samples in the Table were 15.

Table 2 Effect of the solvent systems on the product distribution[a].

Solvent	Time (h)	Conversion (%)	Selectivity (%)		
			Fructose	HMF	Others
Water 5ml	1	76	17	14	59
	3	94	3	10	79
Water 4.5 ml	1	50	26	33	34
DMSO 0.5ml	3	89	4	36	54
Water4.5 ml	1	56	9	36	29
DMSO 0.5 ml					
THF 15 ml	3	78	2	55	27

a: Catalyst, Beta-Cal750 100 mg; Glucose, 0.67 mmol; Temperature, 180 ºC.

Table 3 Transformation of glucose to HMF over Beta zeolites[a].

Catalyst	Acid (mmol/g)[b]		Conv.[c]	Selectivity (carbon %)						
	Brønsted	Lewis	(%)	Fructose	HMF	LVA	Furfural	AHG	C_3	Others
Beta-SDAcal	0.23	0.14	57	5	38	7	4	8	4	36
Beta-Cal500	0.25	0.13	57	4	36	7	4	10	4	35
Beta-Cal500[d]			81	1	50	7	5	3	2	32
Beta-Cal600	0.24	0.14	61	4	37	6	4	8	4	37
Beta-Cal700	0.20	0.17	69	5	50	5	5	6	3	26
Beta-Cal750	0.17	0.18	78	2	55	6	4	4	2	28
Beta-ST500	0.11	0.17	77	6	51	4	5	4	2	28
Beta-ST600	0.09	0.15	78	6	55	5	5	5	3	21

a: Catalyst, 100 mg; Glucose, 0.67 mmol; Water, 4.5 ml; DMSO 0.5 ml; THF 15 ml; Temperature, 180 ºC; Time, 3 h.

b: Each acid amount corresponds to the amount of adsorbed pyridine after evacuation at 250 ºC.

c: Conversion of glucose.

d: Time, 5 h.

Table 4 Dehydration of fructose to HMF over Beta zeolites[a].

Catalyst	Acid (mmol/g)[b]		Conv.[c]	Selectivity (carbon %)				
	Brønsted	Lewis	(%)	HMF	LVA	Furfural	C_3	Others
Beta-SDAcal	0.23	0.14	91	68	6	10	1	15
Beta-Cal500	0.25	0.13	96	70	6	12	1	11
Beta-Cal600	0.24	0.14	93	70	6	13	1	10
Beta-Cal700	0.20	0.17	97	68	5	8	1	18
Beta-Cal750	0.17	0.18	97	66	4	7	1	22
Beta-ST500	0.11	0.17	92	60	7	8	1	24
Beta-ST600	0.09	0.15	91	55	7	6	1	31

a: Catalyst, 100 mg; Fructose, 0.67 mmol; Water, 4.5 ml; DMSO 0.5 ml; THF 15 ml; Temperature, 180 ºC; Time, 1 h.

b: Each acid amount corresponds to the amount of adsorbed pyridine after evacuation at 250 ºC.

c: Conversion of fructose

Table 5 Comparison of catalytic performances with conventional acid catalysts[a].

Catalyst	Acid (mmol/g)[b]		Conv.[c]	Selectivity (carbon %)						
	Brønsted	Lewis	(%)	Fructose	HMF	LVA	Furfural	AHG	C_3	Others
Beta-Cal750	0.17	0.18	78	2	55	6	4	4	2	28
Beta-CV[d]	0.18	0.19	65	9	43	2	5	9	6	26
Mordenite[e]	0.52	0.02	57	3	52	2	2	10	8	23
USY[f]	0.14	0.03	63	2	50	1	4	8	6	29
ZSM-5[g]	0.25	0.05	33	8	19	6	2	9	7	49
Silica-alumina[h]	0.03	0.19	87	14	32	1	2	4	3	44

a: Catalyst, 100 mg; Glucose, 0.67 mmol; Water, 4.5 ml; DMSO 0.5 ml; THF 15 ml; Temperature, 180 ºC; Time, 3 h.

b: Each acid amount corresponds to the amount of adsorbed pyridine after evacuation at 250 ºC.

c: Conversion of glucose.

d: Commercial Beta (JRC-Z-HB25, Si/Al = 12.5) kindly given by Japan reference catalyst.

e: Mordenite (JRC-Z-HM20, Si/Al = 10) kindly given by Japan reference catalyst.

f: USY (CBV-760, Si/Al = 30) purchased from Zeolyst international.

g: ZSM-5 (JRC-Z5-25H, Si/Al = 12.5) kindly given by Japan reference catalyst.

h: Silica-alumina (JRC-SAL-2, Si/Al = 4.7) kindly given by Japan reference catalyst.

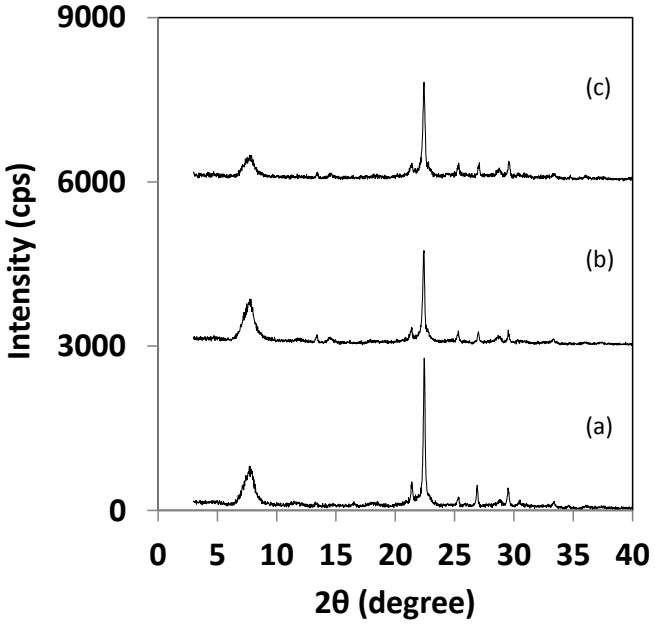

Figure 1 XRD patterns of (a) as-synthesized sample, (b) Beta-SDAcal, (c) Beta-NH_4.

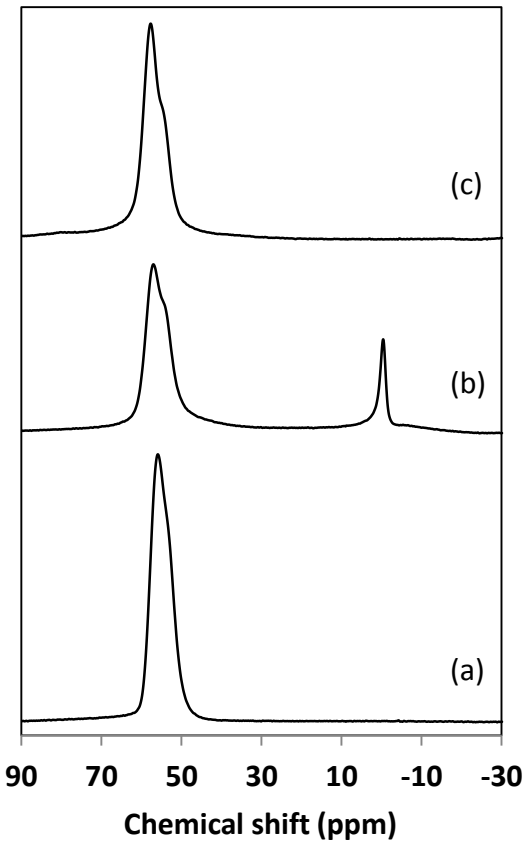

Figure 2 ^{27}Al MAS NMR spectra of (a) as-synthesized sample, (b) Beta-SDAcal, (c) Beta-NH_4.

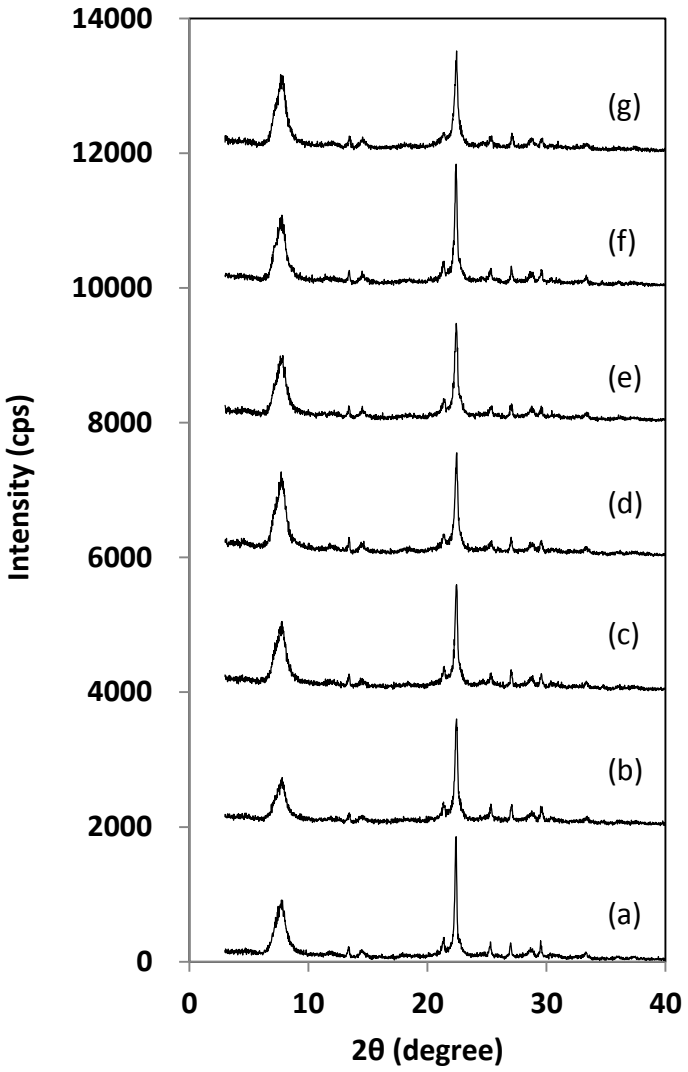

Fig. 3 XRD patterns of dealuminated Beta zeolite samples.

(a) Beta-SDAcal, (b) Beta-Cal500, (c) Beta-Cal600, (d) Beta-Cal700, (e) Beta-Cal750, (f) Beta-ST500, (g) Beta-ST600.

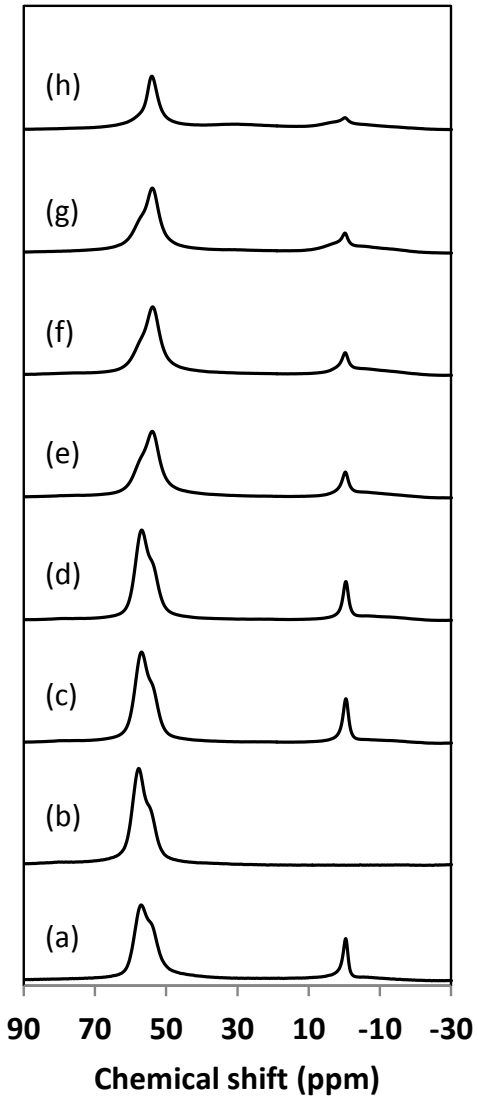

Fig. 4 ^{27}Al MAS NMR spectra of dealuminated Beta zeolites.

(a) Beta-SDAcal (b) Beta-NH_4 (c) Beta-Cal500, (d) Beta-Cal600, (e) Beta-Cal700, (f) Beta-Cal750, (g) Beta-ST500, (h) Beta-ST600.

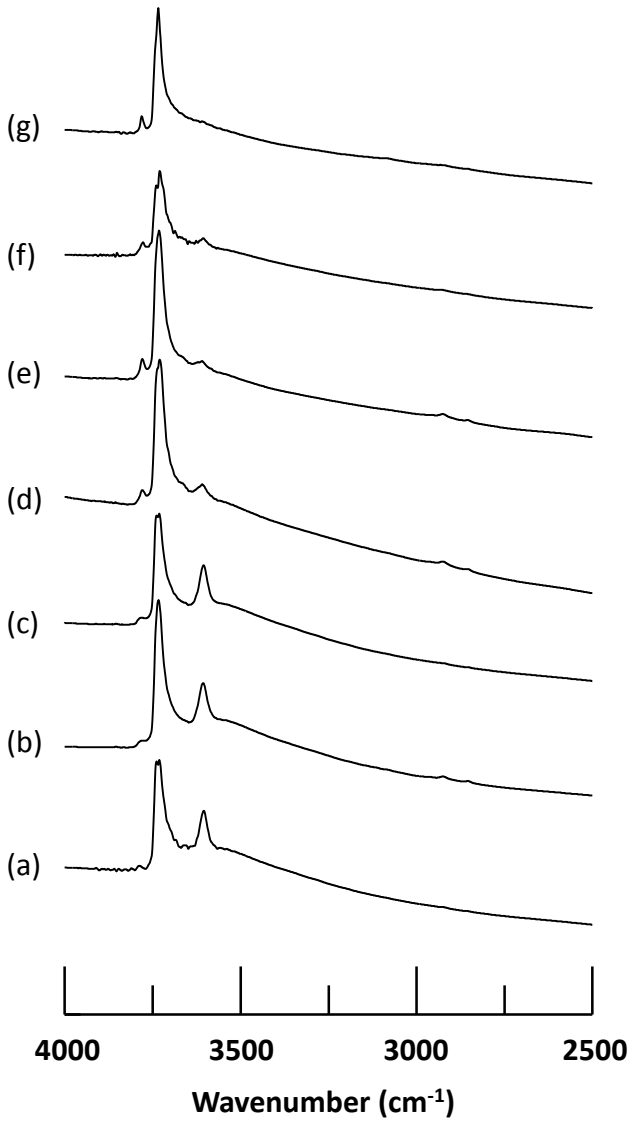

Fig. 5 IR spectra of dealuminated Beta zeolites.

(a) Beta-SDAcal (b) Beta-Cal500, (c) Beta-Cal600, (d) Beta-Cal700, (e) Beta-Cal750, (f) Beta-ST500, (g) Beta-ST600.

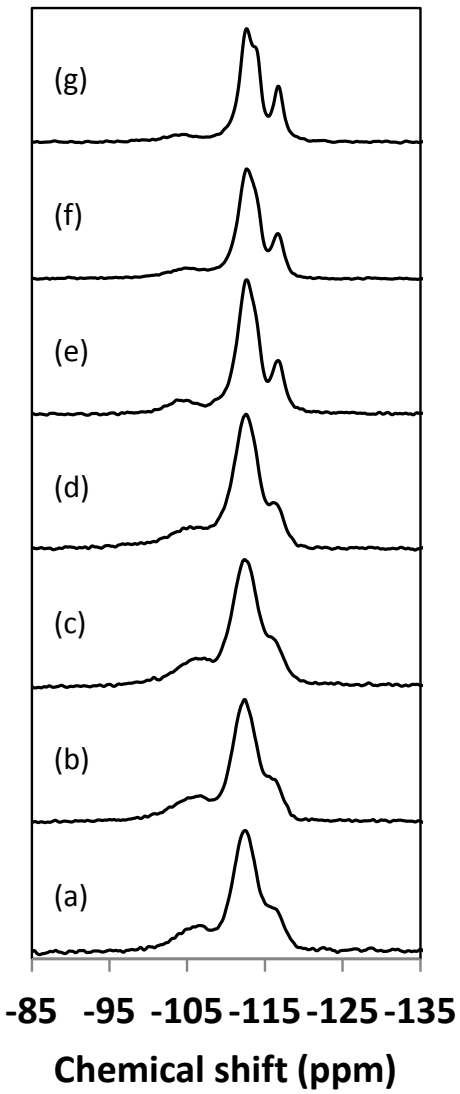

Fig. 6 ^{29}Si MAS NMR spectra of dealuminated Beta zeolites.

(a) Beta-SDAcal (b) Beta-Cal500, (c) Beta-Cal600, (d) Beta-Cal700, (e) Beta-Cal750, (f) Beta-ST500, (g) Beta-ST600.

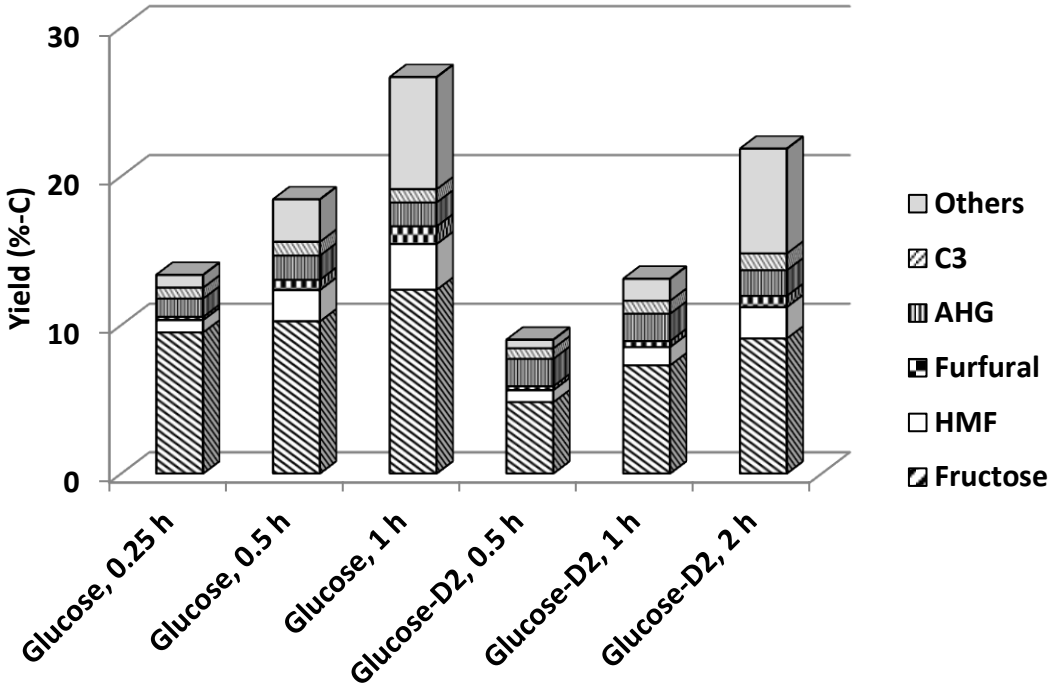

Fig. 7 Isomerization of glucose(-D2) in water using Beta-ST600[a].

a: Beta-ST600, 100 mg; Glucose(-D2), 0.67 mmol; Water, 15 ml; Temperature, 170 ºC.

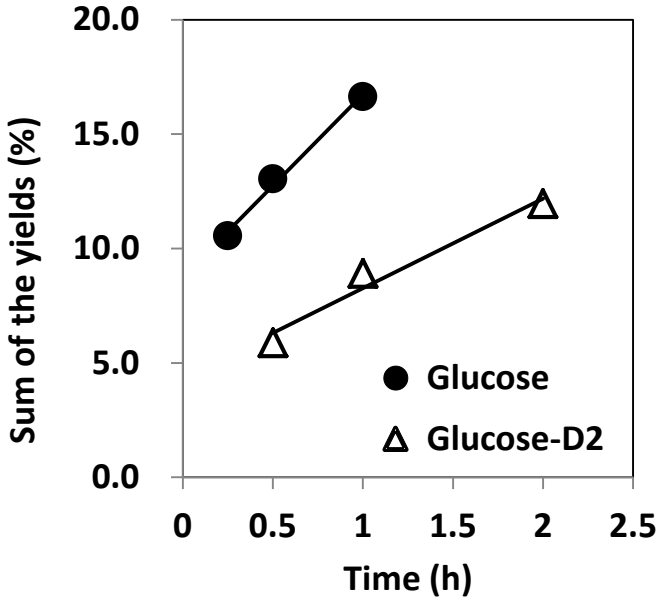

Fgirue 8 Sum of the yields of fructose, HMF and furfural produced in the reaction of glucose and glucose-D2.

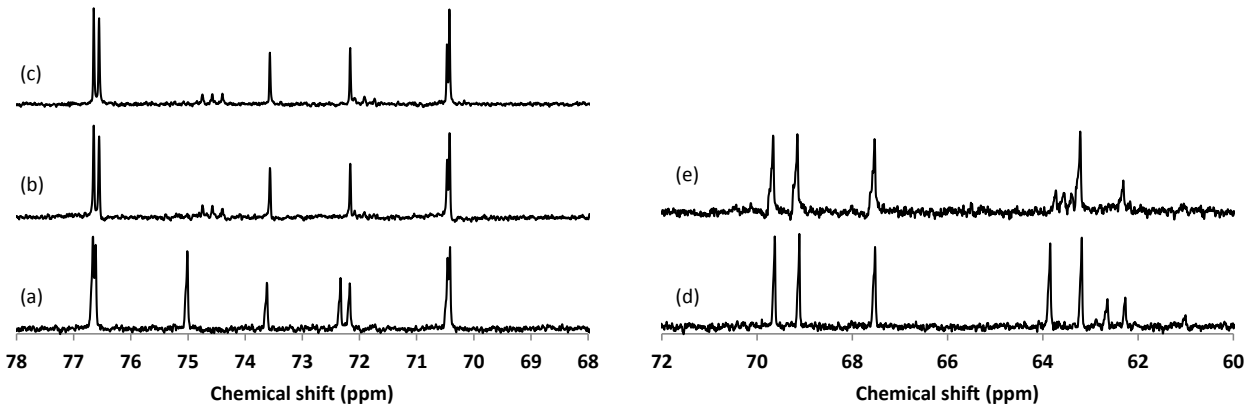

Fig. 9 ^{13}C NMR spectra of unlabeled glucose, unlabeled fructose, and the fractions obtained in the isomerization of glucose-D2 using Beta-ST600.

(a) unlabeled glucose (b) glucose-D2 before reaction (c) glucose-D2 after reaction (d) unlabeled fructose (e) fructose product.

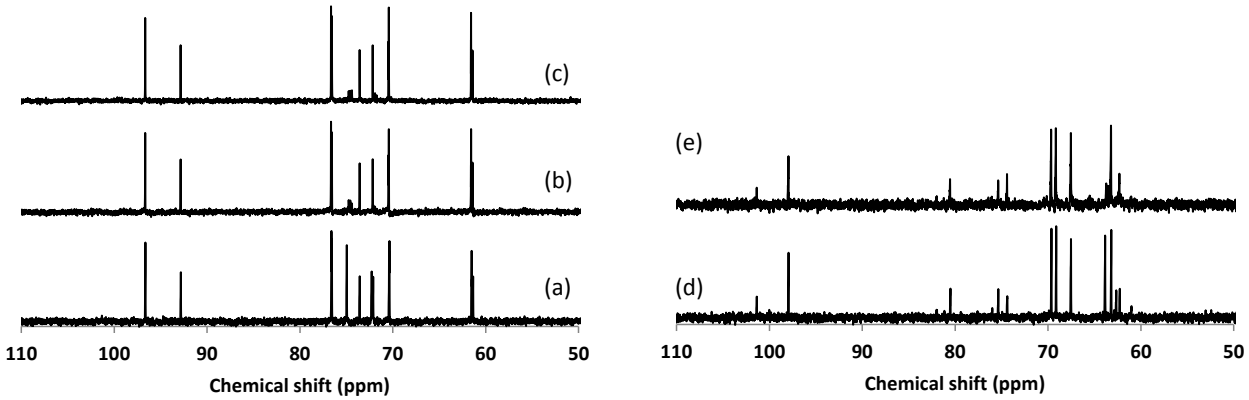

Figure 10 ^{13}C NMR spectra of unlabeled glucose, unlabeled fructose and obtained fractions in the isomerization of glucose-D2 in H_2O solvent using Beta-ST600.

(a) unlabeled glucose (b) glucose-D2 before reaction (c) glucose-D2 after reaction (d) unlabeled fructose (e) fructose product.

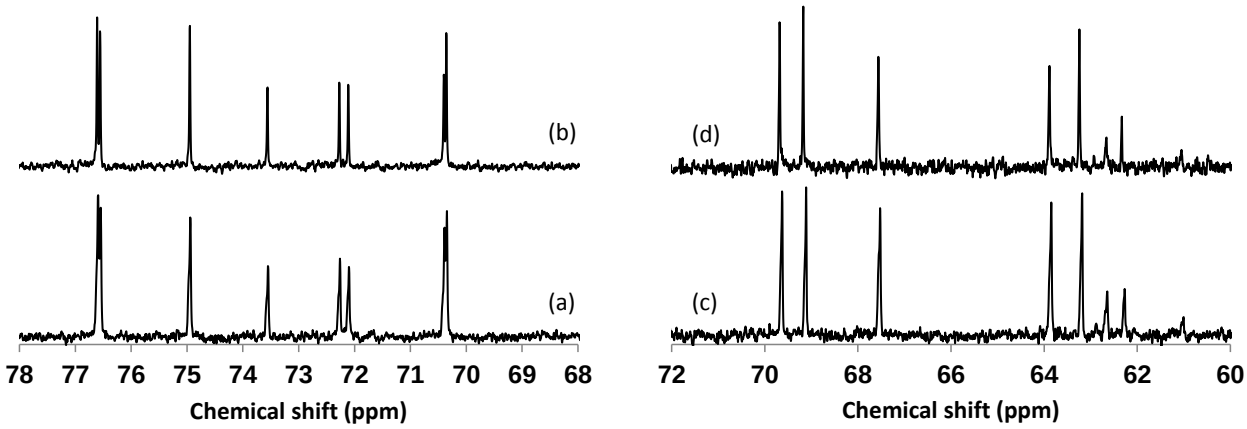

Figure 11 ^{13}C NMR spectra of unlabeled glucose, unlabeled fructose and obtained fractions in the isomerization of glucose in D_2O solvent using Beta-ST600.

(a) unlabeled glucose (b) glucose after reaction (c) unlabeled fructose (e) fructose product.

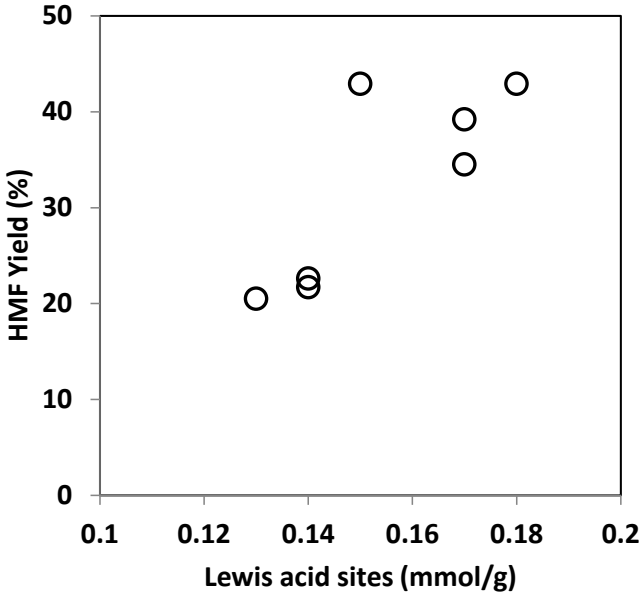

Figure 12 The relationship between the HMF yield and the amount of Lewis acids sites.

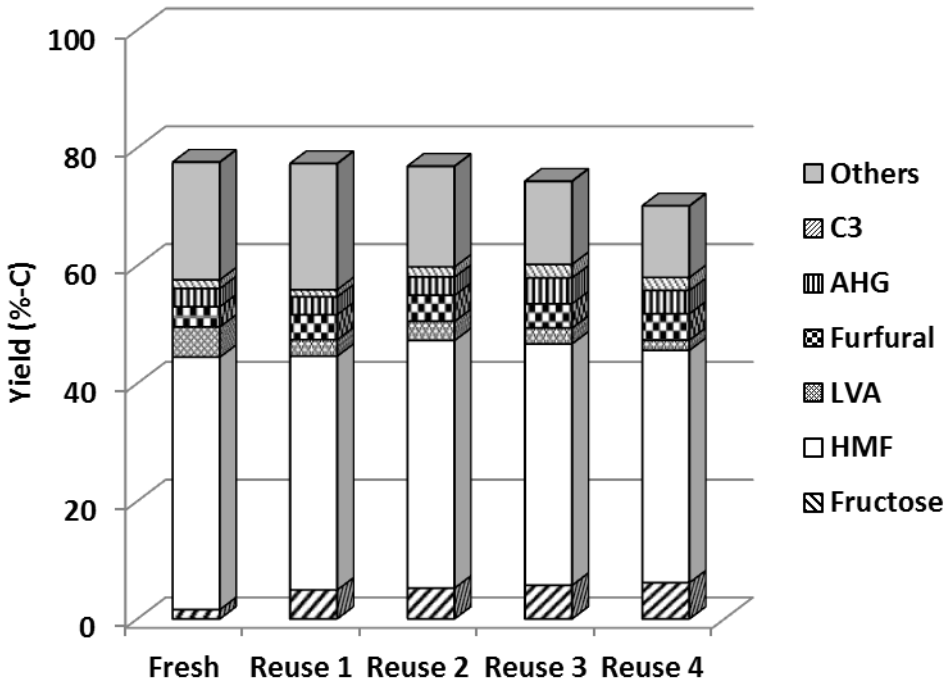

Figure 13 Multiple recycling of Beta-Cal750 catalyst[a, b].

a: Beta-Cal750, 100 mg; Glucose, 0.67 mmol; Water, 4.5 ml; DMSO 0.5 ml; THF 15 ml; Temperature, 180 ºC; Time, 3 h.

b: The catalyst was recovered by filtration after each run and calcined at 550 ºC.

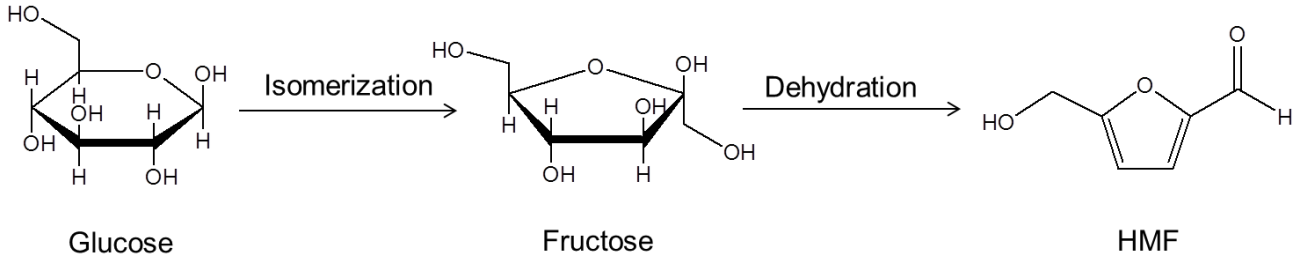

Scheme 1 Transformation of glucose to HMF.

Chapter 3

One-Pot Synthesis of Furfurals from Various Types of Sugars Using Dealuminated Beta Zeolites

Abstract:

The catalytic performance of Beta zeolites in the transformation of various types of sugars to furfurals was investigated. Beta-Cal750, which was prepared by calcination of NH_4-form precursor at 750 ºC and had a relatively large amount of Lewis acid sites formed by the dealumination, effectively promoted the transformation of various types of saccharides including hexoses, oligosaccharides and polysaccharides including cellulose. On the other hand, Beta-Cal500, which had a small amount of Lewis acid sites, showed a better performance in the transformation of xylose than Beta-Cal-750. These results suggest that the suitable acid properties depend on the reactivity of the substrate.

3-1 Introduction

Biomass resources are potential alternatives to crude oil for the production of chemicals and fuels [1-4]. They are mainly composed of polysaccharides in the form of cellulose and hemicellulose. Such polysaccharides are hydrolyzed in the presence of acid catalysts into oligosaccharides, disaccharides and monosaccharides; for example, cello-oligosaccharides, cellobiose, glucose, galactose, mannose, xylose, and arabinose [5,6]. Representative monosaccharides are glucose and xylose, which are a hexose making up the cellulose portion and a pentose constituting hemicellulose portion, respectively. Xylose and glucose can be converted to furfural and 5-hydroxymehtylfurfural (HMF), respectively, through isomerization of aldose to

ketose and subsequent dehydration of ketose to the corresponding furfurals. These compounds are very important because they are intermediate or “plat-form” chemicals for manufacturing chemicals from biomass [7-9]. Therefore, there are many reports on the catalytic transformation of sugars to furfurals.

Aluminosilicate zeolite is a promising candidate as solid acid catalyst for the transformation from the viewpoints of strong acidity, high surface area, hydrothermal stability and cost for its synthesis. The catalytic transformations of sugars over zeolite catalysts have been reported [10-16]. Moreau et al. reported that dealuminated mordenite selectively converted sugars to furfurals [10,11]. Valente et al. reported the catalysis of several kinds of zeolites such as Nu-6(2), ITQ-18, Beta, MCM-22, and ITQ-2 [12-14].

Very recently, I found that the proportion of Lewis acid sites on the zeolite was remarkably increased when the *BEA-type aluminosilicate was simply calcined over 700 ºC or treated with steam over 500 ºC. During these treatments, a part of Si-O-Al bonds surrounding an Al atom were cleaved to form Al species showing Lewis acidity. Thus dealuminated Beta zeolite catalysts were found to be an effective bifunctional catalyst for the transformation of glucose to HMF; the Beta zeolite calcined at 750 ºC with the Si/Al ratio of 15 gave 78 % conversion of glucose in 3 h with a higher selectivity to HMF (ca. 55 %) [17]. I also clarified that Lewis acid sites of the Beta zeolites promote the isomerization of glucose to fructose, which is the rate-determining step in the transformation of glucose to HMF, and Brønsted acid sites enhance the dehydration of fructose to HMF. A catalyst with a relatively large amount of Lewis acid sites gives a high yield of HMF [17].

Complex mixtures of saccharides are produced through hydrolysis of cellulose and hemicellulose, but the isolation and purification of the mixtures are sometimes needed for further reactions. If the mixed saccharides are directly converted to HMF and furfural, the hydrolysis steps of oligo- and di-saccharides into monosaccharides and separation processes can be omitted. Therefore, I investigated the catalytic performance of my developed dealuminated Beta catalyst in the transformation of various types of sugars.

Here, I will report the transformation of various types of saccharides including oligosaccharides and even cellulose to the corresponding furfurals over dealuminated Beta zeolites. Moreover, optimal acid properties of a zeolite catalyst depending on the reactivity of a substrate will be also reported.

3-2 Experimental

3-2-1 Materials

Sugars except for cellulose were purchased from Kanto chemical. Crystalline cellulose was purchased from Aldrich. Other chemicals in reagent grade were purchased from some chemical companies. These compounds were used without any further purification.

3-2-2 Preparation of Beta zeolite catalysts

The aluminosilicate Beta zeolite was synthesized in the media containing fluoride anion according to the previous report [18]. Tetraethylammonium cation was used as structure-directing agent (SDA) in the synthesis. Aluminum isopropoxide (Kanto chemical) was added to tetraethylammonium hydroxide solution (Alfa aesar) with stirring. Then, tetraethyl orthosilicate (TEOS) purchased from Tokyo Chemical Industries was added and the mixture was stirred until the complete evaporation of ethanol. Finally, HF *aq* (Wako) was added. The molar composition of the gel was 1.0 TEOS : 0.5 TEAOH : 0.067 $Al(O^{i}Pr)_3$: 8 H_2O : 0.5 HF. Thus obtained thick gel was transferred to a Teflon-lined stainless steel autoclave and crystallized at 140 ºC for 5 days with tumbling. The solid product was recovered by filtration, washed with distilled water and dried overnight at 100 ºC followed by calcination at 580 ºC to remove SDA. The calcined sample was stirred in 1.0 M NH_4NO_3 solution at 80 ºC for ion-exchange. This treatment was repeated two times to obtain an ammonium form, followed by calcination in air at 500 and 750 ºC.

3-2-3 Catalytic tests

Catalytic reactions were performed in a Teflon-lined stainless-steel autoclave (50 ml), in which the reaction mixture was heated by a heating jacket outside. At a desired point, the reaction was quenched by cooling the autoclave in an ice bath. The reaction mixture was filtered prior to quantitative analysis for removing solid catalyst. For the reactions in the mixed solvent system, the homogeneous solution after the filtration was separated into aqueous phase and organic phase by adding NaCl as salting-out agent. Sugar substrates and water-soluble products in the aqueous phase were analyzed by an HPLC (Shimadzu, LC-20A series) with RI and UV (280 nm) detectors in the ion-exclusion mode. HMF and furfural in the organic phase were analyzed by another HPLC (Shimadzu LC-10A) with UV detectors (260nm). For quantitative calculation, calibration curves were drawn by using the standard materials purchased from chemical companies. Conversion of cellulose was calculated by the weight difference between the recovered unreacted cellulose and the cellulose added.

3-3 Results and discussion

3-3-1 Transformation of mono- and disaccharides to HMF

The dealuminated Beta (Si/Al = 15) were prepared by calcination of NH_4-form Beta zeolite at 750 ºC and it is designated as Beta-Cal750. As a control, typical Beta catalyst (Si/Al = 15), which was obtained by calcination of NH_4-form Beta zeolite at 500 ºC (designated as Beta-Cal500), was used. XRD patterns and physic-chemical properties of these samples are shown in Figure 1 and Table 1.

Beta-Cal750 was able to convert galactose and mannose to HMF with the selectivity over 50 %; Galactose and mannose, which are hexoses abundant in nature as well as glucose, were effectively transformed to HMF (Table 2, Entries 3 and 4). Notably, disaccharides, cellobiose and sucrose, were also directly transformed to HMF in the presence of Beta-Cal750; after 3 h of the reaction, cellobiose was totally consumed and the conversion calculated based on the monomer unit

was 77 % with the selectivity of 52 %. (Table 2, Entry 6). Note that the production of HMF starting from cellobiose was almost similar to that from glucose, indicating that the hydrolysis of cellobiose to glucose was faster than the isomerization of glucose. Sucrose, which consists of glucose and fructose, was more efficiently transformed to HMF with the selectivity of 62 % after 3 h. This is because sucrose more readily hydrolyzed to glucose and fructose, and the reaction of sucrose can be regarded entirely as a reaction of the mixture of glucose and fructose. After 3 h apparent conversions of glucose and fructose units were 76 and 94 %, respectively (Table 2, Entry 7). It was found that disaccharides were directly transformed to HMF with almost the same performances as the transformation of monosaccharides.

3-3-2 Transformation of polysaccharides to HMF

The catalytic application of the dealuminated Beta zeolite was extended to direct transformation of polysaccharides (Table 3). Cornstarch, which is a representative amorphous glucan, was employed as substrate. After 5 h of the reaction at 180 ºC, the reaction mixture was transparent, indicating that polysaccharides immiscible with the solvent were totally converted to lower compounds. The yield of HMF reached to 39 % (Table 3, Entry 3). Upon increasing the reaction temperature to 200 ºC, the HMF yield was improved to 44 % (Table 3, Entry 4), which was slightly lower than that obtained starting from glucose and cellobiose (50 and 49 % respectively, Entries 1 and 2 in Table 3), implying that some losses occurred during the hydrolysis of cornstarch. At present, the selectivity in the transformation of glucose is considered to be a limiting factor for achieving a high yield of HMF from polysaccharides.

Next, the direct transformation of cellulose over the dealuminated Beta zeolite was studied. Cellulose is a crystalline glucan composed of 1,4-β-glycosidic bonds, whose rigid structure makes it difficult to hydrolyze and further transform cellulose. Hence, cellulose has been converted into chemical products via a multi-step transformation (Scheme 1). Prior to the hydrolysis, cellulose is transformed to amorphous glucan by some types of pretreatments such as ball-milling [19-22]. Then

amorphous glucan is hydrolyzed into cello-oligosaccharides in the presence of acid catalysts, followed by the hydrolysis to glucose. Finally, glucose is transformed to desired compounds through various types of chemical reactions. Since such a multi-reaction is energy- and time-consuming, integrated reaction systems have been proposed by some research groups [23-26].

Prior to the investigation of catalytic performance, as a control, the reactivity of cellulose against hydrolysis was examined in the absence of a catalyst because cellulose cannot enter the micropores of the *BEA-type structure. For 5 h of the reaction at 180 ºC, the conversion of cellulose, which is calculated based on the weight, was only 44 % (Table 3, Entry 5). Then the yields of glucose and HMF were 16 and 2 %, respectively and a trace amount of cellobiose was detected (cello-oligosaccharides larger than cellobiose cannot be detected in the present analysis conditions). The increase in the reaction temperature to 200 ºC remarkably improved the reaction rate; the conversion of cellulose was increased to 65 % at 1 h with the glucose yield of 27 % (Table 3, Entry 6). After 3 h, the conversion of cellulose reached to 94 % and 46 % of glucose yield was achieved (Table 3, Entry 7). Once cellulose is hydrolyzed to glucose, the Beta zeolite would catalyze the following transformation to HMF. Therefore, the direct transformation was performed at 200 ºC.

When Beta-Cal750 was introduced into the reaction system, the yield of glucose was decreased along with the increase in the conversion of cellulose but the HMF yield was increased, implying the successive reaction mechanism composed of the hydrolysis of cellulose to glucose and the transformation of glucose to HMF (Table 3, Entries 8 – 10). The conversion of cellulose was not significantly changed by the addition of the catalyst, but the HMF yield was dramatically improved in the presence of the Beta zeolite. These results clearly indicate that cellulose was not catalytically hydrolyzed, but the following transformation to HMF was definitely promoted by the Beta zeolite. When the reaction time was extended to 5 h, the HMF yield reached to 42 %, which is similar to the HMF yield (44 %) obtained in the transformation of cornstarch. Under the conditions, the hydrolysis of cellulose requires longer reaction time than that of cornstarch, but subsequent reactions to HMF similarly proceeded.

To date there have been various types of catalysts applied for the transformation of cellulose to HMF. Antal et al. reported the hydrolysis of cellulose with sulfuric acid formed 5 % yield of HMF as by-product [27]. Raines et al. reported that the combined catalysts of $CrCl_3$ and HCl in dimethylacetamide solvent containing 10 wt% of LiCl showed 33 % yield of HMF from cellulose [28]. Ionic liquids have been extensively used as solvent for the conversion of polysaccharides including cellulose and excellent results have been reported; for example, Chen et al. reported 89 % yield of HMF with $CrCl_2$ catalyst in the imidazolium ionic liquid at 120 ºC for 6 h [29]. Heterogeneous catalysts were also employed but ordinarily the performance was poor compared to homogeneous reaction systems; TiO_2 showed 13 % yield of HMF in water at 250 ºC [30]. My developed Beta zeolite showed 42 % yield of HMF, which is a significantly high performance for a heterogeneous reaction system.

Note that crystalline cellulose can be transformed to HMF in a one pot without any particular treatment prior to the catalytic reaction. I characterized the unreacted cellulose recovered after the reaction and compared with the one before the reaction by XRD, ^{13}C CP/MAS NMR and SEM techniques. Figure 2 shows ^{13}C CP-MAS NMR spectra of the cellulose before and after the reactions. C4 atoms in crystalline domain and in amorphous domain provide the different chemical shifts at 89 and 84 ppm, respectively (assignments of other peaks are inset). The integrated area of these signals indicates crystallinity of glucan [31], but the crystallinity of the cellulose before and after the reaction was not changed, even though organic solvents (THF and DMSO) were contained in the reaction mixture. This result is in accordance with the result on XRD analysis (Figure 3), which is another method for examining the crystallinity of glucan [32,33]anning electron microscopy provides information on the change of morphology of the cellulose during the reaction. Cellulose substrate consists of particles with the size of ~ 50 μm (Figure 4a). In the micrograph for the recovered cellulose, large particles with the length of larger than 50 μm was decreased but smaller particles were extensively found (Figure 4b). It has been reported that particle size and surface area are critical factors determining the reactivity of cellulose [34. It has not been

understood how the particle size was changed during the reaction, the small particle size would contribute to the improved reactivity of crystalline cellulose.

3-3-3 Transformation of xylose to furfural

The catalytic performance of the dealuminated Beta zeolites in the transformation of hemicellulose fractions was also investigated. Figure 5 shows the reaction profiles in the transformation of xylose to furfural over the Beta-Cal500 and -Cal750. As is expected, the transformation proceeded through a successive reaction mechanism in which xylose as aldose is isomerized to xylulose as ketose and thus produced xylulose is dehydrated to furfural, being analogous to the mechanism in the transformation of glucose to HMF. Beta-Cal750, which has a larger amount of Lewis acid sites, showed a higher conversion of xylose than Beta-Cal500, but Beta-Cal500 exhibited a higher furfural yield; the maximum yield of 72 % was achieved at 6 h. Besides, Beta-Cal500 also showed the catalytic activity in the transformation of pentoses other than xylose (Table 4). The different product selectivities in the transformation of xylose are ascribed to the different acid properties. Brønsted acid sites promote the dehydration of xylulose to furfural, but Lewis acid sites cause side reactions of xylulose, reflected in the high selectivity to unknown products of Beta-Cal750 (Figure 5b).

I have found that the selectivity to furfural depends on the ratio of Brønsted acid sites to Lewis acid sites (B/L ratio) and that a catalyst with a high B/L ratio should show a high selectivity to furfural [17]. However, the opposite tendency was seen in the transformation of glucose to HMF (Table 2, Entries 1 and 2), implying that the suitable acid properties vary depending on a kind of reactant and it would be interpreted as follows. Brønsted acid sites are indispensable in all cases for the dehydration of ketoses to furfurals and the catalyst having a high B/L ratio shows high selectivity to furfurals. In addition to Brønsted acid sites, Lewis acid sites enough to promote the isomerization are also indispensable. Hence, the suitable acid properties depend on the amount of Lewis acid sites required for activation of aldoses. Xylose is much more reactive than glucose.

Therefore, a large amount of Lewis acid sites is not necessary; instead, too much amount of Lewis acid sites resulted in a decrease in the selectivity to furfural. On the other hand, glucose requires enough for its activation.

3-4 Conclusions

The catalytic performance of Beta zeolites in the transformation of various types of sugars to furfurals was investigated. Beta-Cal750, which has a relatively large amount of Lewis acid sites formed by the dealumination, can effectively promote the transformation of various types of saccharides including hexoses, oligosaccharides and polysaccharides. Moreover, the reaction system can be applied to the direct conversion of crystalline cellulose to HMF. On the other hand, Beta-Cal500, which has a small amount of Lewis acid sites, shows a better performance in the transformation of xylose than Beta-Cal-750. These results suggest that the suitable acid properties depend on the reactivity of the substrate; For glucose and its derivatives, Lewis acidity is a critical factor and a catalyst having a relatively large amount of Lewis acid sites shows a better catalytic activity and a high yield of HMF, whereas a large amount of Lewis acid sites are not necessary for xylose but a catalyst having a relatively high B/L ratio shows a good selectivity to furfural. My current research is on the further improvement in the selectivity to HMF in the transformation of glucose as well as the changes of cellulose particle during the reaction.

References:

1. J. N. Chheda, G. W. Huber, J. A. Dumesic, Angew. Chem. Int. Ed. 46 (2007) 7164-7183.
2. A. Corma, S. Iborra, A. Velty, Chem. Rev. 107 (2007) 2411-2502.
3. P. Gallezot, Chem. Soc. Rev. 41 (2012) 1538-1558.
4. H. Kobayashi, A. Fukuoka, Green Chem. 15 (2013) 1740-1763.
5. R. Rinaldi, F. Schüth, ChemSusChem, 2 (2009) 1096-1107.
6. P. Mäki-Arvela, T. Salmi, B. Holmbom, S. Willför, D. Y. Murzin, Chem. Rev. 111 (2011) 5638-5666.
7. X. Tong, Y. Ma, Y. Li, Appl. Catal. A: Gen. 385 (2010) 1-13.
8. A. A. Rosatella, S. P. Simeonov, R. F. M. Frade, C. A. M. Afonso, Green Chem. 13 (2011) 754-793.
9. R.-J. van Putten, J. C. van der Waal, E. de Jong, C. B. Rasrendra, H. J. Heeres, J. G. de Vries, Chem. Rev. 113 (2013) 1499-1597.
10. C. Moreau, R. Durand, S. Razigade, J. Duhamet, P. Faugeras, P. Rivalier, P. Ros, G. Avignon, Appl. Catal. A: Gen. 145 (1996) 211-224.
11. C. Moreau, R. Durand, D. Peyron, J. Duhamet, P. Rivalier, Ind. Crop. Prod. 7 (1998) 95-99.
12. S. Lima, M. Pillinger, A. A. Valente, Catal. Commun. 9 (2008) 2144-2148.
13. S. Lima, M. M. Antunes, A. Fernandes, M. Pillinger, M. F. Ribeiro, A. A. Valente, Appl. Catal. A: Gen. 388 (2010) 141-148.
14. M. M. Antunes, S. Lima, A. Fernandes, M. Pillinger, M. F. Ribeiro, A. A. Valente, Appl. Catal. A: Gen. 417-418 (2012) 243-252.
15. R. O'Neill, M. N. Ahmad, L. Vanoye, F. Aiouache, Ind. Eng. Chem. Res. 48 (2009) 4300-4306.
16. S. B. Kim, S. J. You, Y. T. Kim, S. Lee, H. Lee, K. Park, E. D. Park, Korean J. Chem. Eng. 28 (2011) 710-716.
17. R. Otomo, T. Yokoi, J. N. Kondo, T. Tatsumi, Appl. Catal. A: Gen., 470 (2014) 318-326

18. M. A. Camblor, A. Corma, S. Valencia, J. Mater. Chem. 8 (1998) 2137-2145.

19. S. M. Hick, C. Griebel, D. T. Restrepo, J. H. Truitt, E. J. Buker, C. Bylda, R. G. Blair, Green Chem. 12 (2010) 468-474.

20. M. Benoit, A. Rodrigues, Q. Zhang, E. Fourr, K. De Oliveira Vigier, J.-M. Tatibouët, F. Jérôme, Angew. Chem. Int. Ed. 50 (2011) 8964-8967.

21. N. Meine, R. Rinaldi, F. Schüth, ChemSusChem, 8 (2012) 1449-1454.

22. H. Kobayashi, M. Yabushita, T. Komanoya, K. Hara, I. Fujita, A. Fukuoka, ACS Catal., 3 (2013) 581-587.

23. A. Fukuoka, P. L. Dhepe, Angew. Chem. Int. Ed., 45 (2006) 5161-5163.

24. J. B. Binder, R. T. Raines, J. Am. Chem. Soc. 131 (2009) 1979-1985.

25. S. Dutta, S. De, Md. I. Alam, M. M. Abu-Omar, B. Saha, J. Catal. 288 (2012) 8-15.

26. R. Carrasquillo-Flores, M. Käldström, F. Schüth, J. A. Dumesic, R. Rinaldi, ACS Catal. 3 (2013) 993-997.

27. W. S.-L. Mok,d M. J. Antal, Jr., G. Varhegyi, Ind. Eng. Chem. Res. 31 (1992) 94-100.

28. J. B. Binder, R. T. Raines, J. Am. Chem. Soc. 131 (2009) 1979-1985.

29. Y. Zhang, H. Du, X. Qian, E. Y.-X. Chen, Energy Fuels, 24 (2010) 2410-2417.

30. A. Chareonlimkun, V. Champreda, A. Shotipruk, N. Laosiripojana, Fuels, 89 (2010) 2873-2880.

31. R.H. Newman, Holzforschung, 58 (2004) 91-96.

32. L. Segal, J.J. Creely, A.E. Martin Jr., C.M. Conrad, Tex. Res. J. 29 (1962) 786-794.

33. Y Cao, H. Tan, Enzyme Microb. Tech. 36 (2005) 314-317.

34. D. Caulfield, W. E. Moore, Wood Sci. 6 (1974) 375-379.

Table 1 Textural and acid properties of Beta zeolite catalysts.

Catalyst	Si/Al	BET surface area (m^2/g)	Micropore volume (ml/g)	Acid amount (mmol/g)		
				Brønsted	Lewis	B/L
Beta-Cal500	15	632	0.24	0.25	0.13	1.9
Beta-Cal750	15	618	0.23	0.17	0,18	0.94

Table 2 Transformation of hexoses and disaccharides to HMF[a].

Entry	Catalyst	Substrate	Time [h]	Conv.[b] [%]	Selec.[c] [%]
1	Beta-Cal500	Glucose	5	81	50
2	Beta-Cal750	Glucose	3	78	55
3		Galactose	3	80	52
4		Mannose	3	80	55
5		Fructose	1	97	66
6		Cellobiose	3	77	52
7		Sucrose	3	76, 94	62

a: Reaction conditions: catalyst (0.1 g), substrate (0.67 mmol based on monomer unit), water (4.5 ml), DMSO (0.5ml), THF (15 ml), temperature (180 ºC).

b: Conversion of substrate. For disaccharides, conversion based on the monomer unit is shown.

c: Selectivity to HMF.

Table 3 Transformation of polysaccharides to HMF[a].

Entry	Substrate	Conditions	Conv.	Yield [%]	
			[%]	Glucose	HMF
1	Glucose	200 ºC, 2 h	93	-	50
2	Cellobiose	200 ºC, 2 h	> 99	3	49
3	Cornstarch	180 ºC, 5 h	> 99	2	39
4	Cornstarch	200 ºC, 3 h	> 99	3	44
5[b]	Cellulose	180 ºC, 5 h	44	16	2
6[b]	Cellulose	200 ºC, 1 h	65	27	2
7[b]	Cellulose	200 ºC, 3 h	94	46	15
8	Cellulose	200 ºC, 1 h	69	20	17
9	Cellulose	200 ºC, 3 h	88	10	34
10	Cellulose	200 ºC, 5 h	> 99	< 1	42

a: Reaction conditions: catalyst (0.1 g), substrate (0.67mmol based on monomer unit), water (4.5 ml), DMSO (0.5ml), THF (15 ml).

b: Catalyst blank.

Table 4 Transformation of pentoses to furfural[a].

Entry	Substrate	Time [h]	Conv.[b] [%]	Selec.[c] [%]
1	Xylose	3	88	71
2		5	97	74
3	Arabinose	3	77	70
4		5	89	66
5	Xylobiose	3	88	73

a: Reaction conditions: catalyst (0.1 g), substrate (0.67mmol based on monomer unit), water (4.5 ml), DMSO (0.5ml), THF (15 ml), temperature (180 ºC).

b: Conversion of substrate. For xylobiose, conversion based on xylose unit is shown.

c: Selectivity to furfural.

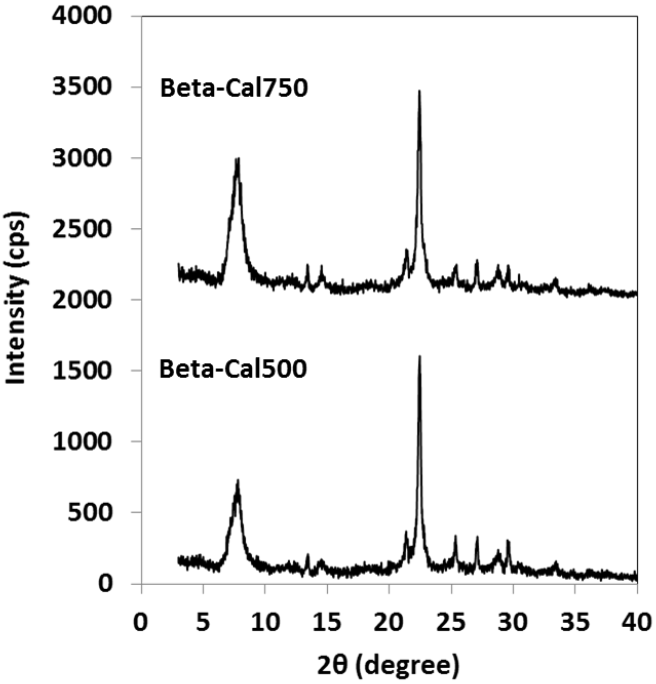

Figure 1 XRD patterns of Beta zeolite catalysts.

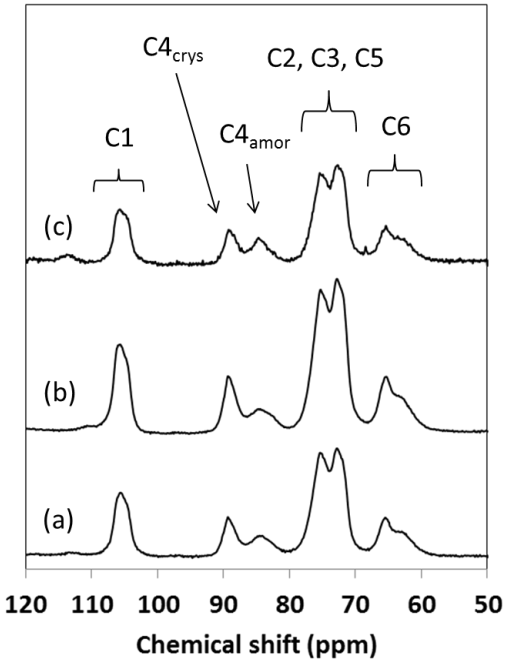

Figure 2 ^{13}C CP-MAS NMR spectra of the cellulose.

a) Before the reaction. b) Recovered after the reaction without a catalyst. c) Recovered after the reaction with Beta-Cal750.

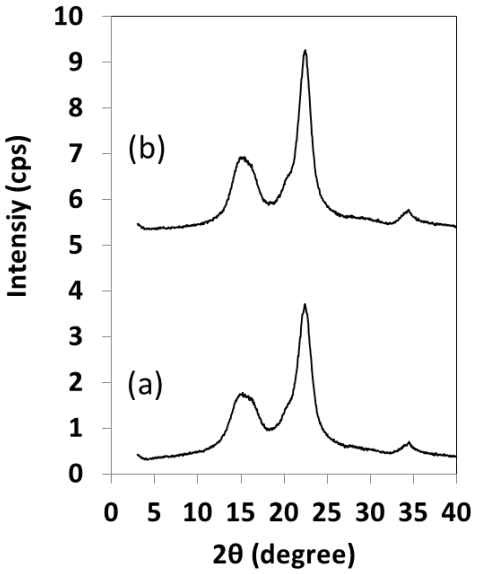

Figure 3 XRD patterns of the cellulose.

a) Before the reaction. b) Recovered after the reaction without a catalyst.

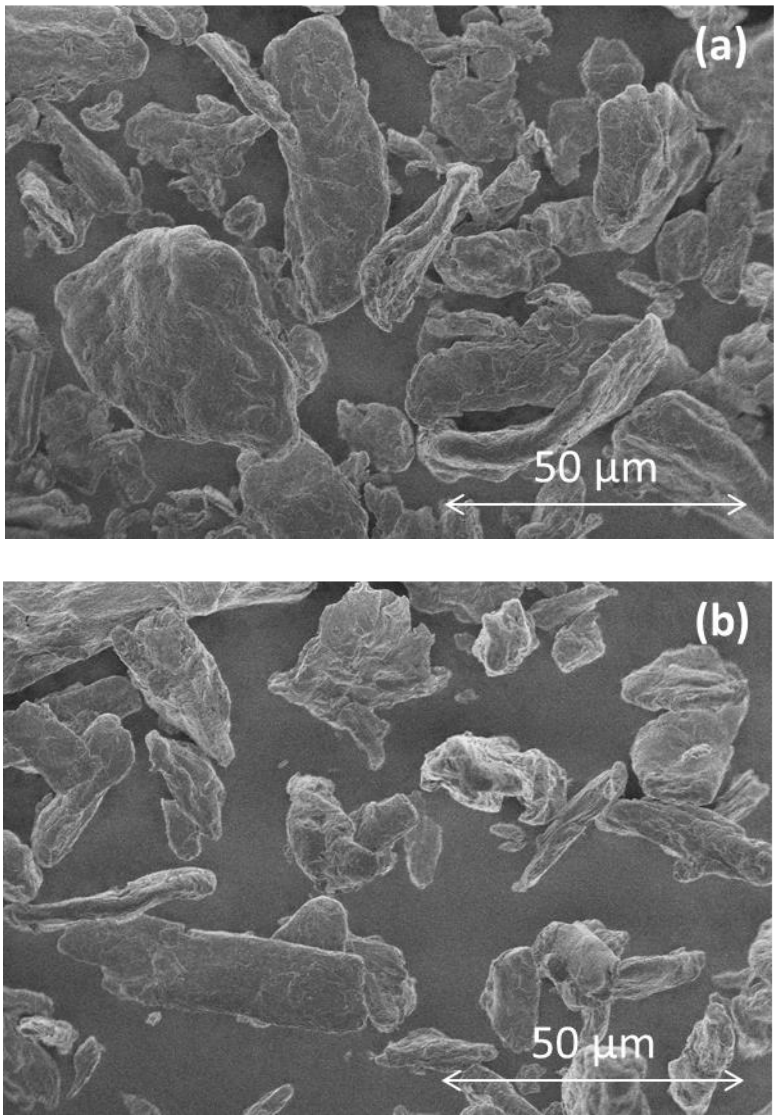

Figure 4 SEM images of the cellulose.

a) Before the reaction. b) Recovered after the reaction without a catalyst.

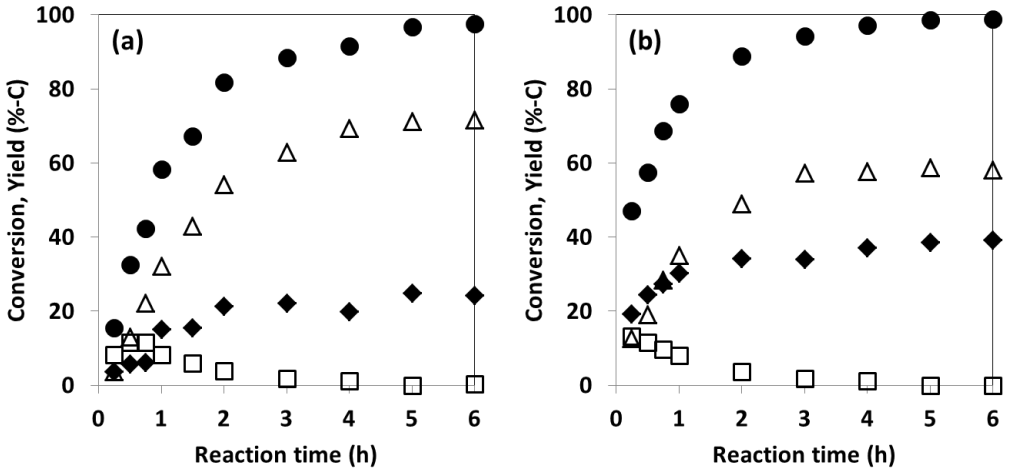

Figure 5 Transformation of xylose to furfural over (a) Beta-Cal500 and (b) Beta-Cal750[a].

(●) xylose conversion, (□) xylulose yield, (△) furfural yield, (◆) unknown yield.

a: Reaction conditions: catalyst (0.1 g), xylose (0.67mmol), water (4.5 ml), DMSO (0.5ml), THF (15 ml), temperature (180 ºC).

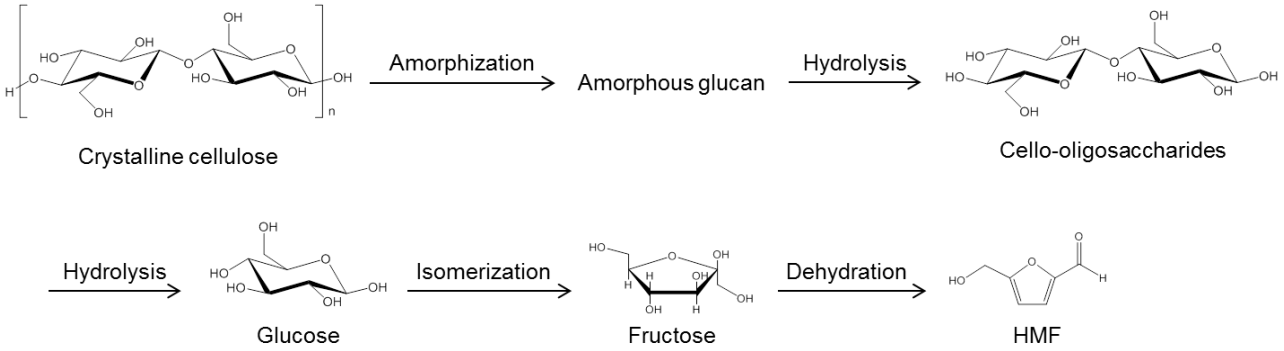

Scheme 1 Multi-step transformation of cellulose to HMF.

Chapter 4

OSDA-Free Beta Zeolite with High Al Content Efficiently Catalyzes a Tandem Reaction for Transformation of Biomass into Useful Chemicals

Abstract:

An environmentally benign route for producing useful chemicals from biomass by using green zeolite catalysts has been successfully developed. Organic structure-directing-agent (OSDA)-free Beta zeolite with a high Al content exhibited a remarkably high catalytic performance in transformation of glucose to 5-hydroxymethylfurfural (HMF); 72 % yield of HMF was achieved at 6 h of the reaction. I found that its high Al content allows OSDA-free Beta zeolite to have the appropriate acid properties for the transformation of glucose to HMF; sufficient amount of Lewis acid sites was generated by calcination of NH_4-form zeolite with a large amount of the original Brønsted acid sites maintained, resulting in the high Brønsted /Lewis acid ratio (B/L ratio) and the proximity of both acid sites.

4-1 Introduction

Beta zeolite, with its intriguing *BEA framework architecture and 3-dimensional 12-membered ring pore system, exhibits excellent catalytic performances in many applications such as acylation of aromatics [1-3] and hydrocracking [4,5]. It also shows unique catalytic properties such as shape-selectivities in particular organic reactions, *e.g.* the rearrangements of allyl benzyl ethers [6], Diels-Alder reactions [7] and Meerwein-Ponndorf-Verley reductions [8-11].

Beta zeolite can be synthesized by a variety of methodologies typically using tetraethylammonium cation as organic structure-directing agent (OSDA) [12-15]. In 2007 Xiao *et al.* reported on the OSDA-free synthesis of Beta zeolite [16]. Since this pioneering report, other groups have also reported the OSDA-free synthesis of Beta zeolite [17-21] and its applications [22]. Today, OSDA-free synthesis is one of the hottest topics in zeolite science, and it has attracted considerable attention because OSDA-free synthesis has several advantages compared to conventional ones using OSDAs. For example, it saves energy consumption, CO_2 and NO_x emission, and cost for an OSDA involved in a zeolite synthesis. Therefore, OSDA-free synthesis of zeolites will certainly contribute to a potential green chemical process if thus prepared zeolites exhibit a high catalytic performance. Unfortunately, Al content of OSDA-free synthesis of zeolites except for the **RTH**-type zeolite (TTZ-1) [23] is generally high and uncontrollable; for OSDA-free Beta, the Si/Al ratio ranges from 4 to 6. Therefore, the dealumination involving steam treatment followed by acid treatment is indispensable for applying the OSDA-free Beta as catalyst for acylation [22].

5-hydroxymethylfurfural (HMF) has been regarded as a bio-based "platform" material into useful chemicals [24-29]. Increasing research interest has been paid to the synthesis of HMF from sugars, particularly glucose because it is the most abundant component of woody biomass. However, this reaction is still a challenging theme because it is a multi-step reaction by way of fructose intermediate, which is more reactive than glucose, and each step requires different types of acids; sufficient Lewis acid sites are necessary to promote the isomerization of glucose to fructose and also Brønsted acid sites are necessary to promote the subsequent dehydration of fructose to HMF [30-34]. A qualitative and quantitative fine-tuning of acid properties is indispensable to achieve a high yield of HMF from glucose.

Herein, I report on an effective transformation of glucose to HMF over OSDA-free Beta zeolite whose acid properties are finely tuned by a facile method making use of its high Al content. The high Al composition of OSDA-free Beta zeolite realizes a high density of acid sites with high

Brønsted/Lewis acid ratio (B/L ratio), which are key factors for selective production of HMF from glucose.

4-2 Experimental

4-2-1 Preparation of Beta zeolite catalysts

Beta(OF) zeolite was prepared following the previous report by Xiao et al. [16]. Sodium aluminate (Wako) was added to NaOH solution and completely dissolved. To the solution was added fumed silica, Cab-O-Sil M5 (Cabot) as Si source and the resulting slurry was stirred for 1 h. After the addition of Beta seed crystal, the obtained aluminosilicate gel with the molar composition of 1.0 SiO_2: 0.02 Al_2O_3: 0.3 Na_2O: 25 H_2O was transferred to a stainless-steel autoclave and hydrothermally treated at 140 ºC for 24 h. The solid product was recovered by filtration, washed with distilled water and dried overnight at 100 ºC. The Na-form sample was stirred in 2.5 M NH_4NO_3 solution at 80 ºC for ion-exchange to ammonium form. The ion-exchange was repeated to obtain a sample free of Na and the sample was calcined at different temperatures (450 – 700 ºC) to obtain proton-form samples.

Beta(TEA) zeolite was synthesized in the media containing fluoride anion [35]. Aluminum isopropoxide (Kanto chemical) was added to tetraethylammonium hydroxide solution (Alfa aesar) with stirring. Then, tetraethyl orthosilicate (TCI) was added and the mixture was stirred until the complete evaporation of ethanol. Finally, hydrofluoric acid (Wako) was added. The molar composition of the gel was 1.0 SiO_2: 0.5 TEAOH: 0.067 $Al(O^iPr)_3$: 8 H_2O: 0.5 HF. Thus obtained thick gel was transferred to a Teflon-lined stainless steel autoclave and crystallized at 140 ºC for 5 days with tumbling. The solid product was recovered by filtration, washed with distilled water and dried overnight at 100 ºC followed by calcination at 580 ºC. The calcined sample was ion-exchanged to NH_4-form in the same way as Beta(OF) zeolites and calcined at 750 ºC.

The commercial USY zeolite was used in this work, which was HSZ-350HUA supplied by Tosoh company.

4-2-2 Characterization of catalysts

Powder X-ray diffraction (XRD) patterns of the prepared samples were collected on a Rigaku Ultima III diffractmeter using a Cu Kα radiation (40 kV, 40 mA). Elemental analyses of the samples (Si/Al ratios) were performed on an inductively coupled plasma-atomic emission spectrometer (ICP-AES, Shimadzu ICPE-9000). Solid-state NMR spectra of hydrated samples were obtained on a JEOL ECA-600 spectrometer. Acid properties of the zeolites were evaluated by FT-IR technique using pyridine as probe molecule. FT-IR spectra were obtained by a Jasco FT-IR 4100 spectrometer equipped with an MCT detector. After the pretreatment at 450 ºC, excess amount of pyridine (~ 1 kPa) was introduced into the cell and the sample was held at that temperature for 15 min. Then the sample was heated to 250 ºC and then the cell was evacuated for 10 min to pump off desorbed pyridine. The sample was cooled to 150 ºC and IR spectra were recorded. For quantitative calculation of adsorbed pyridine, the reported molar extinction coefficient was used [36].

4-2-3 Catalytic tests

Catalytic dehydration experiments were performed in a Teflon-lined stainless-steel autoclave (50 ml), in which the reaction mixture was heated by a heating jacket outside. At a set point, the reaction was quenched by cooling the autoclave in an ice bath. The reaction mixture was filtered prior to quantitative analysis for removing solid catalyst. For the reactions in the mixed solvent system, the homogeneous solution after the filtration was separated into aqueous phase and organic phase by adding NaCl as salting-out agent. Sugar substrates and water-soluble products in the aqueous phase were analyzed by an HPLC (Shimadzu, LC-20A series) with RID and UV (280 nm) detectors in the ion-exclusion mode. HMF and furfural in the organic phase were analyzed by another HPLC (Shimadzu LC-10A) with UV detectors (260nm).

4-3 Results and discussion

4-3-1 Influence of the Brønsted/Lewis acid ratio

First, we evaluated the catalytic performance of OSDA-free Beta zeolite (Si/Al atomic ratio = 5.5) prepared by calcination of the NH_4-form sample at 500 ºC, designated as Beta(OF)-Cal500, in the transformation of glucose to HMF (Figure 1a). The catalytic reactions were performed in the mixed solvent system of water/dimethyl sulfoxide/tetrahydrofuran, which was reported to improve HMF yield and separation efficiency [37]. At early stage of the reaction, the yield of fructose was increased along with the glucose conversion up to the maximum (10 %) at the conversion of 44 %. Then the yield of fructose was continuously decreased and simultaneously the HMF yield was increased. These behaviors imply that the transformation proceeded through a tandem reaction combining the isomerization of glucose to fructose and the subsequent dehydration of fructose to HMF, and that both steps were catalyzed by the single catalyst. The yield of HMF reached to the maximum of 72 % at 6 h, which is the best performance to my knowledge that has been reported so far for a heterogeneous reaction system. At further prolonged reaction time, the HMF yield was gradually decreased due to its consecutive reactions.

For a comparison, catalytic performance of Beta(OF)-Cal700, which was prepared by the calcination of the NH_4-form sample at 700 ºC, was assessed (Figure 1b). The conversion of glucose for Beta(OF)-Cal700 was only a little lower than that for Beta(OF)-Cal500, while the selectivities to fructose and HMF were remarkably different. The maximum yield of fructose was higher (15 %), which was attained at the later point (53 % conversion). The HMF yield was gradually increased along the reaction time and leveled off at 57 %. I consider that the calcination temperature would cause the changes in the state of Al atoms and acid properties of the catalysts, resulting in the different catalytic performances.

Therefore, I investigated the influence of the calcination temperature of Beta(OF) on its structural properties and catalytic performance; the NH_4-form sample of Beta(OF) was calcined with the temperature varied ranging from to 450 to 700 ºC (Table 1). Note that the framework

structure was retained even after the calcination at 700 ºC (Figure 2). The change in the state of Al atoms through the calcination was investigated by the ^{27}Al MAS NMR analyses, revealing that a type of dealumination, a partial cleavage of Si-O-Al bonds of the framework proceeded by the calcination (Figure 3). The NH_4-form sample showed a main peak and a shoulder peak at 57 and 54 ppm, respectively, which are assigned to tetrahedral Al atoms in the ***BEA** framework. Beta(OF)-Cal500 gave a new peak at 0 ppm in addition to two peaks at 54 and 57 ppm, which is assigned to octahedral Al species, indicating that dealumination took place during the calcination at 500 ºC. The calcination at over 600 ºC led to the decrease in the intensity and the broadening of the peaks assigned to the framework Al atoms, suggesting that the calcination at high temperature enhances the dealumination; however, the intensity of the peak at 0 ppm was not increased but decreased. Simultaneously, new broad peaks appeared at 4 and 30 ppm. These peaks are attributed to Al species with distorted octahedral coordination and penta-coordinated Al species, respectively [38,39]. Thus, the calcination of the NH_4-form sample led to the hydrolysis of Si-O-Al bonds in the framework, forming various types of Al species. Other properties of these samples are summarized in Table 2.

Acid properties of these catalysts were evaluated by IR observation using pyridine as probe molecule (Table 1). The amounts of adsorbed pyridine on Brønsted and Lewis acid sites of Beta(OF)-Cal500 were 0.71 and 0.20 mmol/g, respectively. The ratio of the amount of Brønsted acid sites to Lewis acid sites (B/L ratio) was calculated to be 3.6. As the calcination temperature was increased, Brønsted acid sites were decreased due to the dealumination except for the increase from 450 to 500 ºC because NH_4^+ cation is not completely decomposed below 500 ºC, not to form Brønsted acid sites. It is well known that Al species formed by the dealumination show Lewis acidity to promote intra/intermolecular hydride transfer [8-11, 40-43]. The degree of the dealumination was increased along with the increase in the calcination temperature as is seen in the decrease of the peaks at 54 and 57 ppm (Figure 3), but the amount of Lewis acid sites was not so much changed as that of Brønsted acid sites by the calcination temperature. Consequently, the total

amount of apparent acid sites and the B/L ratio were decreased except for the change between 450 and 500 ºC.

The catalytic properties of the Beta(OF) catalysts with different B/L ratios were compared. The product distributions at the glucose conversion of 77-88 % strongly depend on Brønsted acidity of the catalysts. Beta(OF)-Cal450, -Cal500, -Cal550, which have the large amount of Brønsted acid sites (ca. 0.6 - 0.7 mmol/g), showed the high selectivities to HMF (65 - 67 %). On the other hand, the catalysts with a small amount of Brønsted acid sites (ca. 0.2 mmol/g) gave the low selectivities to HMF (45 and 55 %) but the high selectivities to fructose (12 and 15 %). These differences would be attributed to differences in the dehydration rate and its selectivity; the dehydration of fructose to HMF is accelerated by Brønsted acid sites, but Lewis acid sites promote side reactions of fructose, reflected in the amount of unknown products (Figure 1). These results suggest that the catalyst with high B/L ratio shows a high dehydration rate, leading to a high conversion of fructose and a high selectivity to HMF.

Hence, I checked the catalytic performance of Beta(OF) catalysts with different B/L ratios in the dehydration of fructose (Table 3). Beta(OF)-Cal500 with the B/L ratio of 3.6 showed 80 % selectivity at 99 % conversion. The conversion of fructose and the selectivity to HMF were decreased as the B/L ratio was decreased; Beta(OF)-Cal700 with the ratio of 1.1 showed 60 % selectivity at 83 % conversion. There is a correlation between the selectivity to HMF and the B/L ratio (See Figure 4). These results strongly suggest that high B/L ratio is an essential feature for achieving the selective production of HMF [44].

4-3-2 Comparison with conventional zeolite catalysts

As a control, Beta(TEA), which is a conventional Beta catalyst hydrothermally synthesized with tetraethylammonium cation as SDA, was applied to this reaction in order to highlight the advantages of the Beta(OF) catalysts. The catalytic performance of Beta(TEA)-Cal500 with the Si/Al ratio of 15 was evaluated (Table 1, Entry 6). It took 5 h to achieve the conversion of over

80 % because of its low amount of Lewis acid sites. The long reaction time would result in escalated consecutive reactions of HMF, leading to a low selectivity to HMF. The performance of Beta(TEA)-Cal750 having 0.18 mmol/g of Lewis acid sites was also evaluated (Table 1, Entry 7). It showed a low selectivity to HMF (56 %) at a similar conversion (85~86 %), compared to Beta(OF)-Cal500 (66 %). This difference is due to a lower content of Brønsted acid sites on Beta(TEA)-Cal750 (ca. 0.17 mmol/g), which is resulting from its lower Al content because Lewis acid sites that enable the isomerization are generated at the expense of Brønsted acid sites. Effectiveness of the Beta(OF) catalysts was also evaluated by using other zeolites. Since glucose molecule, 0.73 nm in size, is too large to enter the pore of 10-membered ring of zeolites [45-47], USY zeolite with the Si/Al ratio of 5.4 was chosen as representative 12-membered ring zeolite and compared with Beta(OF) catalysts (Table1, Entry 11). USY showed faster reaction rate probably because its large pore openings enhanced the diffusion of glucose molecule. However, Beta(OF)-Cal500 showed the higher selectivity to HMF than USY, even though Beta(OF)-Cal500 and USY have similar Al contents and similar B/L ratios. The reasons for the different catalytic performance between these two types of zeolites are under investigation, but the structure of the zeolite framework might affect its catalytic performance.

4-3-3 Influence of the acid density

As mentioned above, high B/L ratio is a key factor for the selective production of HMF from glucose. Can we obtain HMF in a high yield if a mixture of Beta zeolites with low and high B/L ratios? A mixture of Beta(OF)-Cal700 with a low B/L ratio (1.1) and Beta-B(rich)with a high B/L ratio (8.5) was applied as catalyst with their proportion varied. However, a high catalytic performance was not attained. The combination with 0.1 g of Beta-B(rich) led to the increase in the selectivity to HMF accompanied with the decrease in the selectivity to fructose, indicating that Beta-B(rich) promoted the dehydration of fructose (Table 1, Entries 5 and 8). However, its selectivity to HMF was not higher than that of Beta(OF)-Cal600 in spite of its higher B/L ratio

(Table1, Entries 4 and 8). Furthermore, the combination of 0.1 g of Beta(OF)-Cal700 and 0.5 g of Beta-B(rich) has a B/L ratio similar to that of Beta(OF)-Cal550, while the selectivities to HMF were significantly different; the combination showed 55 % selectivity, but Beta(OF)-Cal550 showed 67 % (Table 1, Entries 3 and 9). These results can be interpreted as follows: The isomerization of glucose was promoted mainly by Lewis acid sites of Beta(OF)-Cal700 (Table1, Entries 5 and 10). Fructose thus generated in micropores of Beta(OF)-Cal700 is subject to consecutive reactions in its micropores due to the high density of acid sites of Beta(OF) catalysts. Hence, the whole selectivity to HMF strongly depends on the selectivity of Beta(OF) catalysts, namely depending on the B/L ratio of Beta(OF) catalysts. Brønsted acid sites should be located close to Lewis acid sites in micropores to effectively producing HMF though the details are under investigation. Furthermore, a large amount of a catalyst led to an increased amount of organic deposition on the catalyst, which partly made up the decrease in the selectivity to HMF.

4-3-4 Reusability of catalyst

The reusability of Beta(OF)-Cal500 catalyst was also checked. The catalyst solid recovered by filtration after each run was thoroughly washed with water and ethanol. After being dried at ambient temperature, the catalyst was used in the next run. Figure 5 shows the conversion of glucose and the product distributions in four consecutive runs. Throughout the runs, the conversion of glucose was steadily constant (86 - 91 %) and the product distributions were almost unchanged either, *e.g.* 65-67 % of HMF selectivity. The amount of Brønsted acid sites was slightly decreased from 0.71 to 0.60 mmol/g and the amount of Lewis acid sites were unchanged after the four runs. Furthermore, it was confirmed that the structural properties of the catalyst are almost unchanged even after the four runs (Figure 6 and 7).

4-4 Conclusions

I have first demonstrated that OSDA-free Beta zeolite can be used without Al atoms leached

as an excellent catalyst for the transformation of glucose to HMF. Beta(OF)-Cal500 gave 72 % yield of HMF at 6 h of the reaction, which is the best performance that has been reported so far for a heterogeneous reaction system. A high B/L ratio and proximity of the two types of acid sites in the Beta catalyst are crucial factors for effectively producing HMF. Beta(OF) catalyst can be reused and the performance were almost retained during the four consecutive runs. The findings shown here will contribute to a sustainable and carbon-saving process in biorefinery.

References:

1. H. K. Heinichen, W. F. Hölderich, J. Catal. 185 (1999) 408-414.
2. U. Freese, F. Heinrich, F. Roessner, Catal. Today, 49 (1999) 237-244.
3. G. Sartori, R Maggi, Chem. Rev. 106 (2006) 1077-1104.
4. E. Blomsma, J. A. Martens, P. A. Jacobs, J. Catal. 165 (1997) 241-248.
5. M. A. Camblor, A. Corma, A. Martínez, V. Martínez-Soria, S. Valencia, J. Catal. 179 (1998) 537-547.
6. J. Wennerberg, F. Ek, A. Hansson, T. Frejd, J. Org. Chem. 64 (1999) 54-59.
7. L. Eklund, A. Axelsson, A. Nordahl, R. Carlson, Acta Chem. Scand. 47(1993) 581-591.
8. E.J. Creyghton, S.D. Ganeshie, R.S. Downing, H. van Bekkum, J. Mol. Catal. A: Chem. 115 (1997) 457-472.
9. P. J. Kunkeler, B. J. Zuurdeeg, J. C. van der Waal, J. A. van Bokhoven, D. C. Koningsberger, H. van Bekkum, J. Catal. 180 (1998) 234-244.
10. O. Bortnovsky, Z. Sobalík, B. Wichterlová, Z. Bastl, J. Catal. 210 (2002) 171-182.
11. B. Akata, J. Warzywoda, A. Sacco Jr., J. Catal. 222 (2004) 397-403.
12. R. L. Wadlinger, G. T. Kerr, E. J. Rosinski, U. S. Pat. 3308069, 1967.
13. R. B. Borade, A. Clearfield, Micropor. Mater. 5 (1996) 289-297.
14. P.R. Hari Prasad Rao, M. Matsukata, Chem. Commun. (1996) 1441-1442.
15. M. A. Camblor, A. Corma, S. Valencia, J. Mater. Chem. 8 (1998) 2137-2145.
16. B. Xie, J. Song, L. Ren, Y. Ji, J. Li, F.-S. Xiao, Chem. Mater. 20 (2008) 4533-4535.
17. G. Majano, L. Delmotte, V. Valtchev, S. Mintova, Chem. Mater. 21 (2009) 4184-4191.
18. Y. Kamimura, W. Chaikittisilp, K. Itabashi, A. Shimojima, T. Okubo, Chem. Asian J. 5 (2010) 2182-2191.
19. Y. Kamimura, S. Tanahashi, K. Itabashi, A. Sugawara, T. Wakihara, A. Shimojima, T. Okubo, J. Phys. Chem. C, 115 (2011) 744-750.

20. B. Xie, H. Zhang, C. Yang, S. Liu, L. Ren, L. Zhang, X. Meng, B. Yilmaz, U. Müller, F.-S. Xiao, Chem. Commun. 47 (2011) 3945-3947.

21. K. Itabashi, Y. Kamimura, K. Iyoki, A. Shimojima, T. Okubo, J. Am. Chem. Soc. 134 (2012) 11542-11549.

22. B. Yilmaz, U. Müller, M. Feyen, S. Maurer, H. Zhang, X. Meng, F.-S. Xiao, X. Bao, W. Zhang, H. Imai, T. Yokoi, T. Tatsumi, H. Gies, T.De Baerdemaeker, D. De Vos, Catal. Sci. Technol. 3 (2013) 2580-2586.

23. T. Yokoi, M. Yoshioka, H. Imai, T. Tatsumi, Angew. Chem. Int. Ed. 48 (2009) 9884-9887.

24. Y. Román-Leshkov, J. N. Chheda, J. A. Dumesic, Science, 312 (2006) 1933-1937.

25. J. N. Chheda, G. W. Huber, J. A. Dumesic, Angew. Chem. Int. Ed. 46 (2007) 7164-7183.

26. X. Tong, Y. Ma, Y. Li, Appl. Catal. A: Gen. 385 (2010) 1-13.

27. M. J. Climent, A. Corma, S. Iborra, Green Chem. 13 (2011) 520-540.

28. A. A. Rosatella, S. P. Simeonov, R. F. M. Frade, C. A. M. Afonso, Green Chem. 13 (2011) 754-793.

29. R.-J. van Putten, J. C. van der Waal, E. de Jong, C. B. Rasrendra, H. J. Heeres, J. G. de Vries, Chem. Rev. 113 (2013) 1499-1597.

30. E. Nikolla, Y. Román-Leshkov, M. Moliner, M. E. Davis, ACS Catal. 1 (2011) 408- 410.

31. C. M. Lew, N Rajabbeigi, M. Tsapatsis, Ind. Eng. Chem. Res. 51 (2012) 5364-5366.

32. Y. J. Pagán-Torres, T. Wang, J. M. R. Gallo, B. H. Shanks, J. A. Dumesic, ACS Catal. 2 (2012) 930-934.

33. J. M. R. Gallo, D. M. Alonso, M. A. Mellmer, J. A. Dumesic, Green Chem. 15 (2013) 85-90.

34. V. Choudhary, S. H. Mushrif, C. Ho, A. Anderko, V. Nikolakis, N. S. Marinkovic, A. I. Frenkel, S. I. Sandler, D. G. Vlachos, J. Am. Chem. Soc. 135 (2013) 3997-4006.

35. M. A. Camblor, A. Corma, S. Valencia, J. Mater. Chem. 8 (1998) 2137-2145.

36. J. Wang, J. C. A. Emeis, J. Catal. 141 (1993) 347-354.

37. Ren, X. Liu, G. Lu, Y. Wang, AIChE J. 59 (2013) 2558-2566.

38. F. Deng, Y. Du, C. Ye, J. Wang, T. Ding, H. Li, J. Phys. Chem. 99 (1995) 15208-15214.

39. S. Li, A. Zheng, Y. Su, H. Fang, W. Shen, Z. Yu, L. Chen, F. Deng, Phys. Chem. Chem. Phys. 12 (2010) 3895-3903.

40. R. M. West, M. S. Holm, S. Saravanamurugan, J. Xiong, Z. Beversdorf, E. Taarning, C. H. Christensen, J. Catal. 269 (2010) 122-130.

41. P. P. Pescarmona, K. P. F. Janssen, C. Delaet, C. Stroobants, K. Houthoofd, A. Philippaerts, C. De Jonghe, J. S. Paul, P. A. Jacobs, B. F. Sels, Green Chem. 12 (2010) 1083-1089.

42. S. Saravanamurugan, M. Paniagua, J. A. Melero, A. Riisager, J. Am. Chem. Soc. 135 (2013) 5246-5249.

43. J. S. Kruger, V. Choudhary, V. Nikolakis, D. G. Vlachos, ACS Catal. 3 (2013) 1279-1291.

44. R. Weingarten, G. A. Tompsett, W. C. Conner Jr., G. W. Huber, J. Catal. 279 (2011) 174.

45. E. Sjoman, M. Manttari, M. Nystrom, H. Koivikko, H. Heikkila, J. Membr. Sci. 292 (2007) 106-115.

46. M. Moliner, Y. Román-Leshkov, M. E. Davis, Proc. Natl. Acad. Sci. USA, 107 (2010) 6164-6168.

47. C. M. Lew, N. Rajabbeigi, M. Tsapastis, Micropor. Mesopor. Mater. 153 (2012) 55-58.

Table 1 Acid properties of Beta(OF) zeolites and their catalytic performances in the transformation of glucose to HMF[a].

Entry	Catalyst	Acidity (mmol/g)[b]			Conversion[c]	Selectivity (%)	
		Brønsted	Lewis	B/L ratio	(%)	Fructose	HMF
1	Beta(OF)-Cal450	0.61	0.21	2.9	81	4	65
2	Beta(OF)-Cal500	0.71	0.20	3.6	86	3	66
3	Beta(OF)-Cal550	0.62	0.22	2.9	88	4	67
4	Beta(OF)-Cal600	0.31	0.24	1.3	86	12	55
5	Beta(OF)-Cal700	0.20	0.19	1.1	80	15	45
6[d]	Beta(TEA)-Cal500	0.25	0.13	1.9	81	1	50
7[d]	Beta(TEA)-Cal750	0.17	0.18	0.94	85	2	56
8[e]	Beta(OF)-Cal700 + Beta-B(rich)			1.5	84	7	55
9[f]	Beta(OF)-Cal700 + Beta-B(rich)			2.9	85	4	55
10	Beta-B(rich)	0.11	0.013	8.5	19	3	39
11	USY	0.42	0.11	3.7	97	3	57

a: Reaction conditions: catalyst, 0.1 g; glucose, 0.67mmol; water, 4.5 ml; DMSO, 0.5ml; THF, 15 ml; temperature, 180 ^{o}C; time, 3 h.

b: Acid properties of the samples were measured by IR observation using pyridine as probe molecule.

c: Conversion of glucose.

d: Time, 5 h.

e: The combination of 0.1 g of Beta(OF)-Cal700 and 0.1 g of Beta-B(rich).

f: The combination of 0.1 g of Beta(OF)-Cal700 and 0.5 g of Beta-B(rich).

Table 2 Structural properties of catalyst samples.

Sample	Si/Al ratio	BET surface area (m^2/g)	Micropore volume (ml/g)
Na-form Beta(OF)	5.4	643	0.25
Beta(OF)-Cal450	5.5	607	0.24
Beta(OF)-Cal500	5.5	603	0.24
Beta(OF)-Cal600	5.5	591	0.23
Beta(OF)-Cal700	5.5	575	0.22
Beta(TEA)-Cal750	15	638	0.25
Beta-Brich	75	663	0.24
USY	5.4	722	0.32

Table 3 Dehydration of fructose to HMF using Beta(OF) zeolite catalysts[a].

Entry	Catalyst	Acidity (mmol/g)			Conversion[b]	Selectivity (%)	
		Brønsted	Lewis	B/L ratio	(%)	Glucose	HMF
1	Beta(OF)-Cal450	0.61	0.21	2.9	98	2	78
2	Beta(OF)-Cal500	0.71	0.20	3.6	99	2	80
3	Beta(OF)-Cal550	0.62	0.22	2.9	96	3	76
4	Beta(OF)-Cal600	0.31	0.24	1.3	85	5	63
5	Beta(OF)-Cal700	0.20	0.19	1.1	83	4	60
6	Beta-Brich	0.11	0.013	8.5	99	1	81

a: Reaction conditions: catalyst, 0.1 g; fructose, 0.67mmol; water, 4.5 ml; DMSO, 0.5ml; THF, 15 ml; temperature, 180 ^{o}C; time, 1 h.

b: Conversion of fructose.

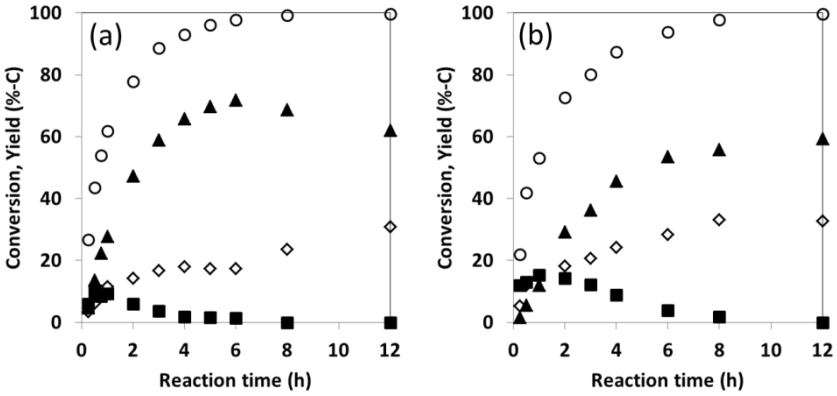

Figure 1 Evolution of glucose conversion (○), fructose yield (■), HMF yield (▲) and unknown products (◇) in the presence of Beta(OF)-Cal500 (a) and Beta(OF)-Cal700 (b).

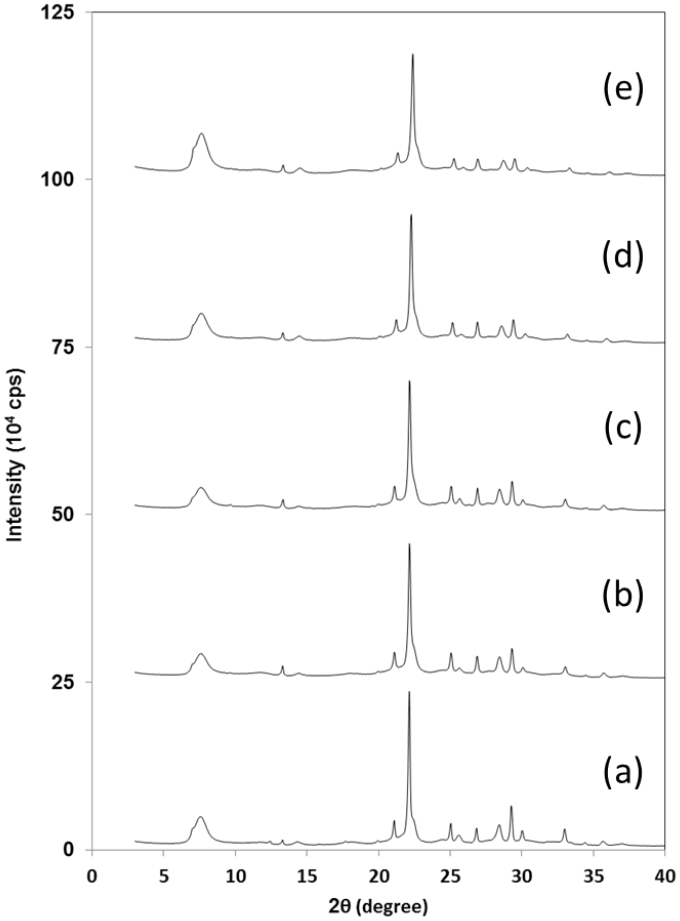

Figure 2 XRD patterns of Beta(OF) samples

(a) Na-form Beta(OF), (b) Beta(OF)-Cal450, (c) Beta(OF)-Cal500, (d) Beta(OF)-Cal600, (e) Beta(OF)-Cal700.

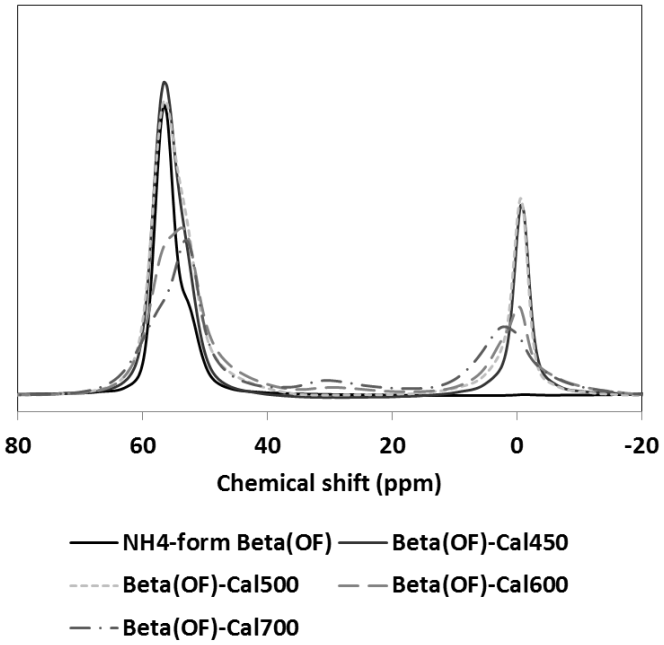

Figure 3 ^{27}Al MAS NMR spectra of Beta(OF) samples.

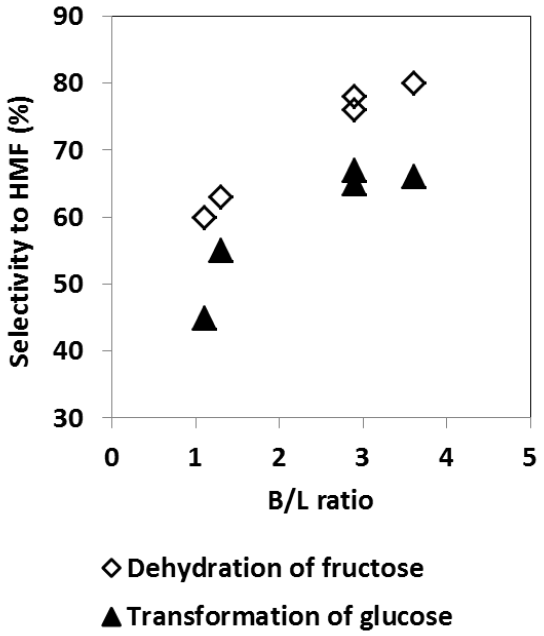

Figure 4 Influence of Brønsted acidity on the catalytic performance.

The selectivities to HMF in the transformation of glucose or dehydration of fructose are plotted.

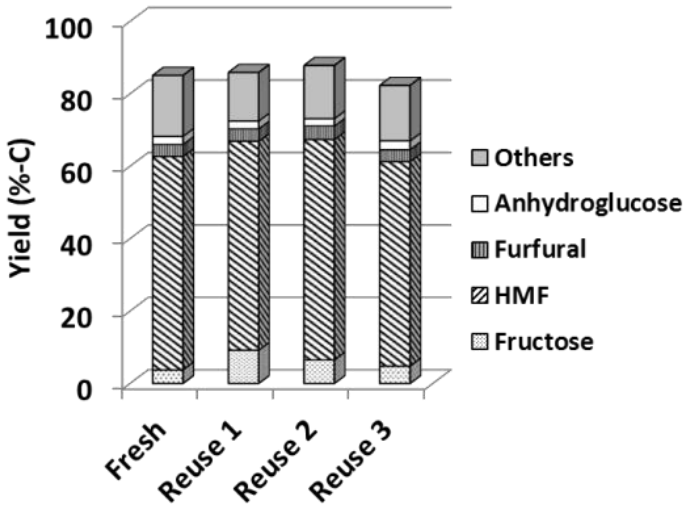

Figure 5 Reuse test of Beta(OF)-Cal500 catalyst[a].

a: Beta(OF)-Cal500, 0.1 g; glucose, 0.67mmol; water, 4.5 ml; DMSO, 0.5ml; THF, 15 ml; temperature, 180 ºC; time, 3 h.

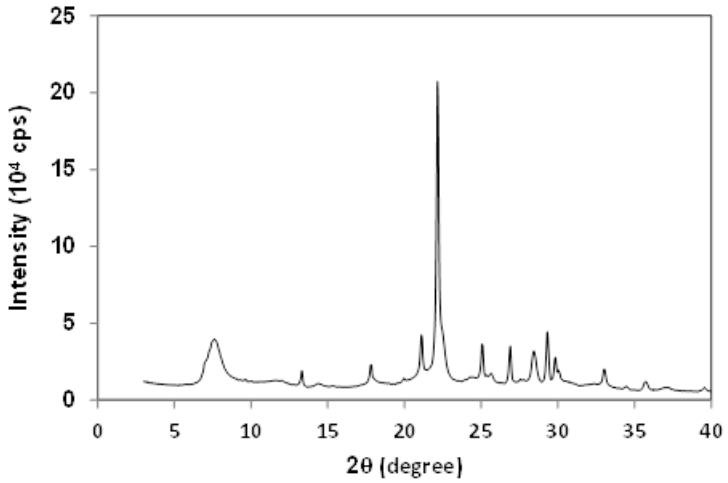

Figure 6 XRD pattern of Beta(OF)-Cal500 after the four consecutive runs.

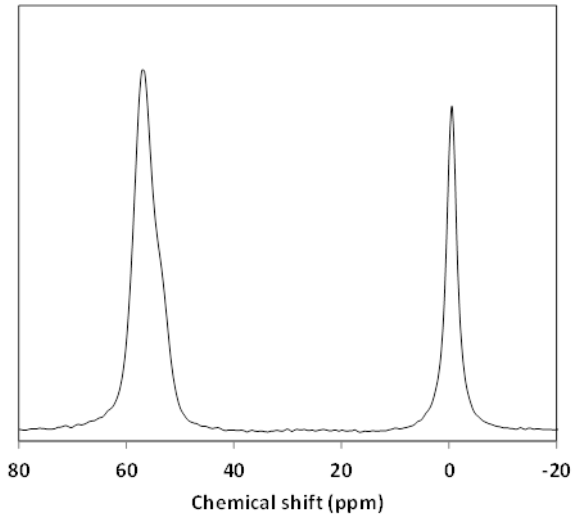

Figure 7 ^{27}Al NMR spectrum of Beta(OF)-Cal500 after the four consecutive runs.

Chapter 5

Synthesis of Beta Zeolite from High-Aluminum Aluminosilicate gel in a High Yield

Abstract:

Beta zeolite was synthesized without using any organic structure-directing agent starting from a sodium aluminosilicate gel with high aluminum composition. The synthesis parameters such as composition of a starting gel, a kind of SiO_2 raw material, and amount of seed crystal were optimized in detail. The amount of NaOH determines the degree of dissolution of SiO_2 raw material and strongly influences the subsequent crystallization process. ***BEA** phase was selectively obtained by using colloidal silica as raw material. Seed crystal directs a growing crystal phase in the syntheses and a certain amount of seed crystal is essential for selectively obtaining ***BEA** phase. Through a mechanistic study, it was found that aluminum atoms dissolved in the mother solution promote the deposition of dissolved species in the form of aluminosilicates onto the surface of seed crystal. Based on this mechanism, increasing the Al content in the starting gel improved a synthesis yield. Under the optimized conditions, highly crystalline Beta zeolite was obtained in >80 % yield, which was significantly high compared to the conventional syntheses.

5-1 Introduction

Synthesis of zeolites without using any organic structure-directing agent (OSDA) has several advantages compared to conventional ones using OSDAs. For example, it saves energy consumption, CO_2 and NO_x emission, and cost for an OSDA involved in a zeolite synthesis. Therefore, OSDA-free synthesis of zeolites is expected to contribute to a potential green chemical

process in the future and today it is one of the hottest topics in zeolite science. Recently increasing types of zeolites have been successfully synthesized without using OSDAs; for example, ECR-1 [1], ZSM-34 [2], Beta [3-8], ZSM-5 small crystal [9,10], RUB-13 [11,12], ZSM-12 [13,14], high-silica ferrierite [15], Levyne [16], nano-sized EMT [17], MFI metallosilicates [18], and Fe-Beta [19].

Among those successful syntheses, the OSDA-free synthesis of Beta zeolite has a significant impact. Beta zeolite, with 3-dimensional 12-membered ring pore system, has been widely investigated and used in industries as catalyst for synthesis of petrochemical and fine chemical products such as hydrocracking [20,21] and acylation of aromatic compounds [22-24]. Beta zeolite shows unique shape-selectivity in the rearrangement of the allyl benzyl ethers [25], Diels-Alder reaction [26] and Meerwein-Ponndorf-Verley reduction [27]. Moreover, increasing attention has been paid to the application as catalyst in NO_x decomposition for automobile exhaust gas [28,29]. In addition to these reported results, as shown in the preceding chapter, Beta zeolite that was prepared by the OSDA-free method reported by Xiao et al. was found to be an effective catalyst for conversion of glucose to5-hydroxymethylfurfural.

In 2007 Xiao et al. first reported on the OSDA-free synthesis of Beta zeolite adopting the seed-direction [3]. Following this report, some research groups have also reported the OSDA-free synthesis of Beta zeolite [4-8] and its catalytic applications [6,30,31]. The critical factors for the seed-assisted synthesis have been reported, but unfortunately the synthesis window was narrow and the synthesis yield was below 30 %. Recently, Xiao et al. reported the rational synthesis method and achieved ~31 % yield [8]. Such low yields are usually found in OSDA-free syntheses of other types of zeolites except for **RTH**-type TTZ-1 [11]. Further improvement of the synthesis yield is strongly desired.

In the present study, I carried out OSDA-free synthesis of Beta zeolite with the assistance of seed crystal starting from sodium aluminosilicate gel with high-aluminum composition. I thoroughly optimized synthesis parameters such as a kind of SiO_2 raw material, alkalinity of the gel and the seed amount. Moreover, I discuss a mechanism for evolution of Beta zeolite during

hydrothermal synthesis.

5-2 Experimental

5-2-1 Materials

Raw materials used in all the syntheses in this work were used as received from chemical companies. Fumed silica (Cab-O-Sil M5, Cabot) or colloidal silica (Ludox HS-40, Aldrich) was used as Si source. Sodium aluminate (Al/NaOH = 0.79, Wako) and aluminum hydroxide (Al_2O_3 content = 55 wt%, Aldrich) were used as Al source in OSDA-free syntheses. $Al(NO_3)_3 \cdot 9H_2O$ (98 %, Wako) and tetraethylammonium hydroxide (TEAOH) solution (35 wt%, Alfa aesar) were used as Al source and OSDA, respectively in synthesis of seed crystal. NaOH (97 %, Wako) was used as alkali source in all the syntheses.

5-2-2 Preparation of seed crystal

Beta zeolite seed crystal was prepared by the conventional hydrothermal synthesis using tetraethylammonium hydroxide as OSDA. Aluminosilicate gel with the composition of 1.0 SiO_2: 0.067 $Al(NO_3)_3$: 0.45 TEAOH: 0.1 NaOH: 20 H_2O was hydrothermally treated at 140 ºC for 3 d. Solid product was recovered by centrifugation, dried at 100 ºC overnight and calcined at 580 ºC for 5 h. The calcined Beta zeolite was soaked into 1 M NaCl solution (100 ml per 1 g of zeolite) and the mixture was stirred at 80 ºC for 2 h to obtain Na-form sample. Finally the recovered Na-form sample was calcined at 580 ºC for 5 h. Thus obtained Na-form Beta zeolite was used as seed crystal in OSDA-free syntheses.

5-2-3 OSDA-Free Synthesis of Beta zeolite

OSDA-free synthesis of Beta zeolite was performed with the gel composition varied. Colloidal silica was used as SiO_2 raw material unless specially notified and its amount was set to 80 mmol for each batch. The composition of other raw materials was varied based on the molar

amount of SiO_2. The composition of the gel was in the following range; 1.0 SiO_2: 0.05-0.18 Al source: 0.4-0.8 NaOH: 25 H_2O: 2.5-20 wt% seed crystal. Gel preparation was performed at ambient temperature and typical procedure for the gel preparation is as follows. Desired amount of Al source was added into NaOH aqueous solution and the mixture was stirred for 30 min. After a SiO_2 raw material was added, the mixture was stirred for 3 h. Beta seed crystal was added and mixed with the gel for 30 min. Thus prepared sodium aluminosilicate gel containing the seed crystal was transferred to a Teflon-lined stainless-steel autoclave (150 ml) and heated at 140 ºC for a set time under static conditions. The solid product was recovered by filtration, thoroughly washed with water and dried at 100 ºC overnight. In some cases, the filtrates were analyzed by NMR spectroscopy.

5-2-4 Characterization of zeolites

Powder X-ray diffraction (XRD) patterns of samples were collected on a Rigaku Ultima III diffractometer using a Cu Kα radiation (40 kV, 40 mA). Chemical compositions of zeolite samples were analyzed by a Shimadzu ICPE-9000 analyzer. Solid-state ^{29}Si MAS NMR spectra were measured on a JEOL ECA-400 spectrometer at a resonance frequency of 79.5 MHz using a 6 mm sample rotor with a spinning rate of 5.5 kHz. Solid-state ^{27}Al MAS NMR spectra were measured on a JEOL ECA-600 spectrometer at a resonance frequency of 156.4 MHz using a 4 mm sample rotor with a spinning rate of 15.0 kHz. ^{29}Si NMR solution NMR spectra were recorded on a JEOL GX500 spectrometer at a resonance frequency of 99.4 MHz using a 5 mm quartz sample tube. The ^{29}Si NMR spectra were recorded with a single pulse acquisition at ambient temperature using a 2/π pulse of 14 μs, a recycle delay of 30 s, and 5000 integrations.

5-3 Results and discussion

5-3-1 Preparation of seed crystal

Aluminosilicate Beta zeolite was prepared by a conventional method using TEAOH as OSDA. The sample after the ion-exchange to Na-form was used as seed crystal. XRD analysis confirmed that thus prepared sample has ***BEA**-type structure (Figure 1). The Si/Al ratio determined by ICP analysis was 13. Scanning electron microscope (SEM) image showed agglomerates of small particles (< 50 nm), indicating that the seed crystal has a large external surface area (Figure 2).

5-3-2 Compositional study

First, influence of the amount of NaOH was investigated by performing hydrothermal syntheses with different amounts of NaOH added. The sodium aluminosilicate gels with the compositions of 1.0 SiO_2: 0.1 $Al(OH)_3$: 0.4-0.8 NaOH: 25 H_2O: 10 wt% seed were crystallized at 140 ºC for 4 days. After the crystallization, the aluminosilicate gel was separated into a solid phase and a liquid phase (mother solution). Figure 3 shows XRD patterns of the recovered solids. In the synthesis at the ratio of $NaOH/SiO_2$ = 0.4, crystallization did not occur at all to give an amorphous material. When the ratio was increased to 0.5, ***BEA**-type crystal mixed with amorphous phase was obtained. At the ratio of 0.6, highly crystalline Beta zeolite was successfully obtained. Its Si/Al ratio was 5.4 and the yield was 53 %, which is significantly improved from the reported results. Further increase of NaOH resulted in the formation of **GIS** phase. At the ratio of 0.8, pure **GIS** crystal was obtained. Note that these syntheses can be perfectly reproduced by using sodium aluminate as Al source. As the amount of NaOH was increased, the Si/Al ratio and the yield of a solid were decreased (Table 1, Entries 1-5). This tendency can be interpreted from the difference in the alkalinity of the mother solution. During the hydrothermal synthesis, alkali including NaOH as mineralizer promotes dissolution of aluminosilicate. The rate and the degree of the dissolution depend on the alkalinity, reflected in a pH value of the solution; as alkalinity of a solution is increased, the rate and the degree of dissolution are increased. Actually, pH values of the filtrates for the hydrothermal syntheses performed with $NaOH/SiO_2$ ratio of 0.4, 0.6 and 0.8 were 11.7, 12.1 and 12.5, respectively. At low alkalinity, crystallization did not occur or very slowly occur. At high

alkalinity undesired crystal phase was obtained, probably because not only amorphous aluminosilicate but also seed crystal dissolved into the solution and the crystallization proceeded without any structure-direction. At moderate alkalinity, both of them partially dissolved into the solution, but amorphous aluminosilicate preferentially dissolved. This study shows that the dissolution rate and the concentration of dissolved species, which are determined by the alkalinity, strongly influence the crystallization rate and resulting crystal phase.

In the seed-directed, OSDA-free synthesis of zeolites, it has been reported that the amount of seed crystal is a critical factor determining the synthesis results [5,10,14]. Therefore, I performed syntheses with different amounts of seed crystal based on the weight of the SiO_2 raw material. The starting gels with the compositions of 1.0 SiO_2: 0.1 $Al(OH)_3$: 0.6 NaOH: 25 H_2O: 0-15 wt% seed were heated at 140 ºC for 4 days. In the synthesis with 10 wt% or higer of seed crystal, crystalline Beta zeolites were obtained (Figure 4). The recovered solid synthesized with a lower amount of seed crystal showed lower X-ray diffraction intensity. In the absence of seed crystal, the peaks assigned to ***BEA**-type framework were not observed at all. These results indicate that the crystallization was initiated by the presence of seed crystal, and the crystallization rate was increased by a large amount of seed crystal.

5-3-3 Crystallization mechanism

Next, the crystallization process was pursued. The sodium aluminosilicate gels with the same composition of 1.0 SiO_2: 0.1 $Al(OH)_3$: 0.6 NaOH: 25 H_2O: 10 wt% seed were prepared in different batches and crystallized at 140 ºC. The hydrothermal treatment was quenched at different points to monitor the crystallization process. XRD patterns in Figure 5 shows the evolution of Beta zeolite. After 1 d of the crystallization, only a halo peak centering at around 25 º was observed. After 2 d, a very small peak superposed on the halo peak appeared at 23.2 º. Thereafter the intensity of the peak increased with the appearance of other peaks assigned to ***BEA**-type structure. At 3.5 d of the crystallization, the halo peak almost disappeared and at 4 d, perfectly crystallized material

was obtained. Further crystallization did not lead to the growth of ***BEA** phase but resulted in the formation of **MOR** phase. Similar evolution processes have been reported for the syntheses starting from the low aluminum composition [6,7]. The recovered solids were characterized by scanning electron microscopy (Figure 6). After 1 d of crystallization, only amorphous material was observed, but after 2 d of crystallization, small crystalline particle (~100 nm) with a specific morphology was observed on the amorphous material. During the crystallization from 2 d to 3.5 d, the size of the crystalline particles was increased to ~1 μm and truncated square-bipyramidal shape of the particle was clearly seen. In the course of the crystallization, the amorphous material was apparently disappeared, which was consistent with the disappearance of the halo peak in the XRD patterns. These samples were also characterized by ^{29}Si MAS NMR (Figure 7). The solids obtained before 2 d gave one very broad band at -102 ppm derived from the amorphous material. When the crystallization time was extended to 2.5 d, the two peaks overlapping the broad band appeared at -105 and -110 ppm. As the crystallization further proceeded, the broad band gradually disappeared. After 4 d of crystallization, four definite peaks appeared at -114.9, -110.2, -104.8 and -99.3 ppm. The peak at -114.9 ppm is assigned to $Si(OSi)_4$ species at T1 and T2 sites [8,32,33]. The peak at -110.2 ppm is assigned to $Si(OSi)_4$ species at T3-T9 sites and $Si(OSi)_3(OAl)$ species at T1 and T2 sites. $Si(OSi)_3(OAl)$ species at T3-T9 sites is expected to appear at around -105 ppm, which corresponds to the peak at -104.8 ppm, but $Si(OSi)_3OH$ species is expected to appears at around -103 ppm, probably overlapping each other. The peak at -99.3 ppm is assigned to $Si(OSi)_2(OAl)_2$ species. The continuous sharpening in the NMR spectra implies that as the crystallization proceeded, Si atoms were settled in geometrically confined locations (T sites) and their coordination environment was defined. Such behaviors were also observed for Al atoms; at first, free or loosely confined Al species were observed as a broad band, but after the crystallization completed, two sharp peaks overlapping each other were observed at 54 and 57 ppm, which are assigned to tetrahedral Al species at T1, T2 sites and T3-T9 sites, respectively.

It is noteworthy that the SiO_2 yields of solid products were unchanged at around 53 % in the

course of crystallization (Table 2). SEM observation reveals that the amorphous material disappeared in the course of crystallization and simultaneously, the crystalline particles grew (Figure 6). These behaviors indicate that during the crystallization, amorphous aluminosilicate dissolves into the solution, but simultaneously dissolved species in the solution were deposited onto a solid. Then deposition preferentially occurs on a seed crystal because amorphous aluminosilicate is more easily dissolved than crystalline seed particle. Consequently the proportion of seed crystal in the solid phase was gradually increased, leading to the growth of crystalline particles. ^{29}Si NMR spectra of the filtrates obtained at 1, 2.5, 4 d during the crystallization are shown in Figure 8. The spectra presents many kinds of (alumino)silicate species including monomer at -72.2 ppm, dimer at -80.8 ppm, trimer -82.3 ppm, and more polymerized species [34-36]. These species appeared in the regions of Q^0 (-72.2 ppm), Q^1 (-78 to -82 ppm), Q^2 (-86 to -91 ppm), Q^3 (-95 to -100 ppm). From 1 d to 4 d, dissolved silicate species and their compositions were almost unchanged, indicating that the dissolution and the deposition of silicate species are in equilibrium. Such dissolution equilibrium was first proposed by Zhdanov in the early days for the synthesis of zeolite A [37]. The concentration of Si atoms in the solution remained constant during the crystallization, but that for Al atoms was changed. The Si/Al ratios of the solids were gradually decreased from 6.0 to 5.4 in the course and Al_2O_3 yield was increased from 89 % to 98 %, indicating that Al species initially present in the solution were incorporated into the solids in the course of crystallization and finally almost completely consumed. Mintova et al. also reported a similar behavior that after the complete crystallization, the Si/Al ratio of the solution becomes infinite and proposed that Al content in the solution is the limiting factor for the crystallization of Beta zeolite [4]. I assume that aluminum species in the mother solution promote the deposition of dissolved species in the form of aluminosilicates onto the surface of seed crystal that is the crystal growth. ^{27}Al NMR spectra of the filtrates showed a broad peak at around 60 ppm, indicating that aluminum atoms were present in the non-monomeric species (not shown).

Possible crystallization mechanism is shown in Figure 9. The behaviors observed in the

present study were similar to those reported for the syntheses of zeolite A through the solution-mediated crystallization mechanism by Zhdanov. Okubo et al. also reported the similar solution-mediated crystallization mechanism for OSDA-free synthesis of Beta zeolite [7]. Therefore, I considered the mechanism with reference to these proposals [37]. (i) Amorphous aluminosilicate gel is separated to a solid phase and a liquid phase with liberation of basic solution from the gel. A part of the gel is dissolved into the solution and these two phases are connected by the solubility equilibrium determined by the compositions of NaOH and Al source (probably also temperature) in the starting gel. (ii) The crystal growth is initiated by the deposition of dissolved aluminosilicate species onto the seed crystal located at the surface of the solid phase. There is an induction period until the equilibrium is formed and the crystal growth starts, which can be observed at 1 d in the crystallization course (Figure 5, 6 and 7).The growth of seed crystal leads to the dissolution of the solid phase, preferentially the amorphous material, into the solution during the crystallization to keep the equilibrium. Because the produced zeolite crystal is less likely to be dissolved, the total reaction moves forward driven by aluminum species in the solution. (iii) Finally the amorphous material was completely consumed and crystallization completes. Then a part of silicate species (in some case, also aluminosilicate species) remains in the solution.

5-3-4 OSDA-free synthesis with high aluminum composition

Based on the above crystallization mechanism, the concentration of Al species in the liquid phase should be high in order to further improve the SiO_2 yield. Therefore, OSDA-free syntheses were performed with the starting Al content increased (Table 3). It is predicted that upon increasing the starting Al content, the formation of undesired crystal phase was likely to occur. However, such sub-phase formation was able to be avoided by increasing the seed amount. In the syntheses performed at starting Si/Al ratio of 8, 15 wt% or higher of seed crystal enabled the selective formation of ***BEA** phase (Entries 1-3). A larger amount of seed crystal facilitates higher surface area on which dissolved aluminosilicate species are deposited, leading to the selective formation of

the desired crystal phase. When the Al content of the starting gel was further increased, Beta zeolites were also successfully obtained. XRD patterns of these samples are shown in Figure 10. Finally when the Si/Al ratio of the starting gel was 5.5, 84 % yield was achieved, which was a significantly high yield compared to the results in early reports. The SiO_2 yield was plotted against the Si/Al ratio in a starting gel in Figure 11. Obviously, the SiO_2 yield was improved by the increase in the Al content in the gel. This correlation strongly supports the mechanism that Al atoms in the solution combined with silicate species deposited onto the seed crystal.

In the syntheses starting from high aluminum content, it took a longer time to complete the crystallization. Such a long crystallization time can be explained from the two reasons. (i) There is an induction time for dissolving amorphous aluminosilicate species until seed crystal is exposed to the solution, but a large amount of the amorphous material covers the seed crystal in a synthesis with high aluminum content. (The SiO_2 yield in the amorphous solid recovered after 1 d was 81 %.) Therefore, it takes a longer induction time. (ii) After the crystal growth is initiated, a certain amount of dissolved species deposited on the surface of the seed crystal. With high aluminum content, a larger amount of deposition occurs until crystallization completes. Moreover, the concentration of silicate species is low at a late stage compared to a synthesis with low aluminum content. Therefore, it takes a longer time for the crystal growth. The decreased concentration resulted in the increase of basicity of the solution. The pH value of the filtrate for Entry 12 in Table 2 was 12.5, while the pH value for Entry 3 in Table 1 was 12.1. Under such stronger basic conditions, a part of aluminosilicate species remains in the solution, which is reflected in the small decrease of Al_2O_3 yield to ~90 %. Moreover, Beta zeolite product would be partly dissolved into the solution under highly basic conditions. Consequently, there is an upper limitation of SiO_2 and Al_2O_3 yields.

The Si/Al ratios of the obtained products were in the narrow range of 5 – 5.5, even though these samples were synthesized from the different starting ratios of 5.5 – 10. Moreover, ^{27}Al MAS NMR spectra of these samples show similar spectra (Figure 12). Based on these results, I speculate that a particular aluminosilicate species deposits onto the surface of seed crystal following some

manners, leading to the similar aluminum distribution in the products. Okubo et al. proposed that *mor* composite building unit in the synthesis solution piles up on the surface of seed crystal [38], but unfortunately, I have not identified the species in the obtained filtrate.

5-3-5 OSDA-free synthesis with fumed silica

The OSDA-free syntheses were performed using fumed silica as Si source and it turns out that a type of SiO_2 raw material is very influential. Figure 13 shows XRD patters of the obtained solids using fumed silica. After 1 d of hydrothermal treatment, the recovered solid shows a small peak at 23.2 º, which was observed after 2 d for the synthesis with colloidal silica (Figure 5). XRD pattern after 3 d of the treatment shows weak diffraction peaks assigned to ***BEA** phase but very weak peaks derived from **MOR** phase were also observed. When the crystallization time was extended to 4 d, diffraction peaks of not only ***BEA** phase but also **MOR** phase became intense. Although fumed silica allowed faster crystallization than colloidal silica, it cannot avoid the formation of **MOR** phase. After the syntheses at 1 d and 4 d, dissolved species in the filtrates were analyzed by ^{29}Si NMR (Figure 8). Some peaks appearing Q^2 and Q^3 regions, particularly at -89.4, -89.8 and -97.3 ppm, were observed with high intensities, while these peaks were ambiguous in the spectra for colloidal silica. I assume that high reactivity of fumed silica, which was reflected in the shorter induction period, produced a variety of dissolved species a part of which was favorable for the formation of **MOR** phase. Similar high reactivity of freeze-dried silica were reported by Mintova et al. [4]. As the crystallization time was prolonged, the Al_2O_3 yield was decreased in the syntheses with fumed silica, while the yield was increased for colloidal silica. Although reasons for this difference have not been elucidated, it might be related to the different crystallization kinetics.

5-4 Conclusions

OSDA-free synthesis of Beta zeolite was successfully achieved starting from high aluminum

composition. A moderate amount of NaOH is necessary for selective formation of ***BEA** phase. At a low alkalinity, dissolution of SiO_2 raw material is insufficient and crystallization did not proceed. At a high content, seed crystal as well as SiO_2 raw material was completely dissolved and the structure direction by the seed crystal was diminished. The crystallization was initiated by the presence of seed crystal, and the crystallization rate was increased by a large amount of seed crystal. The kind of SiO_2 raw material is also important; colloidal silica is more suitable than fumed silica.

Under the hydrothermal conditions employed in this work, crystallization proceeds through the deposition of dissolved species in the form of aluminosilicate onto the surface of seed crystal driven by aluminum species in the solution. When increasing the initial Al content of the starting gel, highly crystalline Beta zeolite was obtained in 84 % yield.

The synthetic strategy presented here is based on the crystallization mechanism and enables a high-yield synthesis in the absence of OSDA, which would be extended to other types of zeolites in the future.

References:

1. J. W. Song, L. Dai, Y. Y. Ji, F.-S. Xiao, Chem. Mater. 18 (2006) 2775-2777.
2. Z. F. Wu, J. W. Song, Y. Y. Ji, L. M. Ren, F.-S. Xiao, Chem.Mater. 20 (2008) 357-359.
3. B. Xie, J. Song, L. Ren, Y. Ji, J. Li, F.-S. Xiao, Chem. Mater. 20 (2008) 4533-4535.
4. G. Majano, L. Delmotte, V. Valtchev, S. Mintova, Chem. Mater. 21(2009) 4184-4191.
5. Y. Kamimura, W. Chaikittisilp, K. Itabashi, A. Shimojima, T. Okubo, Chem. Asian J. 5 (2010) 2182-2191.
6. B. Xie, H. Zhang, C. Yang, S. Liu, L. Ren, L. Zhang, X. Meng, B. Yilmaz, U. Müller, F.-S. Xiao, Chem. Commun. 47 (2011) 3945-3947.
7. Y. Kamimura, S. Tanahashi, K. Itabashi, A. Sugawara, T. Wakihara, A. Shimojima, T. Okubo, J. Phys. Chem. C, 115 (2011) 744-750.
8. H. Zhang, B. Xie, X. Meng, U. Müller, B. Yilmaz, M. Feyen, S. Maurer, H. Gies, T. Tatsumi, X. Bao, W. Zhang, D. De Vos, F.-S. Xiao, Micropor. Mesopor. Mater. 180 (2013) 123-129.
9. G. Majano, A. Darwiche, S. Mintova, V. Valtchev, Ind. Eng. Chem. Res. 48 (2009) 7084-7091.
10. N. Ren, Z.-J. Yang, X.-C. Lv, J. Shi, Y.-H. Zhang, Y. Tang, Micropor. Mesopor. Mater. 131 (2010) 103-114.
11. T. Yokoi, M. Yoshioka, H. Imai, T. Tatsumi, Angew. Chem. Int. Ed. 48 (2009) 9884-9887.
12. M. Yoshioka, T. Yokoi, M. Liu, H. Imai, S. Inagaki, T. Tatsumi, Micropor. Mesopor. Mater. 153 (2012) 70-78.
13. K. Iyoki, Y. Kamimura, K. Itabashi, A. Shimojima, T. Okubo, Chem. Lett. 39 (2010) 730-731.
14. Y. Kamimura, K. Itabashi, T. Okubo, Micropor. Mesopor. Mater. 147 (2012) 149-156.
15. H. Zhang, Q. Guo, L. Ren, C. Yang, L. Zhu, X. Meng, C. Li, F -S. Xiao, J. Mater. Chem. 21 (2011) 9494-9497.
16. H. Zhang, C. Yang, L. Zhu, X. Meng, B. Yilmaz, U. Müller, M. Feyen, F.-S. Xiao, Micropor. Mesopor. Mater.155 (2012) 1-7.
17. E.-P. Ng, D. Chateigner, T. Bein, V. Valtchev, S. Mintova, Science, 335 (2012) 70-73.

18. J. Gu, Y. Jin, Y. Zhou, M. Zhang, Y. Wu, J. Wang, J. Mater. Chem. A, 1 (2013) 2453-2460.
19. H. Zhang, L. Chu, Q. Xiao, L. Zhu, C. Yang, X. Meng, F.-S. Xiao, J. Mater. Chem. A, 1 (2013) 3254-3257.
20. E. Blomsma, J. A. Martens, P. A. Jacobs, J. Catal. 165 (1997) 241-248.
21. M. A. Camblor, A. Corma, A. Martínez, V. Martínez-Soria, S. Valencia, J. Catal. 179 (1998) 537-547.
22. H. K. Heinichen, W. F. Hölderich, J. Catal. 185 (1999) 408-414.
23. U. Freese, F. Heinrich, F. Roessner, Catal. Today, 49 (1999) 237-244.
24. G. Sartori, R Maggi, Chem. Rev. 106 (2006) 1077-1104.
25. J. Wennerberg, F. Ek, A. Hansson, T. Frejd, J. Org. Chem. 64 (1999) 54-59.
26. L. Eklund, A. Axelsson, A. Nordahl, R. Carlson, Acta Chem. Scand. 47(1993) 581-591.
27. E.J. Creyghton, S.D. Ganeshie, R.S. Downing, H. van Bekkum, J. Mol. Catal. A: Chem. 115 (1997) 457-472.
28. B. Coq, M. Mauvezin, G. Delahay, J.-B. Butet, S. Kieger, Appl. Catal. B: Environ. 27 (2000) 193-198.
29. J. Pérez-Ramírez, J.C. Groen, A. Brückner, M.S. Kumar, U. Bentrup, M.N. Debbagh, L.A. Villaescusa, J. Catal. 232 (2005) 318-334.
30. B. Yilmaz, U. Müller, M. Feyen, S. Maurer, H. Zhang, X. Meng, F.-S. Xiao, X. Bao, W. Zhang, H. Imai, T. Yokoi, T. Tatsumi, H. Gies, T.De Baerdemaeker, D. De Vos, Catal. Sci. Technol. 3 (2013) 2580-2586.
31. T. De Baerdemaeker, B. Yilmaz, U. Mueller, M. Feyen, F.-S. Xiao, W. Zhang, T. Tatsumi, H. Gies, X. Bao, D. De Vos, J. Catal. 308 (2013) 73-81.
32. J. Pérez-Pariente, J. Sanz, V. Fornés, A. Corma, J. Catal. 124 (1990) 217-223.
33. G. Valerio, A. Goursot, R. Vetrivel, O. Malkina, V. Malkin, D. R. Salahub, J. Am. Chem. Soc. 120 (1998) 11426-11431.
34. A. Thangaraj, R. Kumar, Zeolites, 10 (1990) 117-120.

35. H. Cho, A. R. Felmy, R. Craciun, J. P. Keenum, N. Shah, D. A. Dixon, J. Am. Chem. Soc. 128 (2006) 2324-2335.
36. M. Haouas, F. Taulelle, J. Phys. Chem. B, 110 (2006) 3007-3014.
37. S.P. Zhdanov, in: E.M. Flanigen, L.B. Sand (Eds.), Molecular Sieve Zeolites-I, ACS Adv. Chem. Ser., vol. 101, 1971, p. 20-43.
38. K. Itabashi, Y. Kamimura, K. Iyoki, A. Shimojima, T. Okubo, J. Am. Chem. Soc. 134 (2012) 11542-11549.

Table 1 Summary of OSDA-free syntheses performed at starting Si/Al ratio of 10.

Entry	$NaOH/SiO_2$	Seed (wt%)	Time (d)	Phase	Si/Al	SiO_2 yield (%)	Al_2O_3 yield (%)
1	0.4	10	4	amorphous	7.1	67	94
2	0.5	10	4	***BEA** + amorphous	6.0	57	96
3	0.6	10	4	***BEA**	5.4	53	98
4	0.7	10	4	**GIS** + unknown	3.5	34	97
5	0.8	10	4	**GIS**	3.9	32	81
6	0.6	0	4	amorphous	6.0	52	87
7	0.6	2.5	4	***BEA** + amorphous	6.2	55	89
8	0.6	5	4	***BEA** + amorphous	5.8	53	91
9	0.6	15	4	***BEA**	5.9	57	97

Table 2 Summary of OSDA-free syntheses performed at starting Si/Al ratio of 5.5 - 8.

Entry	Time (d)	Phase	Si/Al	SiO_2 yield (%)	Al_2O_3 yield (%)
1	1	amorphous	6.0	54	89
2	2	amorphous	6.1	54	88
3	2.5	*__BEA__ + amorphous	5.7	52	91
4	3	*__BEA__ + amorphous	5.7	54	95
5	3.5	*__BEA__	5.7	53	92
6	4	*__BEA__	5.4	53	98
7	5	*__BEA__ + __GIS__ + __MOR__	5.2	49	94

Table 3 Summary of OSDA-free syntheses performed at starting Si/Al ratio of 5.5 - 8.

Entry	Si/Al	NaOH	Seed (wt%)	Time (d)	Phase	Si/Al	SiO_2 Yield (%)	Al_2O_3 Yield (%)
1	8	0.6	10	4	*BEA + GIS + MOR	5.5	60	87
2	8	0.6	15	4	*BEA	5.6	63	89
3	8	0.6	20	4	*BEA	6.1	68	89
4	7	0.6	15	4	*BEA	5.5	71	90
5	7	0.65	15	4	*BEA	5.3	69	91
6	7	0.7	15	4	*BEA + trace MOR	4.8	62	90
7	6	0.55	15	6	*BEA	5.5	80	88
8	6	0.6	15	4	*BEA + amorphous	5.4	79	88
9	6	0.6	15	5	*BEA	5.2	77	89
10	6	0.65	15	5	*BEA + GIS	4.8	69	87
11	5.5	0.6	15	1	amorphous			
12	5.5	0.6	15	5	*BEA + amorphous	5.1	81	87
13	5.5	0.6	15	6	*BEA	5.2	84	89
14	5.5	0.65	15	5	*BEA + GIS	4.5	72	88

Table 4 Summary of OSDA-free syntheses using fumed silica as raw material

Entry	Time [d]	Phase	Si/Al	SiO_2 yield [%]	Al_2O_3 yield [%]
1	1	amorphous	5.6	48	87
2	2	*__BEA__ + amorphous	5.5	45	82
3	3	*__BEA__ + trace __MOR__	5.0	42	84
4	4	*__BEA__ + __MOR__	5.1	42	81

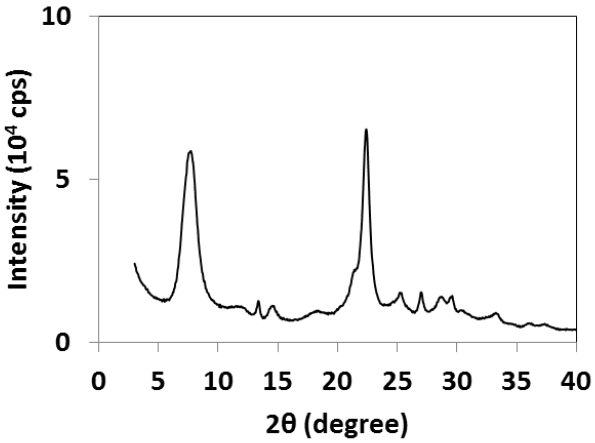

Figure 1 XRD pattern of the seed crystal.

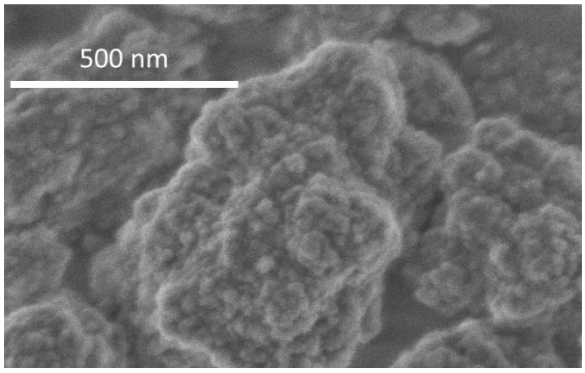

Figure 2 SEM image of the seed crystal.

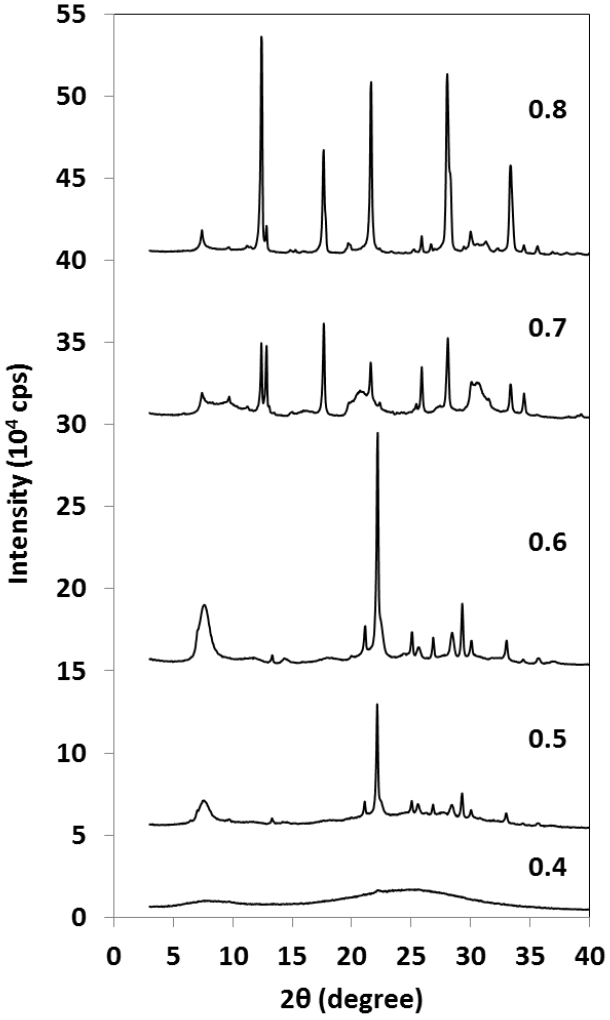

Figure 3 XRD patterns of samples synthesized with different Na amounts.

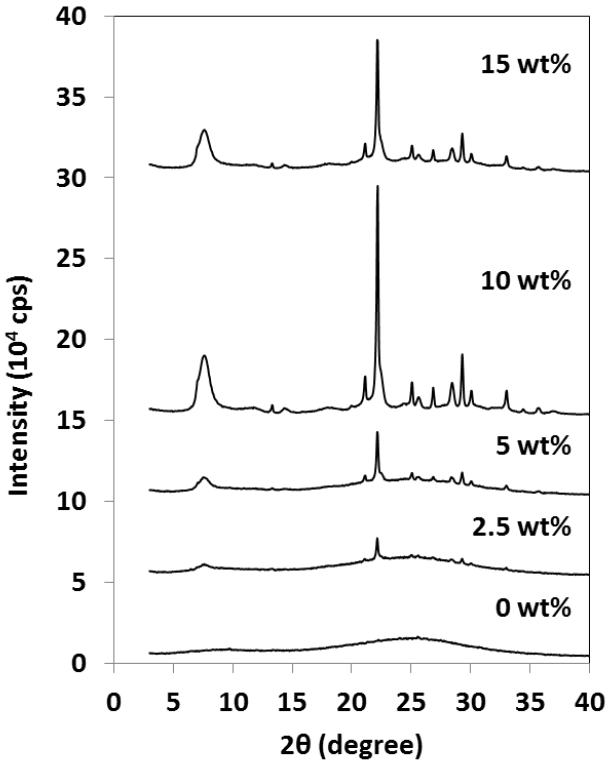

Figure 4 XRD patterns of samples synthesized with seed amount varied.

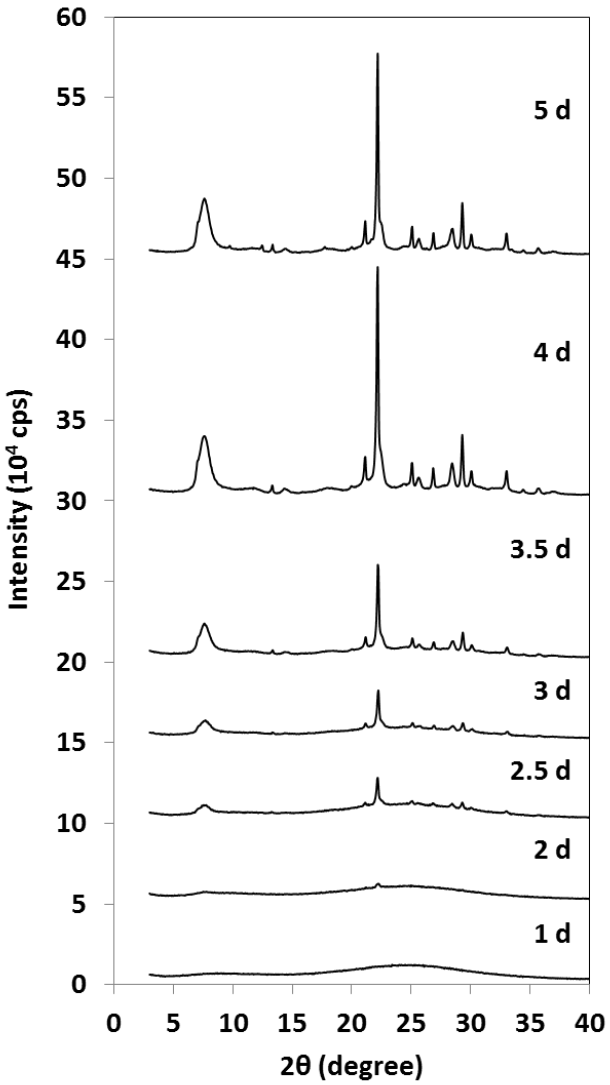

Figure 5 Monitoring the evolution of Beta zeolite by XRD analysis.

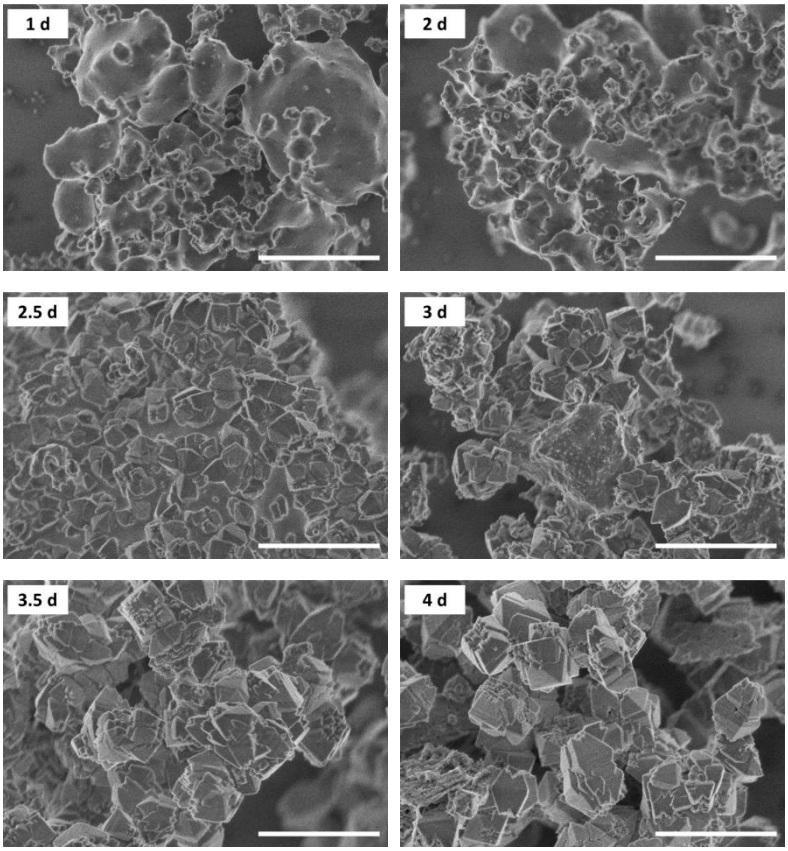

Figure 6 Monitoring the evolution of Beta zeolite by SEM observation. Scale bar in each corresponds to 2 μm.

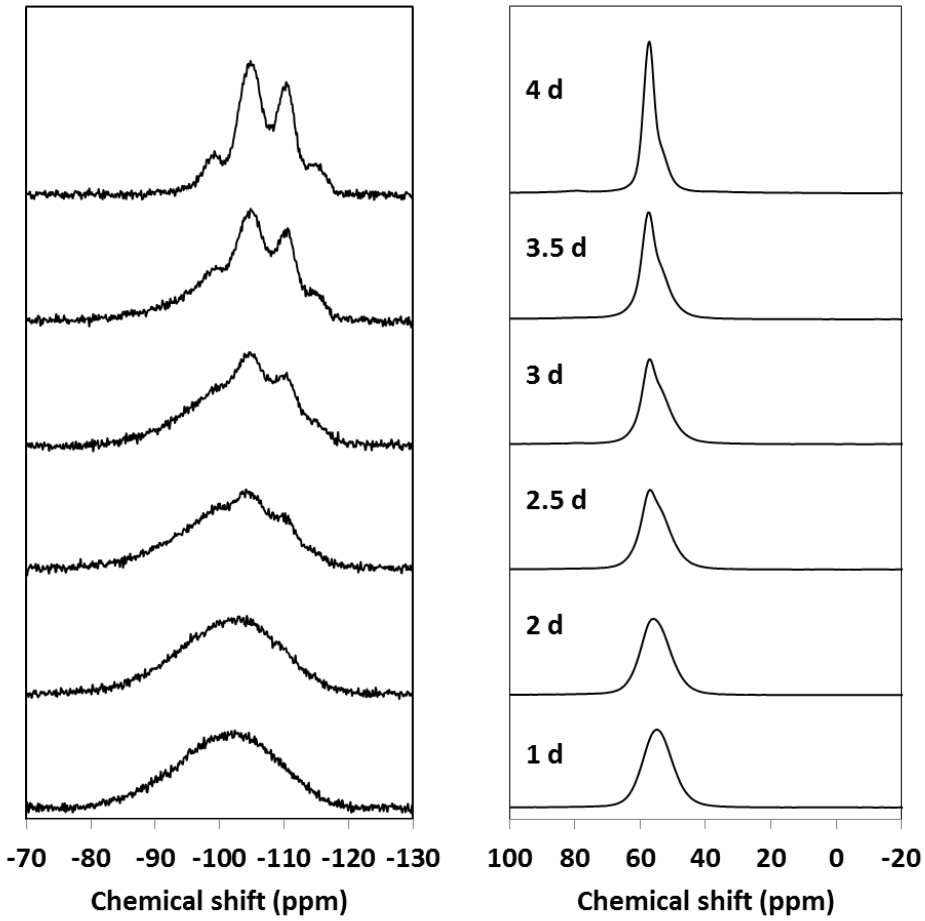

Figure 7 Monitoring the evolution of Beta zeolite by (left) 29Si and (right) ^{27}Al MAS NMR spectroscopy.

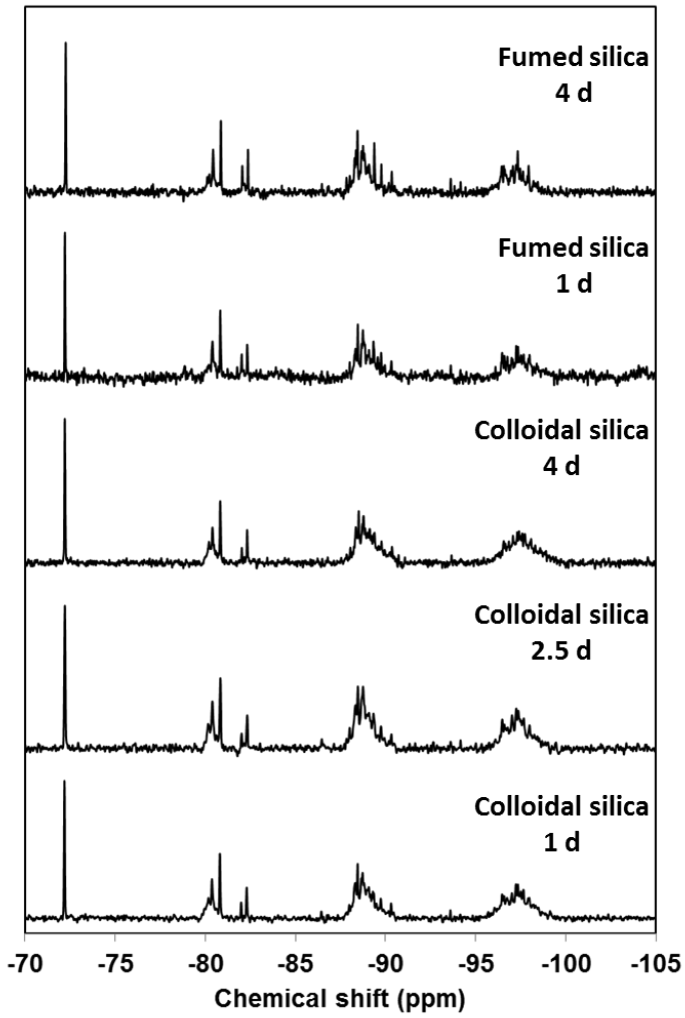

Figure 8 ^{29}Si NMR spectra of the filtrates at different crystallization times.

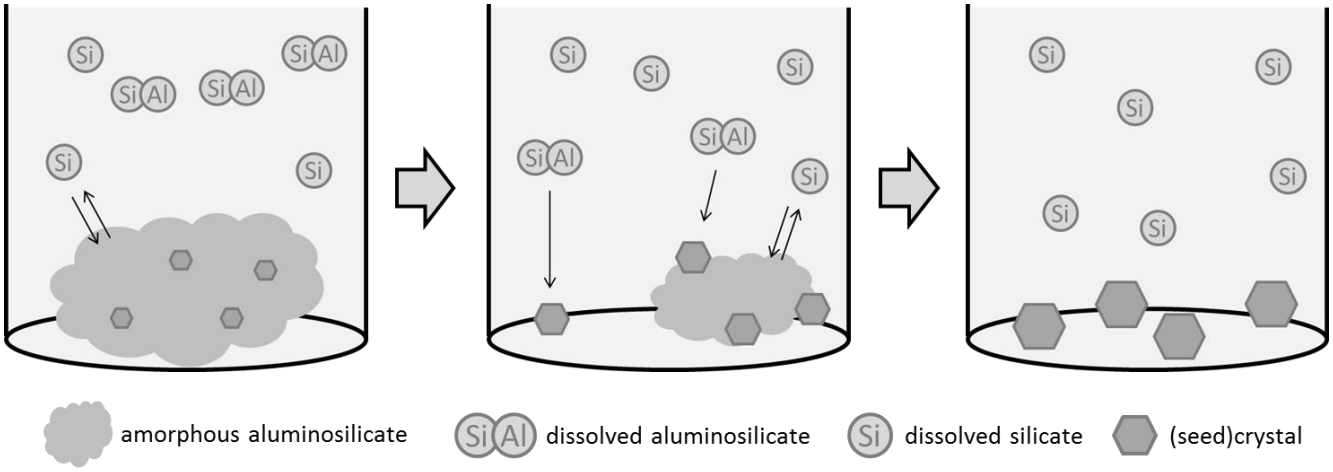

Figure 9 Schematic illustration of evolution Beta zeolite in the absence of OSDA

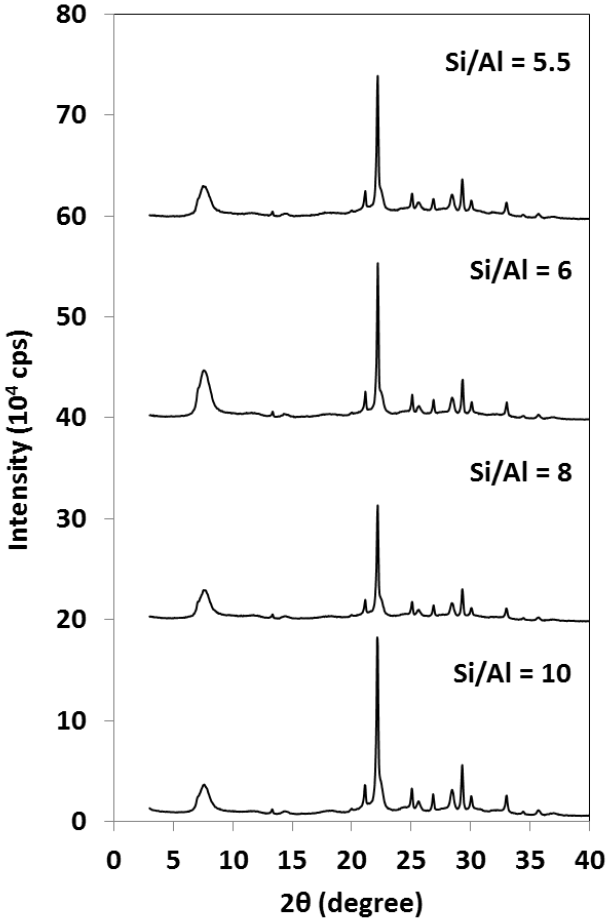

Figure 10 XRD patterns of Beta zeolites synthesized with various starting Si/Al ratios.

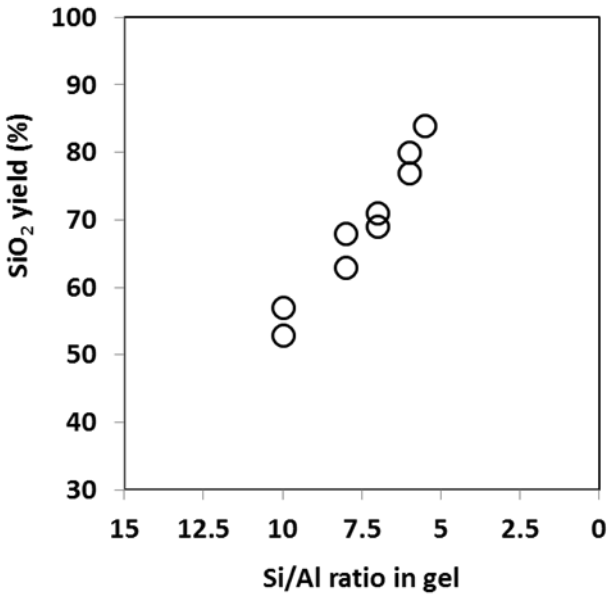

Figure 11 The relationship between SiO_2 yield and Si/Al ratio in a starting gel.

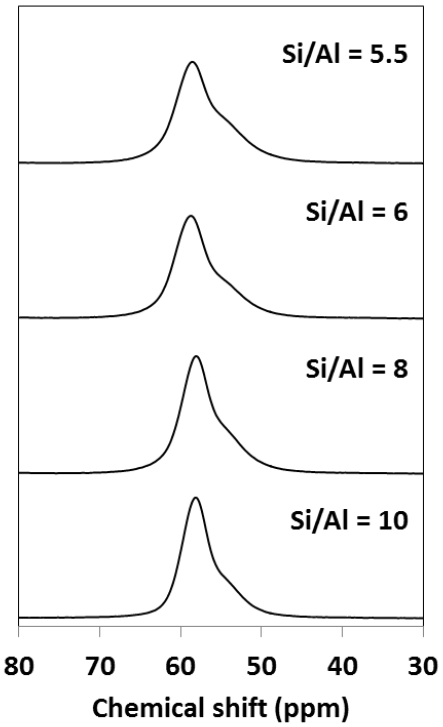

Figure 12 ^{27}Al NMR spectra of Beta zeolites synthesized with various starting Si/Al ratios.

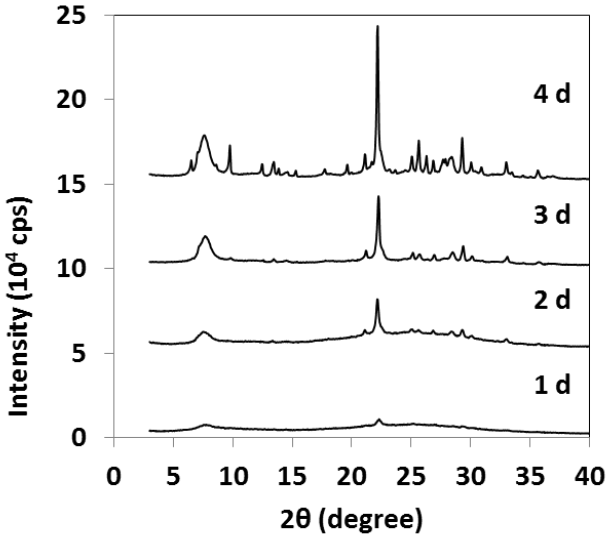

Figure 13 Monitoring of evolution of Beta zeolite synthesized with fumed silica.

Chapter 6

High-silica Beta Zeolite as Efficient Catalyst for Dehydration of Sorbitol to Isosorbide

Abstract:

Dehydration of sorbitol in water was thoroughly studied using aluminosilicate zeolites as heterogeneous catalysts. Catalytic performance of a zeolite strongly depends on structural and compositional properties. 3-dimensinal large pore structure is favorable to enhance the diffusion of sorbitol and/or dehydration products. Zeolite catalysts with high-silica compositions showed superior catalytic performances due to their hydrophobicity. Hydrothermal stability is another critical factor determining the performance of a catalyst; some USY zeolites were hydrothermally unstable under the reaction conditions and showed poor activities, but other types of zeolites showed high hydrothermal stability. Among the zeolite catalysts tested, ***BEA**-type zeolites showed remarkably high catalytic performances; especially, Beta zeolite with Si/Al ratio of 75 achieved 82 % yield of isosorbide. The influence of reaction parameters e.g. temperature and catalyst dosage were also investigated. Finally, the reusability of a catalyst was also investigated.

6-1 Introduction

Extensive research has been carried out to study the utilization of biomass into useful chemicals and fuels [1-5]. Sorbitol is a promising material derived from biomass and it is ranked as one of the top 12 important targets from biomass [6-8]. Conventionally, sorbitol has been produced in industry through hydrogenation of glucose derived from starch by using modified Raney-Ni catalysts and other supported metal catalysts [9-11]. In the past decade, however, increasing

research effort has been devoted to the production of sorbitol from cellulose as non-food biomass because it is renewable, abundant in the worldwide, available in a large scale, and cheap. In 2006 Fukuoka et al. first reported the hydrogenolysis of cellulose to sorbitol and mannitol over Pt/γ-Al_2O_3 [12]. Later other research groups reported the production of sorbitol from cellulose by using the supported metal catalysts [13-20]. Recently, Schüth et al. reported the two-step process combining mechanocatalytic depolymerization of cellulose and subsequent hydrogenolysis to achieve 91% yield of sorbitol [21].

Isosorbide (1,4:3,6-dianhydro-D-sorbitol) is one of the most important chemical compounds, which is produced through double intramolecular dehydration of sorbitol (Scheme 1). Because of tis high stability and two functional groups, isosorbide has many applications in wide industrial fields and there is a review on the properties, production route and applications of isosorbide [22]. The most important application of isosorbide is in the pharmaceutical field. It can reduce blood pressure for brain tumors, head injuries and glaucoma. It is also the medicine for Ménière's disease and a diuretic agent [7]. Isosorbide mononitrate and dinitrate are medicines for angina pectoris and they are more effective than glycerol trinitrate in several points [23]. Another important application of isosorbide is as plastic monomer [24,25]. Poly-(ethylene-co-isosorbide)terephthalate (PEIT) is bio-based alternative to PET and shows a high glass transition temperature by increasing the proportion of isosorbide monomer, which is advantageous for using the PEIT bottle with hot water filled [26]. Isosorbide also replaces bisphenol A in the production of polycarbonate and epoxy resins with high functionality [27,28].

Dehydration of sorbitol to isosorbide has been investigated by many researchers and many types of acid catalysts including homogeneous [29-37] and heterogeneous catalysts [38-45] have been used. Huchette and Flèche reported that sorbitol was dehydrated to isosorbide in 77 % yield by using sulfuric acid as catalyst *in vacuo* at 135 ºC for 15 h [31]. This process achieved the high yield, but requires neutralization and decoloration of the dark-colored mixture. Later, Yamaguchi et al. reported the dehydration of sorbitol in water at high temperature without any acid catalysts added

[33]. Recently, Makkee et al. reported the production of isosorbide from cellulose in molten salt hydrate medium and they achieved 95 % yield [34,35]. For industrial application, a heterogeneous system has advantages in many points. Therefore, many types of heterogeneous catalysts have been explored; for example, modified metal oxides [38-41], metal phosphates [42], supported heteropoly acids [43], supported metals [44], and ion-exchange resin [31,45]. Among those solid acid catalysts, sulfated titania catalyst exhibited the best performance, ~75 % yield of isosorbide under reduced pressure (0.3 bar) [41].

In the present study, we focused on aluminosilicate zeolites and evaluated their catalytic performances in the dehydration of sorbitol to isosorbide. Influence of the properties of zeolites such as framework type, framework composition and crystallinity was extensively investigated. Moreover, the reaction parameters were thoroughly optimized. Among the zeolite catalysts tested, high-silica Beta zeolite was found to be a promising catalyst for the dehydration of sorbitol to isosorbide.

6-2 Experimental

6-2-1 Materials

The aluminosilicate zeolites used in this work except for MCM-68 were purchased from chemical companies or kindly given by Catalysis Society of Japan as follows: ZSM-5 (Si/Al = 13, Catalysis Society of Japan, JRC-Z5-25H), ZSM-5 (Si/Al = 40, Zeolyst, CBV8014), ZSM-5 (Si/Al = 140, Zeolyst, CBV28014), Mordenite (Si/Al =10, Catalysis Society of Japan, JRC-Z-HM20(2)), Mordenite (Si/Al = 45, Catalysis Society of Japan, JRC-Z-HM90), Mordenite (Si/Al = 110, Tosoh, HSZ-690HOA), Beta (Si/Al =13, Catalysis Society of Japan, JRC-Z-HB25), Beta (Si/Al = 75, Catalysis Society of Japan, JRC-Z-HB150), Beta (Si/Al = 150, Zeolyst, CP-811C-300), Y (Si/Al = 3, Catalysis Society of Japan, JRC-Z-HY5.6(2)), USY (Si/Al = 5, Tosoh, HSZ-350HUA), USY (Si/Al = 30, Zeolyst, CBV760), USY (Si/Al = 55, Tosoh, HSZ-385HUA). All the catalysts were calcined at 550 ºC for 6 h prior to the use. Zeolite samples are designated with their Si/Al ratios in the

parentheses. Other chemicals were purchased from chemical companies and used without any further purification: D-sorbitol (Wako), 1,4-anhydro-D-sorbitol (1,4-AHSO, Tronto Research Chemicals), 1,5-anhydro-D-sorbitol (1,5-AHSO, Wako) and 2,5-anhydro-D-sorbitol (2,5-AHSO, Tronto Research Chemicals) were used.

6-2-2 Preparation of MCM-68 catalysts

The aluminosilicate zeolite MCM-68 was synthesized according to the previous report [46]. *N*,*N*,*N'*,*N'*-tetraethyl-*exo*,*exo*-bicyclo[2.2.2]oct-7-ene-2,3:5,6-dipyrrolidinium diiodide was used as structure-directing agent (SDA) in the synthesis. $Al(OH)_3$ (Aldrich) was added to colloidal silica solution (Ludox HS-40, Aldrich) with stirring. Then, KOH (Wako) was added and the mixture was stirred for 30 min at ambient temperature. Finally, the SDA was added and the mixture was stirred for 3 h. The molar composition of the gel was 1.0 SiO_2: 0.1 $Al(OH)_3$: 0.1 SDA: 0.37 KOH: 8 H_2O. Thus obtained gel was transferred to a Teflon-lined stainless steel autoclave and crystallized at 160 ºC for 16 days with tumbling. The solid product was recovered by centrifugation, washed with distilled water and dried overnight at 100 ºC followed by calcination at 600 ºC to remove SDA. The calcined sample was stirred in 1.0 M NH_4NO_3 solution at 80 ºC for ion-exchange and the obtained ammonium form sample was calcined at 550 ºC to give a proton-form sample. A dealuminated MCM-68 was prepared by acid treatment of the calcined sample with 1.0 M HNO_3 *aq* at 80 ºC. The composition of the proton-form sample and the dealuminated sample analyzed by ICP-AES were 9 and 64, respectively.

6-2-3 Characterization of catalysts

Powder X-ray diffraction (XRD) patterns of the samples were collected on a Rigaku Ultima III diffractometer using a Cu Kα radiation (40 kV, 40 mA). Solid-state ^{29}Si MAS NMR spectra were measured on a JEOL ECA-400 spectrometer at a resonance frequency of 79.5 MHz using a 6 mm sample rotor with a spinning rate of 5.5 kHz. ^{13}C CP/MAS NMR spectra were recorded on a JEOL

ECA-600 spectrometer at a resonance frequency of 150.9 MHz using a 4 mm sample rotor with a spinning rate of 15.0 kHz.

6-2-4 Catalytic tests

Catalytic dehydration experiments were performed in a Teflon-lined stainless-steel autoclave (50 ml). In a typical reaction, 15 ml of reactant solution containing 7.5 mmol of sorbitol (0.5 mol/l) was poured into the autoclave and to the solution desired amount (sorbitol/Al = 50, molar basis) of a zeolite was added. The reaction mixture was heated by a heating jacket outside the autoclave and stirred at approximately 800 rpm. At a set time, the reaction was quenched by cooling the autoclave in an ice bath. The reaction mixture was filtered prior to quantitative analysis to remove a solid catalyst. The recovered catalyst was washed with water and dried at ambient temperature, and characterized or in some cases reused. Reaction results at different reaction times were performed in separate batches and combined results were plotted in a figure.

Sorbitol and water-soluble products were analyzed by an HPLC (Shimadzu, LC-20A) with RI detector equipped with an REZEX RCM-monosaccharide column (300 mm x 7.8 mm, Phenomenex). The products were identified by comparing their retention times with those of the standard materials and quantified based on the calibration curves of the standard materials.

Mixtures of anhydrosorbitol (AHSO) isomers are produced in dehydration of sorbitol *via* elimination of a water molecule between hydroxyl groups at different positions and each isomer has very similar molecular structure. For example, 1,4-AHSO and 3.6-AHSO are epimers each other and they cannot be completely separated from one another. Therefore, the combined amount of 1,4- and 3,6-isomers is measured and expressed as 1,4-AHSO. 1,5-AHSO and 2.5-AHSO are also detected in reaction products, but the combined amount of these two isomers are always below 5 % in selectivity and the combined amount is expressed as 1,5-AHSO

6-3 Results and discussion

6-3-1 Influence of structural and compositional properties

First, I evaluated catalytic performances of various types of zeolites in the dehydration of sorbitol. Because sorbitol and dehydration products have bulky structures, 12-membered pore zeolites (***BEA**, **FAU**, **MOR** and **MSE**) are mainly examined, but **MFI**-type zeolites are also examined as representative 10-membered pore zeolite. Figure 1 shows conversion of sorbitol and product distribution in the catalytic runs performed at 200 ºC for 2 h. The ratio of sorbitol to Al atoms in a zeolite was fixed to 50 by varying the amount of a catalyst. In the absence of a catalyst, the conversion of sorbitol was 10 %. Only 1,4-AHSO was detected by the HPLC analysis, but the color of the reaction mixture became pale brown after the reaction, indicating the formation of colored species other than 1,4-AHSO, which is included in unknown products. It turns out that the framework type has a significant influence on the catalytic performance; the sorbitol conversion is in the following order; ***BEA** > **MSE** > **MOR** > **MFI** > **FAU**. 12-membered pore zeolites except for **FAU**-type showed better performances than **MFI**-type zeolites. Among ***BEA**-, **MSE**- and **MOR**-type 12 membered pore zeolites, it is obvious that a multi-dimensional pore system is favorable; ***BEA**-, **MSE**-, and **MOR**-type structures have 3-dimensinally-connected 12 membered pores, a 12-membered pore connected with two different 10-membered pores, and a uni-dimensional 12-membered pore, respectively. The large pore openings and multi-dimensional pore system could enhance the diffusion of sorbitol and/or cyclic products, leading to the high catalytic activity. For all the catalysts, the main product was 1,4-AHSO, which is produced through elimination of a water molecule. As conversion of sorbitol was increased, the isosorbide yield was increased, indicating a successive reaction mechanism for the production of isosorbide (the details on the reaction pathway will be discussed in the later section).

Notably, the framework composition is an also important factor determining a catalytic performance. Zeolites having high-silica compositions showed better performances for any types of frameworks. For example, the catalytic performances of mordenite zeolites with different Si/Al

ratios were increased along with the increase of the Si/Al ratios. In contrast, low-silica zeolites such as ZSM-5(13) and Y(3) gave similar results to the blank run, indicating that they are not active in the dehydration of sorbitol.

Beta(75) showed much better performance than Beta(13) as expected, but the performance of Beta(150) was poor compared to that of Beta(75). This phenomenon was also observed in ZSM-5 zeolites; ZSM-5(40) showed better performance than not only ZSM-5(13) but also ZSM-5(140). These results imply other factors determining a catalytic performance. One of them should be crystallinity of a zeolite. Beta(75) gave higher X-ray diffraction intensity than Beta(150), as shown in Figure 2. Moreover, Beta(75) showed sharp peaks with high proportion of Q^4 species in ^{29}Si MAS NMR spectroscopy (Figure 3). On the other hand, Beta(150) showed broad peaks overlapping each other and the peak of Q^3 species was definitely observed with relatively high proportion. Based on these results, Beta(75) has a lower amount of defects, which is a cause of its high catalytic performance.

Of all the catalysts tested, Beta(75) showed the best performance; 87 % sorbitol conversion and then 33 % selectivity to isosorbide with the co-production of 1,4-AHSO in 44 % selectivity. Its 3-dimensional 12-membered pore structure, high-silica composition and high crystallinity would contribute to the high catalytic performance.

Next, I evaluated the catalytic performance of the representative zeolites on the basis of catalyst mass (Figure 4). It is expected that the difference in the catalytic performance between high-silica zeolites and high-aluminum zeolites becomes small because of a relatively large amount of Al atoms for high-aluminum zeolites. Actually, the difference between Beta(13) and Beta(75) became small compared to the difference in the results performed at the constant sorbitol/Al ratio (Figure 1), but Beta(75) still exhibited better performance despite its lower amount of active sites. This was also observed between Mordenite(10) and Mordenite(45). These results support the importance of high-silica composition aforementioned. One of the reasons for that importance can be attributed to hydrophobicity of a catalyst [47]. There is some literature on catalysis of high-silica

zeolites in water. Yashima et al. reported hydrolysis of ethyl acetate by high-silica zeolites in aqueous solution [48]. Kono et al. reported hydration of cyclohexene using high-silica ZSM-5 [49,50]. In these reports it was proposed that as the Si/Al ratio increases, the surface of a zeolite becomes more hydrophobic and possesses stronger affinity for the organic molecules, leading to a high catalytic activity. In the present study, low-silica zeolites such as ZSM-5(13), Mordenite(10) and Y(3) showed almost no activity in the dehydration of sorbitol, and the catalytic activity was increased with the Si/Al ratio increased. This is probably due to the difference in hydrophobicity of catalysts, which may be reflected in H_2O adsorption amount. Actually, Beta(13) showed significantly high adsorption amount of H_2O compared to the other Beta zeolites (Figure 5). Hydrophobic property of a catalyst must play an important role in the dehydration reaction. There are numerous studies on favorable adsorption of organic molecules on hydrophobic surface of a zeolite as well as studies on unfavorable adsorption of water on such surface; for example, a high-silica zeolite have a larger adsorption capacity for organic molecules such as *n*-hexene and benzene than water [51]. Olson et al. reported that the water adsorption capacity was decreased as the Si/Al ratio decreased [52]. The early reports mainly concern the favorable adsorption of oleophilic molecules on hydrophobic surface of a zeolite, but hydrophobic property is also advantageous for adsorption and catalytic reactions of water-soluble compounds. For example, Deem et al. recently reported that the favorable entropy effect promotes the transfer of glucose molecule from water solution to pure-silica *__BEA__-type framework [53]. In another report, Davis et al. reported that isomerization of glucose in water over Lewis acid center (Ti^{4+} or Sn^{4+}) is not limited by intrazeolitic reactant diffusion, irrespective of whether or not intrazeolitic void spaces are filled with solvent molecules, but the isomerization rate constants reflect differences of kinetic origin [54]. Although it has not been clarified whether transportation limitation or kinetic barrier crucially determines the catalytic activities of high-silica zeolites in the dehydration of sorbitol, it is reasonably anticipated that hydrophobicity originating from high-silica composition facilitates the adsorption of sorbitol molecule on zeolite surface and assists the dehydration reaction.

6-3-2 Importance of hydrothermal stability

FAU-type zeolites showed the poor activities in the screening tests, though they have 3-dimensional 12-membered pores. These poor activities can be attributed to their hydrothermal stability. Figure 6 shows XRD patterns of the **FAU**-type zeolites recovered after the catalytic reactions performed at the constant sorbitol/Al molar ratio. For Y(3) and USY(5) their framework structures were completely retained after the reactions. Howeve, the situation was completely different in the high-silica USY zeolites; USY(30) recovered showed only a halo peak, indicating that the framework was completely collapsed during the reaction to form an amorphous material. USY(55) showed weakened diffraction peaks superposed on a halo peak, indicating a partial collapse of the framework during the reaction. Note that diffraction intensities of the peaks appearing below 20 degree were decreased after the reactions, but this decrease was derived from organic compounds occluded in the micropores, which hinder diffractions in long ranges. Therefore, this decrease does not correlate with the decrease of crystallinity. The XRD analyses indicate that USY zeolites become unstable under the reaction conditions as the Si/Al ratio increased. Sievers et al. has reported similar behaviors that during the treatment in hot water, zeolite Y with a Si/Al ratio of 14 or higher is transformed into an amorphous material, and the rate of this degradation increases with increasing Si/Al ratio [55]. Although high-silica USY zeolites are expected to show high catalytic performances intrinsically due to their large pores and high-silica compositions, their poor hydrothermal stability results in the poor activities. Accordingly, **FAU**-type zeolites are, on the whole, low active in dehydration of sorbitol in water.

The hydrothermal stability of other catalysts was also investigated. Figure 7 shows XRD patterns of **MFI**-, **MOR**- and ***BEA**-type zeolite catalysts with the high-silica compositions before and after the reactions. Obviously, the framework structures of these types of zeolites were totally retained after the reactions. The influence of framework composition of a zeolite on its hydrothermal stability is different depending on the framework type. Also from this point, the framework type is a crucial for the catalytic performance of a zeolite.

6-3-3 Reaction pathway

The time course change of sorbitol conversion and product selectivity was investigated. Figure 8 shows the conversion of sorbitol and the yield of products in the presence of ZSM-5(40), Mordenite(110) and Beta(75), which showed good performances in the screening tests. For Beta(75), the conversion of sorbitol was monotonously increased along with the reaction time and reached over 99 % at 8 h. Initially, the main product was 1,4-AHSO and it was increased to the maximum and then decreased, accompanied with the increase of isosorbide. The isosorbide yield was increased to 77 % at 12 h and then the yield was slowly increased to 78 % at 18 h, which is the maximum. The yield of 1,5-AHSO was increased along with the increase of the conversion, but the yield was below 2 % throughout the reaction. Mordenite(110) showed slower reaction rate; 98 % conversion was achieved at 24 h. The yield of 1,4-AHSO was initially increased, but the yield was fairly constant after 4 h. Moreover, the rate for the isosorbide production was gradually slow down. It is well known that uni-dimensional pore zeolites are likely to deactivate because of deposition of organic compounds to block the micropores and I ascribe the cause of the deactivation due to organic moieties in the micropore. ZSM-5(40) showed much slower reaction rate, but the yield of isosorbide was increased along with the reaction time to 58 % at 24 h. The yield of 1,5-AHSO was high (~7 %) compared to the other zeolites.

The reaction profiles suggest reaction pathways starting from sorbitol (Scheme 1). 1,4-AHSO (including 3,6-isomer) is produced through the dehydration of sorbitol and subsequent dehydration of 1,4-AHSO produces isosorbide. In parallel with the dehydration to 1,4-AHSO, the formation of 1,5- and 2,5-AHSO occurred through the dehydration between the corresponding hydroxyl groups. Besides anhydrosorbitol isomers, a small amount of galactitol (~1 %) was found in the products. Note that mannitol was also found, but its amount was much smaller than galactitol, which is neglected. Because it has been reported that galactitol can be converted to isosorbide [35, 56], dehydration of galactitol was performed by using Beta(75) in order to check the possibility of galactitol being a precursor for isosorbide. Yet, the main product was isoidide and a trace amount of

isosorbide was found (not shown). Also, I have assessed the possibility of the isomerization between isosorbide, isoidide and isomannide by performing the reaction of isosorbide under the same conditions as the dehydration of sorbitol. Equilibrium composition of these isomers at 220 ºC is 7 % of isoidide, 36 % of isosorbide and 57 % of isomannide [31]. Thermodynamically, the isomerization of isosorbide is expected to produce a mixture with a similar composition. In fact the conversion of isosorbide was 14 % at 12 h, when a trace amount of the other two isomers was found (Table 1). Obviously, the isomerization was kinetically hindered under the reaction conditions and isosorbide is stable compared to sorbitol and 1,4-AHSO. Based on these results, I conclude that isosorbide is not produced by way of galactitol or isoidide, and under the conditions subsequent reactions of isosorbide did not significantly occur.

It was found that isoidide was formed by way of galactitol with the elimination of two water molecules. The first dehydration of galactitol generates 1,4-anhydrogalactitol, in which the hydroxyl group at C3 is in *trans* position against hydrogen atom at C4. However, this structure prohibits the following dehydration between the hydroxyl groups at C3 and C6 because thus formed *trans*-fused tetrahydrofuran rings would have a large strain and it is energetically unstable. Therefore, chirality inversion at C4 and C5 should occur to form 1,4-anhydroiditol, a precursor of isoidide [56].

6-3-4 Influence of reaction temperature

The catalytic reactions were performed at different temperatures. In addition to the result at 200 ºC shown in Figure 8(a), reaction results at 180 ºC and 220 ºC are shown in Figure 9. The reaction rate of sorbitol strongly depended on the temperature; at 180 ºC, the conversion of sorbitol after 2 h was 43 %, while >99 % conversion of sorbitol was observed at 220 ºC. At all the temperatures, 1,4-AHSO was initially produced, but the maximum yield of 1,4-AHSO was different depending on the reaction temperature, which was 42, 38, 32 % for 180, 200 and 220 ºC, respectively. The decrease of the maximum yield along with the increase of the reaction temperature

means a strong dependence of the dehydration rate of 1,4-AHSO, indicating a high activation energy for the step, which is the rate-determining. This is compatible with the reported kinetics [30,33,37]. The combined yield of 1,5-AHSO and 2,5-AHSO was not changed by the temperature and it was always below 3 %. The isosorbide yield became constant at prolonged reaction time for all the temperatures, but the maximum isosorbide yield and the reaction time taken to reach the maximum was different. The maximum yield for each temperature was 82, 77 and 74 % and the time taken to reach the maximum was 60, 12 and 4 h. The decrease of the maximum yield at the high temperature would be derived from side reactions of sorbitol to form unidentified products, which was significant at high temperature, reflected in the unknown yield. The yield of unknown products for 180 ºC was 7-10 %, but that for 220 ºC was around 17 %. For achieving a high yield of isosorbide, operation at a low temperature is favorable, though it needs a long reaction time. Anyway, 82 % yield of isosorbide achieved at 180 ºC is, to my best knowledge, the best performance that has been reported for a heterogeneous reaction system.

6-3-5 Influence of catalyst dosage

To improve the productivity of isosorbide, the catalytic reactions were run with the amount of Beta(75) varied at 200 ºC (Figure 10). The catalyst dosage was adjusted to set the sorbitol/Al atom molar ratio equal to 25, 50 and 100 (Figure 8(a) shows the reaction result obtained at the ratio of 50). As the catalyst dosage was increased, the sorbitol and 1,4-AHSO dehydration rates were significantly increased. At the molar ratio of 25, the isosorbide yield reached the maximum (64 %) at 9 h, while the maximum yield (78 %) was obtained at 18 h at the ratio of 50. As for the ratio of 100, the isosorbide yield seemed to be still increasing after 48 h and at that point the yield was 80 %. Although the large amount of catalyst certainly speeded up the dehydrations, it also resulted in the decrease of the isosorbide yield. Simultaneously, the molar balance became worse, indicating the increased production of undetected species. One of them is probably deposition of organic matters on the catalyst surface. Figure 11 shows the unknown yield calculated from the molar balance and

the amount of organic moiety of the recovered catalysts as a function of a reaction time. For the run performed at the ratio of 50, the unknown yield was rapidly increased to 16 % during the first 1 h of the reaction, when conversion of sorbitol was 66 %, and thereafter remained fairly constant. These behaviors were similar to the behaviors of the organic deposition on a catalyst; it was increased to 9 wt% during 1 h and thereafter remained 9-10 wt%. It is obvious that the organic deposition accounts for a part of unknown products. For the run at the ratio of 25, the unknown yield was high (26-29 %) compared to the run at the ratio of 50. Similarly, organic deposition on the catalyst was also high (17-18 wt%). It can be concluded that the escalated production of unknown species including the deposition on the catalyst was a cause of the decrease in the isosorbide yield at high temperature.

6-3-6 Reuse test

Because the deposition of organic compounds on a catalyst is significant in this reaction as mentioned in preceding section, the reusability of Beta(75) was examined. Figure 12 shows the conversion of sorbitol and product distribution during the recycle runs performed at the sorbitol/Al ratio of 50 at 200 ºC for 2 h. Conversion of sorbitol was gradually decreased through the consecutive runs from 87 % to 68 %. However, the combined selectivity to 1,4-AHSO and isosorbide was increased from 77 % to 89 %. The decrease of the sorbitol conversion is mainly due to the suppressed formation of unknown products including deposition on the catalyst. Consequently the selectivity to the desired products was improved. The amounts of the deposition on the catalyst after each run were 10.1 wt%, 12.2 wt%, 13.6wt% and 13.9 wt%, respectively. Clearly, the amount of the deposition newly accumulated during each run substantially decreased. These results implies an upper limitation of the accumulation of organic matters on the catalyst and the deposition does not so much influence the dehydration rates of sorbitol and 1,4-AHSO.

The catalyst recovered after the fourth run was characterized by XRD analysis and it turns out that the crystalline structure of Beta(75) was totally retained even after the four times of usage

(Figure 13). ^{13}C CP/MAS NMR spectra of the recovered catalyst showed multiple peaks in the region of 23-35 ppm and 68-88 ppm (Figure 14). The peaks at the low field are assigned to carbon atoms connected with OH groups derived from sorbitol or dehydration products, but assignment of the peaks at the high field has not been established. Generally, methylene carbon atoms appear at that region of chemical shift, but neither sorbitol nor anhydrosorbitols have methylene carbon atom. These peaks indicate that unexpected reactions occured during reactions and the deposition on the catalyst was formed.

6-4 Conclusions

Dehydration of sorbitol to isosorbide in water was performed using aluminosilicate zeolites as heterogeneous catalysts. Catalytic performance of a zeolite strongly depends on structural and compositional properties. 3-dimensinal large pore zeolites like *__BEA__- and **MSE**-types showed high catalytic activities probably because the large pore openings and multi-dimensional pore systems enhanced the diffusion of sorbitol and/or dehydration products. High-silica zeolites showed better catalytic performances probably due to their hydrophobicity. However, further studies are needed for fully understanding the role of hydrophobic property. Hydrothermal stability is an important factor determining the performance of a catalyst in hot liquid water and it is different depending on the framework type; some USY zeolites were hydrothermally unstable and showed poor activities.

Among the catalysts tested, Beta zeolite with the Si/Al ratio of 75 achieved 82 % yield of isosorbide, which is the best result that has been reported. Furthermore, this catalyst can be reused by a simple washing with water and the yields of 1,4-AHSO and isosorbide remained constant during four consecutive runs.

References:

1. A. Corma, S. Iborra, A. Velty, Chem. Rev. 107 (2007) 2411-2502.
2. J. N. Chheda, G. W. Huber, J. A. Dumesic, Angew. Chem. Int. Ed. 46 (2007) 7164-7183.
3. P. Gallezot, Chem. Soc. Rev. 41 (2012) 1538-1558.
4. D. M. Alonso, J. Q. Bond, J. A. Dumesic, Green Chem., 2010, 12, 1493-1513.
5. G. W. Huber, S. Iborra, A. Corma, Chem. Rev. 106 (2006) 4044-4098.
6. T. Werpy, G. Petersen, A. Aden, J. Bozell, J. Holladay, A. Manheim, D. Eliot, L. Lasure, S. Jones, *Top Value Added Chemicals from Biomass;* U.S. Department of Energy: Oak Ridge, TN, 2004; vol. 1.
7. H. Kobayashi, A. Fukuoka, Green Chem. 15 (2013) 1740-1763.
8. J. Zhang, J. Li, S.-B. Wu, Y. Liu, Ind. Eng. Chem. Res. 52 (2013) 11799-11815.
9. P. J. Cerino, G. Fleche, P. Gallezot, Stud. Surf. Sci. Catal. 59 (1991) 231-236.
10. A P. Gallezot, P. Cérino, B. Blanc, G. Flèche and P. Fuertes, J. Catal. 146 (1994) 93-102.
11. B. W. Hoffer, E. Crezee, P. R. M. Mooijman, A. D. van Langeveld, F. Kapteijn, J. A. Moulijn, Catal. Today, 79/80 (2003) 35-41.
12. A. Fukuoka, P. L. Dhepe, Angew. Chem., Int. Ed. 45 (2006) 5161-5163.
13. W. Deng, X. Tan, W. Fang, Q. Zhang, Y. Wang, Catal. Lett. 133 (2009) 167-174.
14. J. Geboers, S. Van de Vyver, K. Carpentier, K. de Blochouse, P. A. Jacobs, B. F. Sels, Chem. Commun. 46 (2010) 3577-3579.
15. R. Palkovits, K. Tajvidi, A. M. Ruppertc, J. Procelewska, Chem. Commun. 47 (2011) 576-578.
16. H. Kobayashi, Y. Ito, T. Komanoya, Y. Hosaka, P. L. Dhepe, K. Kasai, K. Hara, A. Fukuoka, Green Chem. 13 (2011) 326-333.
17. J. Geboers, S. Van de Vyver, K. Carpentier, P. A. Jacobs, B. F. Sels, Chem. Commun. 47 (2011) 5590-5592.
18. J. W. Han, H. Lee, Catal. Commun. 19 (2012) 115-118.

19. P. Yang, H. Kobayashi, K. Hara, A. Fukuoka, ChemSusChem, 5 (2012) 920-926.

20. S. Van de Vyver, J. Geboers, W. Schutyser, M. Dusselier, P. Eloy, E. Dornez, J. W. Seo, C. M. Courtin, E. M. Gaigneaux, P. A. Jacobs, B. F. Sels, ChemSusChem, 5 (2012) 1549-1558.

21. J. Hilgert, N. Meine, R. Rinaldi and F. Schüth, Energy Environ. Sci. 6 (2013) 92-96.

22. M. Rose, R. Palkovits, ChemSusChem, 5 (2012) 167-176.

23. J. D. Parker, J. O. Parker, N. Engl. J. Med. 338 (1998) 520-531.

24. H. R. Kricheldorf, J. Macromol. Sci., Rev. Macromol. Chem. Phys. C37 (1997) 599-631.

25. F. Fenouillot, A. Rousseau, G. Colomines, R. Saint-Loup, J.-P. Pascault, Prog. Polym. Sci. 35 (2010) 578-622.

26. R. M. Gohil, Polym. Eng. Sci. 49 (2009) 544-553.

27. S. Chatti, G. Schwarz, H. R. Kricheldorf, Macromolecules, 39 (2006) 9064-9070.

28. X. Feng, A. J. East, W. B. Hammond, Y. Zhang, M. Jaffe, Polym. Adv. Technol. 22 (2011) 139-150.

29. J. C. Goodwin, J. E. Hogde, D. Weisleder, Carbohydr. Res. 79 (1980) 133-141.

30. K. Bock, C. Pedersen, H. Thøgersen, Acta. Chem. Scand. B, 35 (1981) 441-449.

31. G. Flèche, M. Huchette, Starch, 38 (1986) 26-30.

32. J. Defaye, A. Gadelle, C. Pedersen, Carbohydr. Res. 205 (1990) 191-202.

33. A. Yamaguchi, N. Hiyoshi, O. Sato, M. Shirai, Green Chem. 13 (2011) 873-881.

34. R. Menegassi de Almeida, J. Li, C. Nedelof, P. O'Connor, M. Makkee, J. A. Moujin, ChemSusChem, 3 (2010) 325-328.

35. J. Li, A. Spina, J. A. Moujin, M. Makkee, Catal. Sci. Technol. 3 (2013) 1540-1546.

36. J. U. Oltmanns, S. Palkovits, R. Palkovits, Appl. Catal. A: Gen. 456 (2013) 168-173.

37. B. O. de Beek, J. Geboers, S. Van der Vyver, J. Van Lishout, J. Snelders, W. J. J. Huijgen, C. M. Courtin, P. A. Jacobs, B. F. Sels, ChemSusChem, 6 (2013) 199-208.

38. Z.-C. Tang, D. H. Yu, P. Sun, H. Li, H. Huang, Bull. Korean Chem. Soc. 31 (2010) 3679-3683.

39. J. Xia, D. Yu, Y. Hu, B. Zou, P. Sun, H. Li, H. Huang, Catal. Comm. 12 (2011) 544-547.

40. N. A. Khan, D. K. Mishra, I. Ahmed, J. W. Yoon, J.-S. Hwang, S. H. Jhung, Appl. Catal. A: Gen. 452 (2013) 34-38.

41. I. Ahmed, N. A. Khan, D. K. Mishra, J. S. Lee, J.-S. Hwang, S. H. Jhung, Chem. Eng. Sci. 93 (2013) 91-95.

42. M. Gu, D. Yu, H. Zhang, P. Sun, H. Huang, Catal. Lett. 133 (2009) 214-220.

43. P. Sun, D. H. Yu, Y. Hu, Z. C. Tang, J. J. Xia, H. Li, H. Huang, Korean J. Chem. Eng. 28 (2011) 99-105.

44. C. Montassier, J. C. Menezo, J. Moukolo, J. Naja, L. C. Hoang, J. Barbier and J. P. Boitiaux, J. Mol. Catal. 70 (1991) 65-84.

45. N. A. Khan, D. K. Mishra, J.-S. Hwang, Y.-W. Kwak, S. H. Jhung, Res. Chem. Intermed. 37 (2011) 1231-1238.

46. T. Shibata, S. Suzuki, H. Kawagoe, K. Komura, Y. Kubota, Y. Sugi, J. H. Kim, G. Seo, Micropor. Mesopor. Mater. 116 (2008) 216-226.

47. T. Okuhara, Chem. Rev. 102 (2002) 3641-3666.

48. S. Namba, N. Hosonuma, T. Yashima, J. Catal. 72 (1981) 16-20.

49. M. Kono, Y. Fukuoka, O. Mitsui, H. Ishida, Nippon Kagaku Kaishi, (1989) 521-527.

50. H. Ishida, Y. Fukuoka, O. Mitsui, M. Kono, Stud. Surf. Sci. Catal. 83 (1994) 473-480.

51. H. Nakamoto, H. Takahashi, Zeolites, 2 (1982) 67-68.

52. D. H. Olson, W. O. Haag, R. M. Lago, J. Catal. 61 (1980) 390-396.

53. P. Bai, I. Siepmann, M. W. Deem, AIChE J. 59 (2013) 3523-3529.

54. R. Gounder, M. E. Davis, J. Catal. 308 (2013) 176-188.

55. R. M. Ravenelle, F. Schüβler, A. D'Amico, N. Danilina, J. A. van Bokhoven, J. A. Lercher, C. W. Jones, C. Sievers, J. Phys. Chem. C, 114 (2010) 19582-19595.

56. M. Kurszewska, E. Skorupowa, J. Madaj, A. Konitz, W. Wojnowski, A. Wiśniewski, Carbohydr. Res. 337 (2002) 1261-1268.

Table 1 Reactivity of isosorbide in the presence of Beta(75)[a].

Temperature	Time (h)	Conversion (%)	Product distribution (%)	
			Detected	Unkown
200 ºC	12	13.9	1.8	12.1
220 ºC	12	19.8	2.5	17.3

a: 0.5 M isosorbide aqueous solution, 15ml; the ratio of isosorbide/Al = 50.

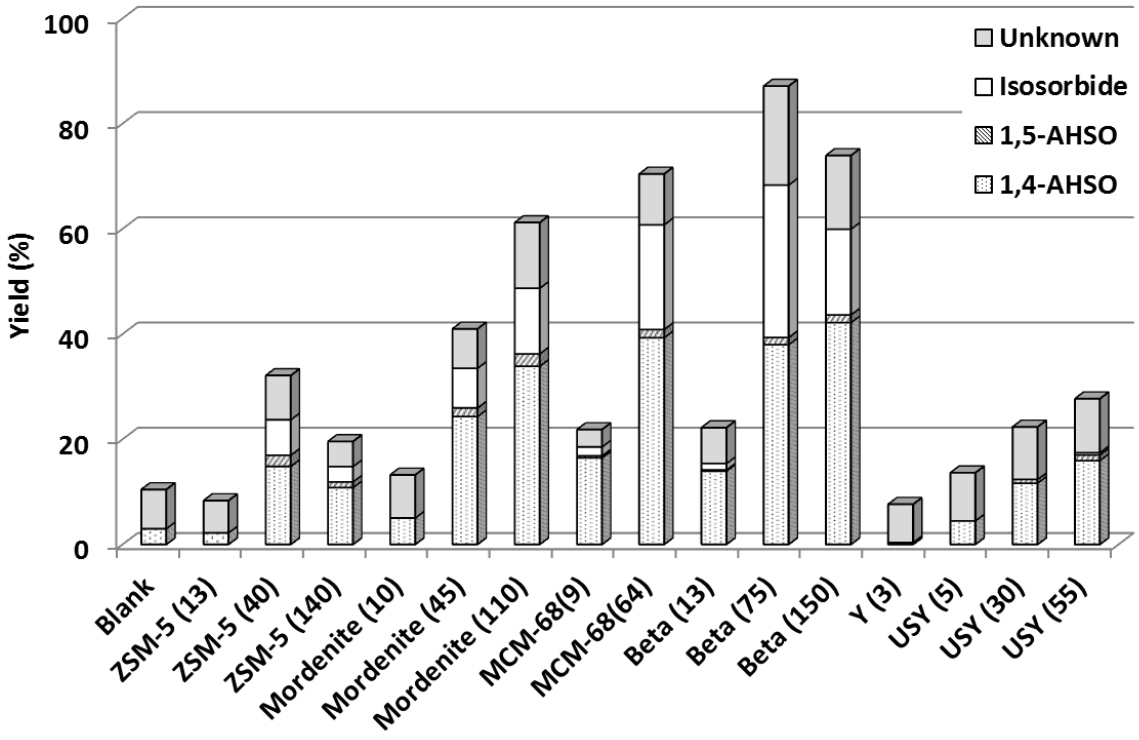

Figure 1 Dehydration of sorbitol over various types of zeolites performed at the ratio of sorbitol to aluminum atoms equal to 50.

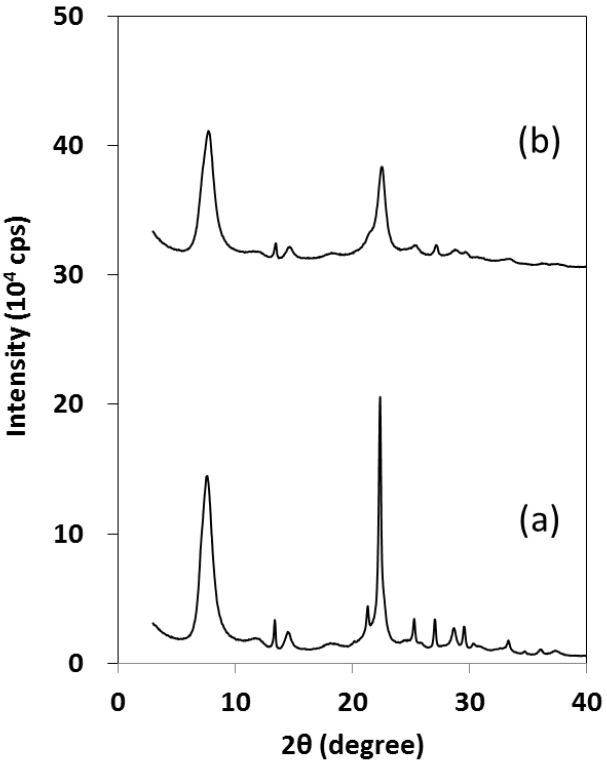

Figure 2 XRD patterns of (a) Beta(75) and (b) Beta(150).

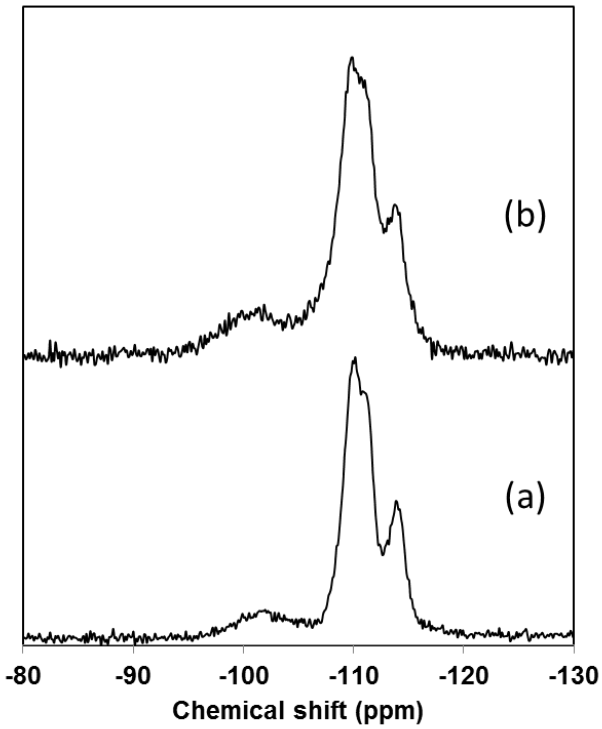

Figure 3 ^{29}Si MAS NMR spectra of (a) Beta(75) and (b) Beta(150).

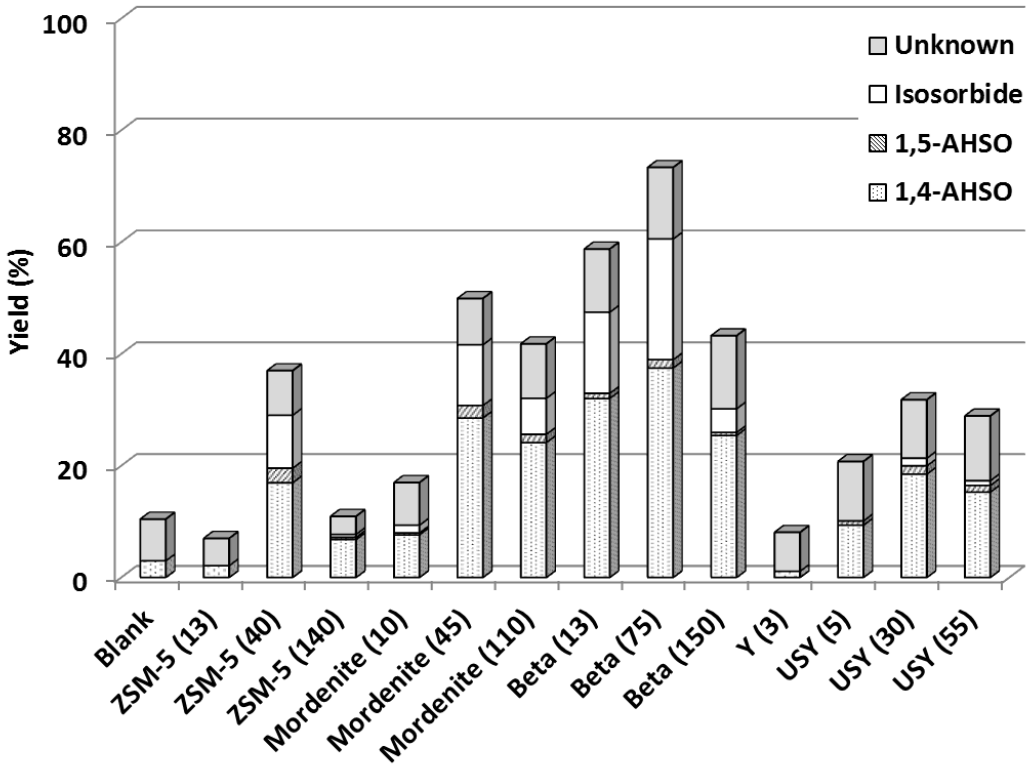

Figure 4 Dehydration of sorbitol over various types of zeolites performed with 0.5 g of a catalyst.

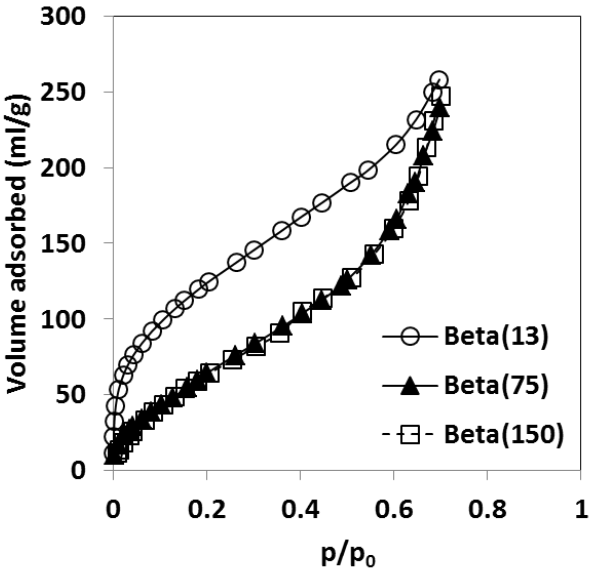

Figure 5 H_2O adsorption isotherms of Beta zeolites measuered at 25 ºC.

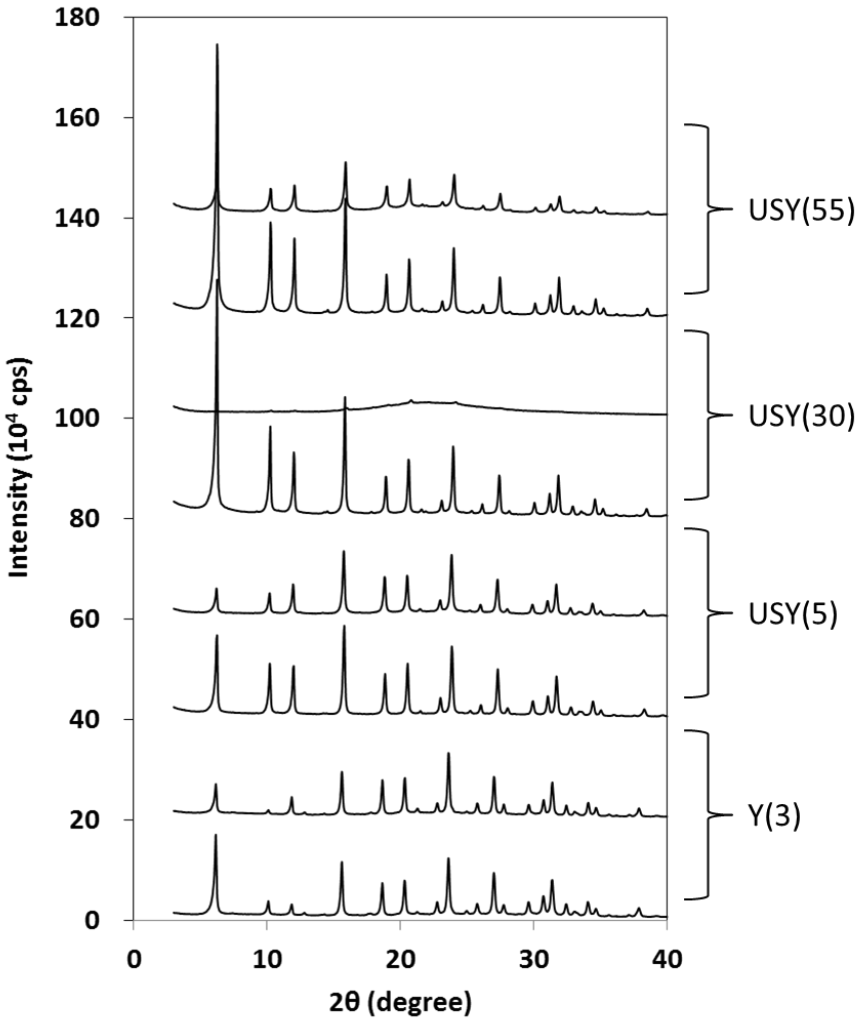

Figure 6 XRD patterns of **FAU**-type zeolites (lower) before and (upper) after the catalytic runs.

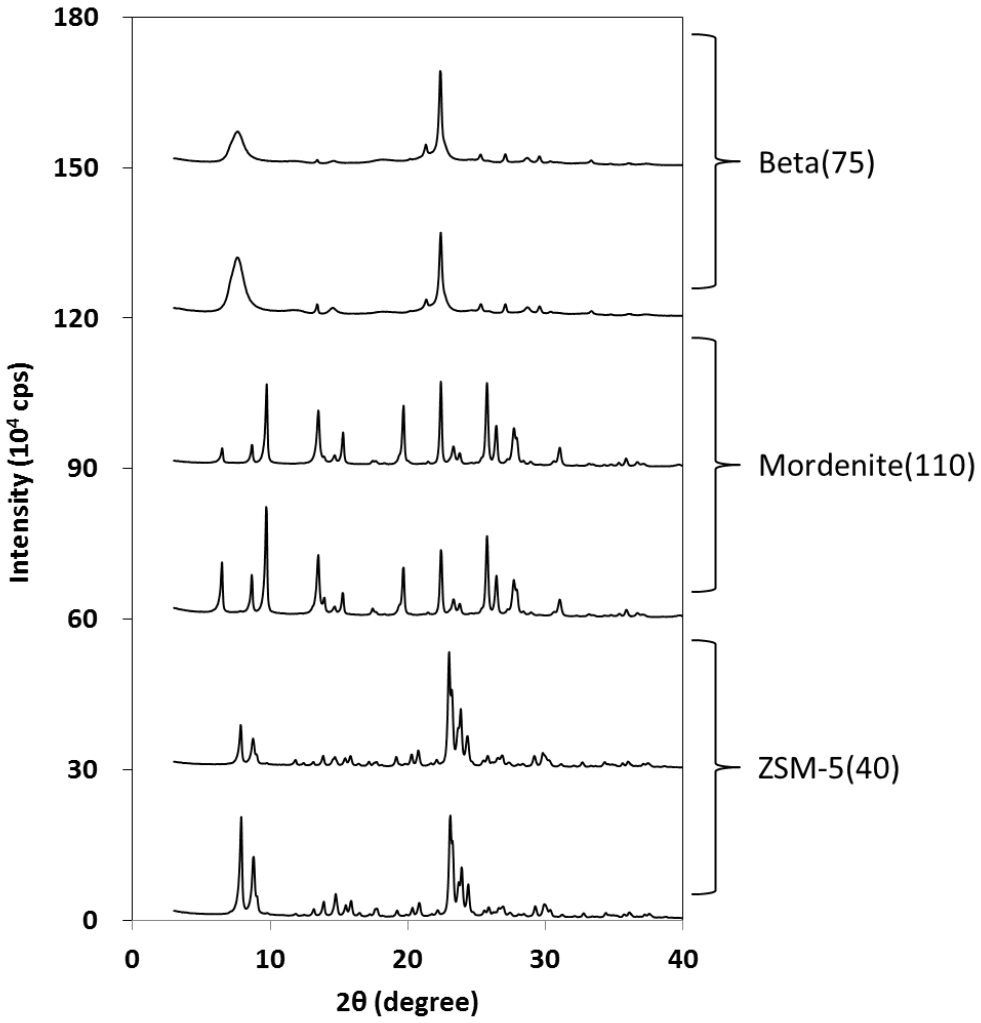

Figure 7 XRD patterns of zeolites (lower) before and (upper) after the catalytic run.

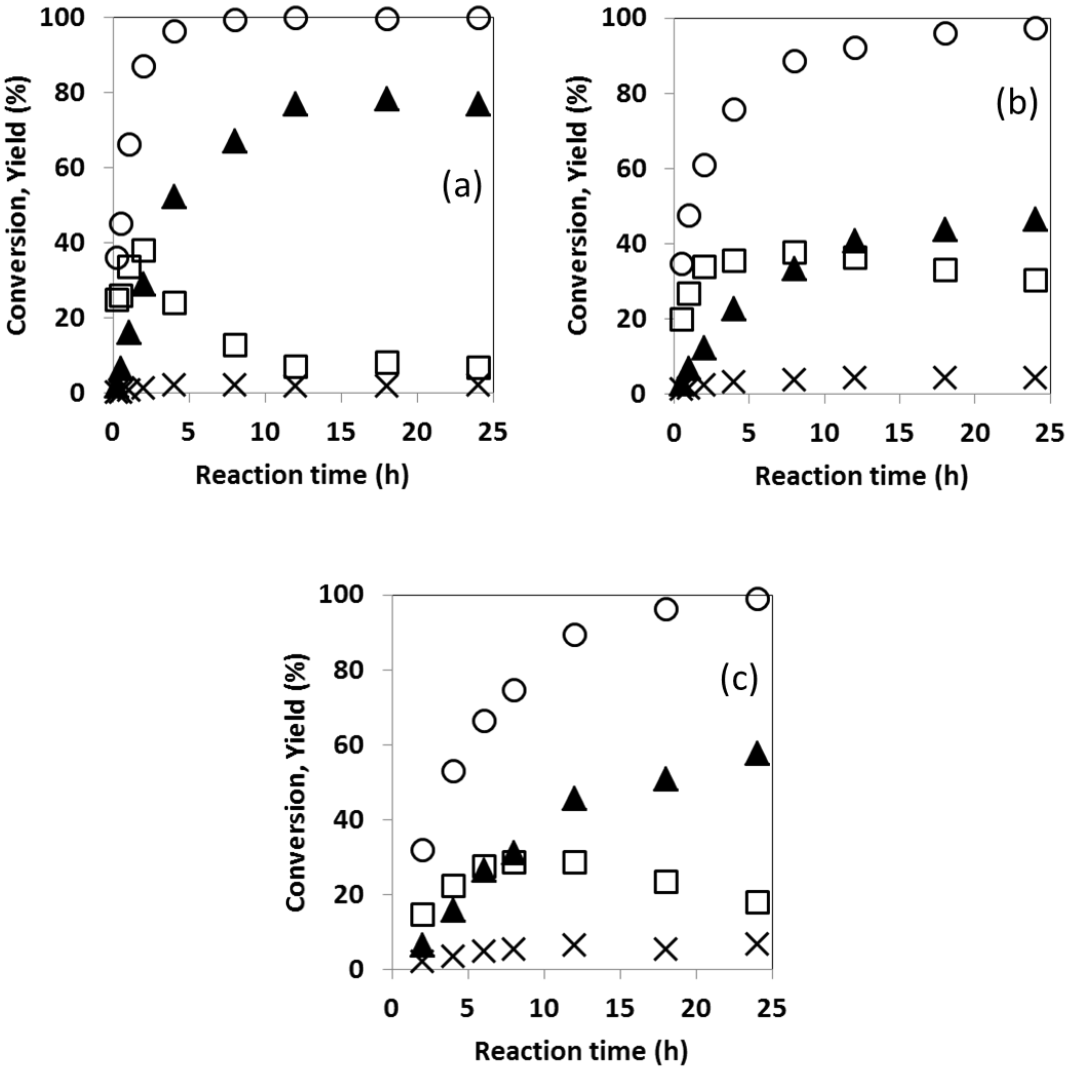

Figure 8 Dehydration of sorbitol with (a) Beta(75), (b) Mordenite(110) and (c) ZSM-5(40).

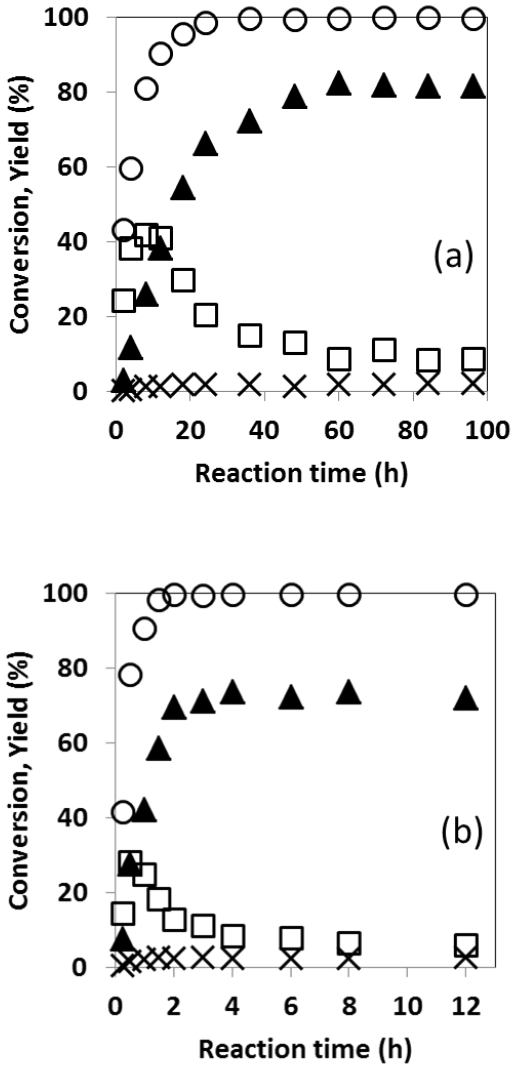

Figure 9 Dehydration of sorbitol with Beta(75) at (a) 180 ºC and (b) 200 ºC.

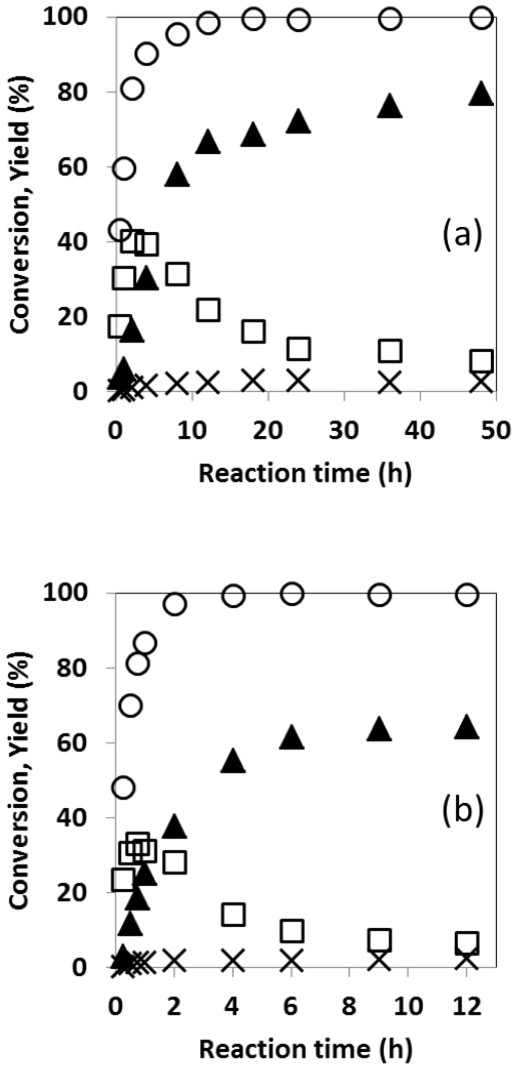

Figure 10 Dehydration of sorbitol with different amount of Beta(75) used. The sorbitol/Al ratios are (a) 100 and (b) 25.

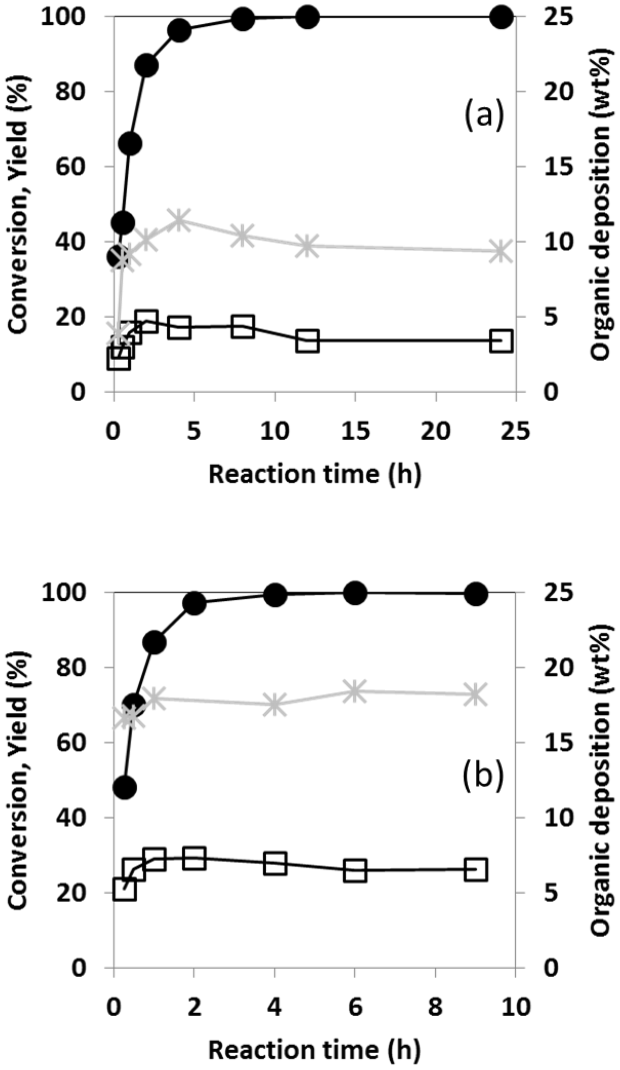

Figure 11 The time course change of sorbitol conversion, unknown yield and organic deposition on Beta(75). The sorbitol/Al ratios are (a) 50 and (b) 25.

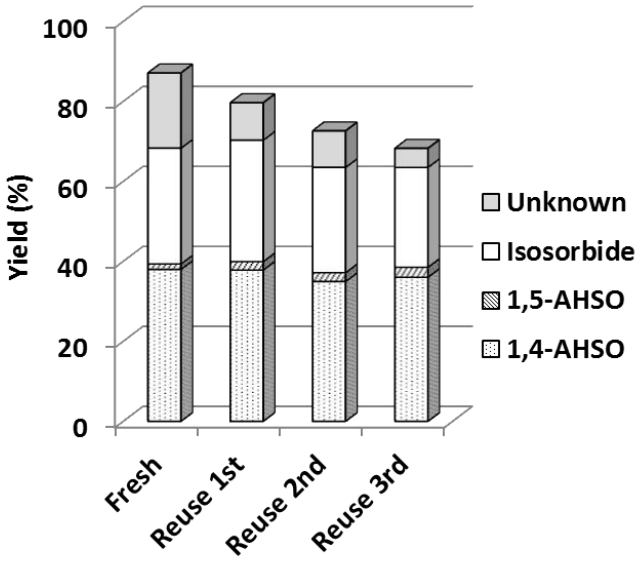

Figure 12 Product distribution in recycling runs with Beta(75).

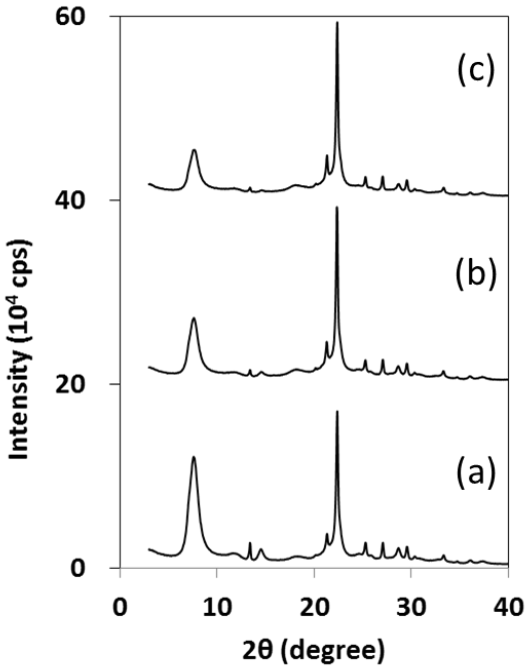

Figure 13 XRD patterns of Beta(75) in recycling runs. (a) fresh, (b) after the first run and (c) after the fourth run.

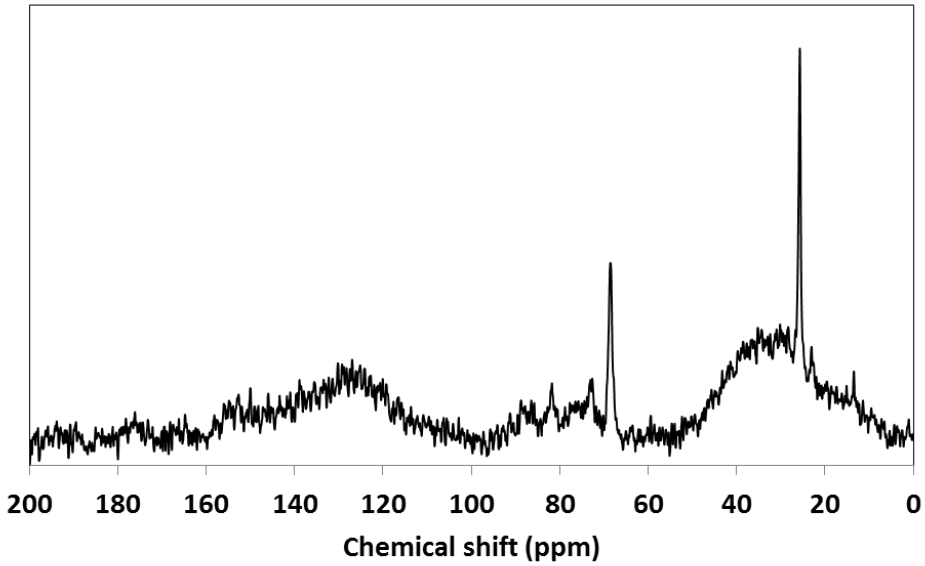

Figure 14 ^{13}C CP-MAS NMR spectrum of Beta(75) after the consecutive four runs.

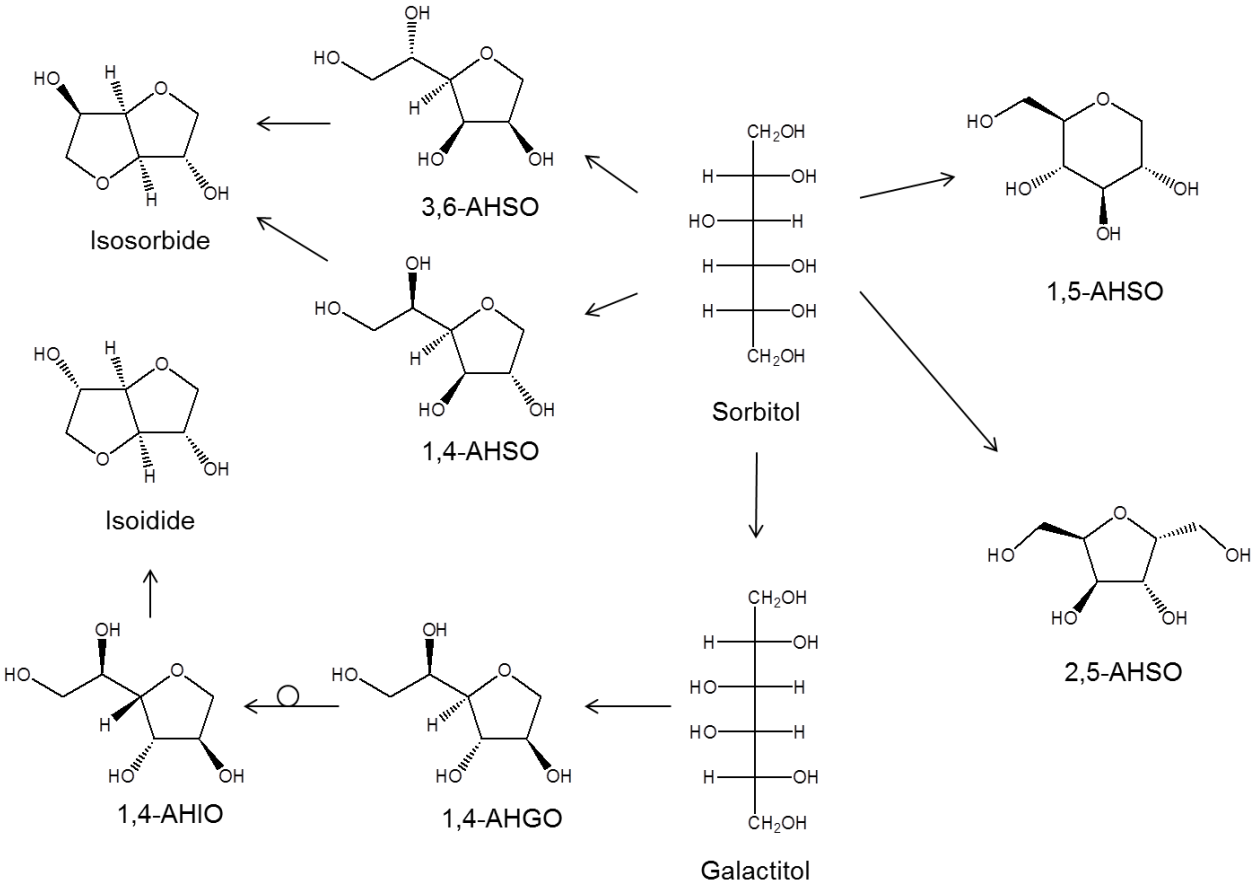

Scheme 1 Reaction pathways of sorbitol in the presence of zeolite catalysts.

Chapter 7

Summary

Chapter 2

Lewis acid sites on the zeolite were remarkably increased when *__BEA__-type aluminosilicate was simply calcined over 700 ºC or treated with steam over 500 ºC. Thus treated Beta zeolites had sufficient amount of Lewis acid sites to promote the isomerization of glucose in addition to the original Brønsted acid sites. Those zeolites with acid properties controlled were effective bifunctional catalysts for the direct transformation of glucose to HMF (55 % selectivity at 78 % glucose conversion). A ^{13}C NMR technique revealed that glucose molecule was isomerized to fructose through an intramolecular hydride transfer. The generated fructose was dehydrated to HMF over Brønsted acid sites.

Chapter 3

Beta-Cal750, which has a relatively large amount of Lewis acid sites formed by the dealumination, can effectively promote the transformation of various types of saccharides including hexoses, oligosaccharides and polysaccharides. Moreover, the reaction system can be applied to the direct conversion of crystalline cellulose to HMF. On the other hand, Beta-Cal500, which has a small amount of Lewis acid sites, shows a better performance in the transformation of xylose than Beta-Cal-750. These results suggest that the suitable acid properties depend on the reactivity of the substrate.

Chapter 4

OSDA-free Beta zeolite can be used without Al atoms leached as an excellent catalyst for the transformation of glucose to HMF. A high B/L ratio and proximity of the two types of acid sites in the Beta catalyst are crucial factors for effectively producing HMF. Beta(OF)-Cal500 gave 72 % yield of HMF at 6 h of the reaction, which is the best performance that has been reported so far for a heterogeneous reaction system.

Chapter 5

OSDA-free synthesis of Beta zeolite was successfully achieved starting from high aluminum composition based on the crystallization mechanism. A moderate amount of NaOH is necessary for selective formation of ***BEA** phase. The crystallization was initiated by the presence of seed crystal, and the crystallization rate was increased by a large amount of seed crystal. Under the hydrothermal conditions employed in this work, crystallization proceeds through the deposition of dissolved species in the form of aluminosilicate onto the surface of seed crystal driven by aluminum species in the solution. When increasing the initial Al content of the starting gel, highly crystalline Beta zeolite was obtained in 84 % yield.

Chapter 6

Dehydration of sorbitol to isosorbide in water was performed using aluminosilicate zeolites as heterogeneous catalysts. Catalytic performance of a zeolite strongly depends on structural and compositional properties. 3-dimensinal large pore zeolites showed high catalytic activities. Probably due to their hydrophobicity, high-silica zeolites showed better catalytic performances. Hydrothermal stability is an important factor determining the performance of a catalyst in hot liquid water and it is different depending on the framework type. Among the catalysts tested, Beta zeolite with the Si/Al ratio of 75 achieved 82 % yield of isosorbide, which is the best result that has been reported.

List of publications

1. Takeshi Suzuki, Toshiyuki Yokoi, Ryoichi Otomo, Junko N. Kondo, Takashi Tatsumi
   "Dehydration of xylose over sulfated tin oxide catalyst: Influence of the preparation conditions on the structural properties and catalytic performance"
   Applied Catalysis A: General 408 (2011) 117-124

2. Ryoichi Otomo, Toshiyuki Yokoi, Junko N. Kondo, Takashi Tatsumi
   "Dealuminated Beta zeolite as effective bifunctional catalyst for direct transformation of glucose to 5-hydroxymethylfurfural"
   Applied Catalysis A: General 470 (2014) 318-326
   (Chapter 2)

3. Ryoichi Otomo, Toshiyuki Yokoi, Junko N. Kondo, Takashi Tatsumi
   "One-Pot Synthesis of Furfurals from Various Types of Sugars Using Dealuminated Beta Zeolites"
   in preparation
   (Chapter 3)

Acknowledgement

First of all, I would like to express my deep and sincere gratitude to my supervisor, Professor Takashi Tatsumi and Professor Junko Nomura for giving me an opportunity to do my research at their laboratory. I am grateful for their guidance, constructive suggestion, and encouragement throughout my studies.

I am deeply grateful to Assistant Professor Toshiyuki Yokoi for his kind encouragement. He is always hard-working with a big smile. His jokes always make me very happy! He is always supporting me in my whole laboratory life.

I wish to express my thanks to Dr. Kiyotaka Nakajima and Dr. Masaaki Kitano for their suggestive discussion in research. Special thanks to Dr. Nakajima for teaching me the preparation of mesoporous silica materials in beginning of my research.

The author is grateful to his contemporaries, Mr. Hiroshi Yamazaki, Mr. Hiroshi Mochizuki and Mr. Min Liu for working hard together and encouragement.

Thanks are due to Prof. Seitaro Namba, Ms. Kazuko Iwane, Dr. Masato Yoshioka, Dr. Hiroyuki Imai, and all members in Tatsumi-Nomura laboratory for encouragement a lot.

Finally, I wish to expresses my sincere gratitude to my family, Mr. Akihiko Otomo, Mrs. Kazuko Otomo, Dr. Daisuke Hoshino, Mrs. Kaori Hoshino and Michitaro Hoshino for their kind and steady supporting and heart-warming mood. I am very proud of being a family with them.